

**DEVELOPMENT OF (MICROFLUIDIC) PAPER-BASED ANALYTICAL
DEVICES FOR COLORIMETRIC DETECTION OF SOIL PRIMARY
MACRONUTRIENTS**



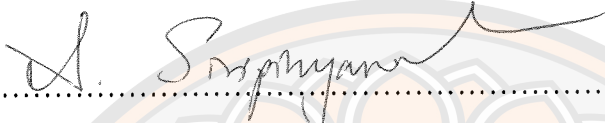
**A Thesis Submitted to the Graduate School of Naresuan University
in Partial Fulfillment of the Requirements
for the Doctor of Philosophy Degree in Chemistry
January 2021
Copyright 2021 by Naresuan University**

Thesis entitled “Development of (Microfluidic) Paper-Based Analytical Devices for
Colorimetric Detection of Soil Primary Macronutrients”

By THINIKAN THONGKAM


has been approved by the Graduate School as partial fulfillment of the requirements
for the Doctor of Philosophy in Chemistry of Naresuan University


Oral Defense Committee


..... Chair
(Associate Professor Atitaya Siripinyanond, Ph.D.)



..... Advisor
(Assistant Professor Khuanjit Hemavibool, Ph.D.)


..... Internal Examiner
(Assistant Professor Dr. Yuthapong Udnan, Ph.D.)


..... Internal Examiner
(Assistant Professor Jintana Klamtet, Ph.D.)


..... Internal Examiner
(Assistant Professor Sairoong Ouypornkochagorn, Ph.D.)

Approved


.....
(Professor Paisarn Muneesawang, Ph.D.)

For Dean of the Graduate School

12 JAN 2021

ACKNOWLEDGEMENTS

First and foremost, I would like to express my sincere gratitude to my dissertation advisor, Assistant Professor Khuanjit Hemavibool for her kind guidance, patience and encouragement throughout the course of this research.

My sincere appreciation is extended to the chairman and external examiner of the thesis defense, Associate Professor Dr. Atitaya Siripinyanond from Mahidol University for her kindness in providing invaluable suggestions and comments. I also wish to thank the internal examiners, Assistant Professor Dr. Yuthapong Udnan, Assistant Professor Dr. Jintana Klamtet, and Assistant Professor Dr. Sairoong Ouypornkochagorn for their suggestions regarding the completion of my dissertation.

I would like to thank the Department of Chemistry, Faculty of Science at Naresuan University, for the use of their research facilities and instrumentation. I also thank Mr. Paul Freund and Mr. Peter Barton of Naresuan University Writing Clinic, for their editing assistance.

I especially would like to thank Kemira (Thailand) Ltd. and Aditya Birla Chemicals (Thailand) Ltd. for the chemical support.

Finally, I would like to give my grateful thanks to my family for their support and encouragement throughout my study, my classmates for their help and wishes for the success of this dissertation.

Thinikan Thongkam

Title DEVELOPMENT OF (MICROFLUIDIC) PAPER-BASED ANALYTICAL DEVICES FOR COLORIMETRIC DETECTION OF SOIL PRIMARY MACRONUTRIENTS

Author Thinikan Thongkam

Advisor Assistant Professor Khuanjit Hemavibool, Ph.D.

Academic Paper Thesis Ph.D. in Chemistry, Naresuan University, 2020

Keywords Microfluidic paper-based analytical devices, Macronutrient, Soil, Nitrate, Ammonium, Phosphate, Potassium

ABSTRACT

The purpose of this dissertation was to fabricate new and simpler paper-based analytical devices (PADs) for the rapid detection of primary macronutrients in soil. The fabrication method using a simple, inexpensive screen-printing method together with new hydrophobic materials was developed. The study consisted of four parts including new paper-based analytical devices with colorimetric assay application to the determination of nitrate, ammonium, phosphate, and potassium, respectively. The first part of study presented an environmentally friendly microfluidic paper-based analytical device (μ PAD) that uses beeswax as a new hydrophobic material with a screen-printing method for determination of nitrate in soil. Functionality of the new μ PAD was optimized for colorimetric determination of nitrate in soil. A linear range was obtained in the range of 0.5–40 mg L⁻¹ with a limit of detection (LOD) and limit of quantitation (LOQ) of 0.41 mg L⁻¹ and 1.35 mg L⁻¹, respectively. The respective RSD values for nitrate was 1.15–2.24% (inter-day precision), and 1.50–2.16% (intra-day precision). The reaction time of this method was obtained in 10 min. The second part focused on a convenient and low-cost PAD for ammonium measuring in soil. This PAD has been developed using an inexpensive UV resin solution, as a new hydrophobic material, with a screen-printing method to create hydrophobic areas. The paper-based colorimetric device was developed using a modified Berthelot reaction in which salicylate and dichloroisocyanurate are used to produce a green compound of 2-2 dicarboxyindophenol in the presence of ammonium.

A variety of tests was carried out to optimize and evaluate various aspects of the PAD's fabrication and utilization. A linear range was obtained in the range of 10–100 mg L⁻¹ with a LOD and LOQ of 0.50 mg L⁻¹ and 1.65 mg L⁻¹, respectively. The relative standard deviation of intra-day measurements was 1.57–2.58% and the inter-day precision was 1.86–3.81% with good reproducibility. The analysis time was obtained in 10 min. The third part demonstrated a one-step fabrication method for a μ PAD using epoxy resin as a novel hydrophobic material in conjunction with the screen-printing method. The μ PAD was applied to analysis the phosphate in soil, by using the molybdenum blue method. This method provided a linear range of 0.5–40 mg L⁻¹ phosphate with the LOD and the LOQ being 0.25 mg L⁻¹ and 0.83 mg L⁻¹, respectively. The relative standard deviation of intra-day measurements was 1.52–2.46% and the inter-day precision was 1.89–2.74% with good reproducibility. The reaction time of this method was obtained in 10 min. The final part explored the indirect determination of potassium based on ion pair extraction of dibenzo-18-crown-6 - K⁺ complex into dichloromethane with an excess amount of calmagite as the counter ion. The remaining calmagite in aqueous phase after extraction was examined on a paper based platform and digitized with a smartphone, allowing the amount of potassium in the original test solution to be calculated. This method provided a linear range from 20–120 mg L⁻¹ with the LOD and LOQ at 5.41 and 18.03 mg L⁻¹, respectively. The respective RSD values for nitrate were 2.02–3.51% (inter-day precision), and 2.42–3.86% (intra-day precision). The analysis of this method was obtained in 5 min. Furthermore, the four propose methods were applied to detect nitrate, ammonium, phosphate, and potassium, respectively in a variety of actual soil samples, and the results were validated against spectrophotometric results using a paired t-test, which showed good accuracy. The developed methods are simple, fast, inexpensive, disposable, and requires no expensive instrument suitable for highly limited regions.

CONTENTS

Chapter	Page
I INTRODUCTION.....	1
Introduction.....	1
Research aim.....	3
The scope of the study.....	3
Expected outcomes.....	4
II LITERATURE REVIEWS.....	5
Soil.....	5
Soil nutrients.....	6
Nitrogen.....	6
Phosphorus.....	7
Potassium.....	8
Microfluidic paper-based analytical devices (μPADs).....	10
Photolithography.....	12
Wax printing.....	13
Inkjet printing.....	14
Screen printing.....	15
Plotting.....	16
Stamping.....	17
Cutting.....	18
Colorimetric detection.....	22
Nitrate.....	22
Ammonium.....	25
Phosphate.....	29
Potassium.....	31

CONTENTS (CONT.)

Chapter	Page
III FABRICATION OF ENVIRONMENTAL FRIENDLY MICROFLUIDIC PAPER-BASED ANALYTICAL DEVICES FOR THE DETERMINATION OF NITRATE.....	34
Introduction.....	34
Experimental.....	38
Chemicals.....	38
Apparatus.....	38
Preparation of solutions.....	38
Optimization of the beeswax screen-printing method.....	39
Optimization of the Griess reaction on μ PAD.....	41
Interference.....	43
Analytical Method Validation.....	43
Optimization of the stability of the μ PAD.....	44
Application in real samples.....	44
Spectrophotometric method.....	44
Results and discussion.....	45
The μ PAD fabrication using beeswax screen printing method ...	45
Effect of colorimetric detection of nitrate.....	51
Effect of interference	54
Analytical performance.....	55
Stability of the μ PAD.....	55
Sample analysis.....	56
Conclusions.....	58

CONTENTS (CONT.)

Chapter	Page
IV FABRICATION OF 3D PAPER-BASED ANALYTICAL DEVICES BY USING THE UV RESIN SCREEN PRINTING METHOD FOR THE DETERMINATION OF AMMONIUM.....	59
Introduction.....	59
Experimental.....	61
Chemicals.....	61
Apparatus.....	61
Preparation of solutions.....	61
Optimization of the UV resin screen-printing method.....	62
Optimization of the modified Berthelot's reaction on 3D PAD...	64
Interference.....	66
Analytical Method Validation.....	66
Application in real samples.....	67
Spectrophotometric method.....	67
Results and discussion.....	68
Effect of the UV resin screen-printing method.....	68
Effect of modified Berthelot's reaction on 3D PAD.....	71
Effect of interference.....	73
Analytical Performance.....	74
Sample analysis.....	75
Creation of convenient paper color comparison chart.....	78
Conclusions.....	78
V FABRICATION OF 3D PAPER-BASED ANALYTICAL DEVICES BY USING ONE-STEP EPOXY RESIN SCREEN PRINTING METHOD FOR THE DETERMINATION OF PHOSPHATE.....	79
Introduction.....	79

CONTENTS (CONT.)

Chapter	Page
Experimental.....	80
Chemicals.....	80
Apparatus.....	80
Preparation of solutions.....	81
Optimization of the epoxy resin screen-printing method.....	81
Optimization of the molybdenum blue reaction on 3D PAD.....	83
Interference.....	85
Analytical Method Validation.....	85
Stability of the μ PAD.....	86
Application in real samples.....	86
Spectrophotometric method.....	87
Results and discussion.....	87
Effect of the epoxy resin screen-printing method	87
Effect of the molybdenum blue method on 3D PADs.....	91
Effect of interference	95
Analytical Performance.....	96
Stability of the μ PAD.....	96
Sample analysis.....	97
Conclusions.....	99

VI INDIRECT DETERMINATION OF POTASSIUM BY EXTRACTION WITH DIBENZO-18-CROWN-6 AND CALMAGITE USING PAPER-BASED PLATFORM IN CONJUNCTION WITH SMARTPHONE.....

SMARTPHONE	101
Introduction.....	101
Experimental.....	103
Chemicals.....	103

CONTENTS (CONT.)

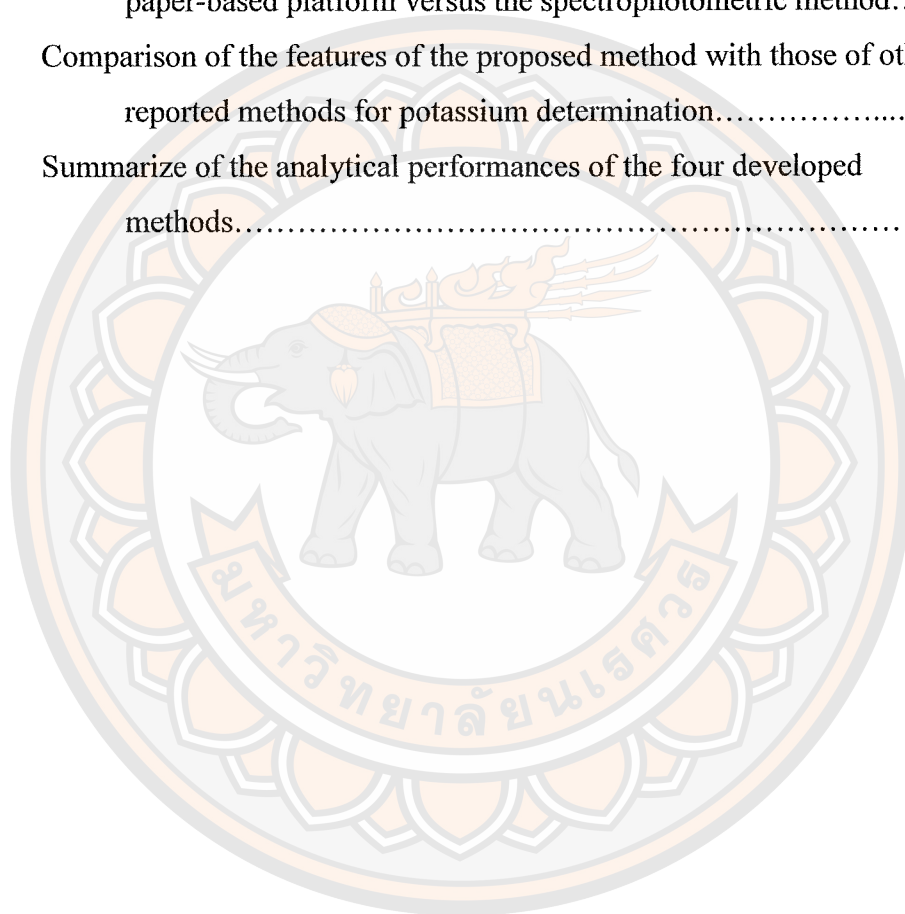
Chapter	Page
Apparatus.....	103
Preparation of solutions.....	104
Preparation of the paper-based platform.....	105
Optimization of extraction conditions.....	105
Interference.....	107
Application to paper-based platform with smartphone read out...	107
Application in real samples.....	109
Results and discussion.....	110
Effect of selection of counter ions.....	110
Effect of pH	111
Effect of the dibenzo 18-crown-6 concentrations.....	113
Effect of the reaction time.....	113
Effect of interference.....	114
Paper-based platform in conjunction with smartphone for potassium determination.....	116
Sample analysis.....	117
Conclusions.....	120
VII CONCLUSIONS.....	121
Conclusions.....	121
Future works.....	123
REFERENCES.....	124
BIOGRAPHY.....	148

LIST OF TABLES

Table	Page
1 Forms in which Plant of nutrients are utilized by plants	10
2 Guidelines for interpreting nutrients levels in soil for rice grown.....	10
3 Hydrophobic materials used for the paper's pattern	19
4 Summary of the main advantages and disadvantages of different method for producing paper-based microfluidic devices	20
5 Summary of colorimetric detection of different from various samples in μ PADs.....	21
6 Viscosity and density data of the prepared beeswax emulsion	46
7 Effect of melting temperature and time on wax barrier formation	47
8 Comparison of nitrate detection results in soil using the μ PAD versus the spectrophotometric method.....	57
9 Comparison of the features of the proposed μ PADs with those of other reported methods for nitrate determination.....	58
10 Comparison of ammonium detection results and recovery rate in various soil samples using the 3D PAD versus the spectrophotometric method.....	76
11 A comparison of the features of the proposed μ PAD with those of other reported methods for ammonia/ammonium determination.....	77
12 Optimization of the mixing ratios between the epoxy resin and the curing agent, and the effects of the curing temperatures.....	88
13 Comparison of phosphate detection results from soil samples using the 3D PAD versus the spectrophotometric method.....	98
14 Comparison of the features of the proposed μ PADs with those of other reported methods for phosphate determination.....	99
15 Comparison of potassium detection results by using varied counter ions at various pH levels.....	111
16 The effect of pH on linearity of potassium.....	112

LIST OF TABLES (CONT.)

Table		Page
17	Comparison of potassium detection results from soil samples using the paper-based platform versus the spectrophotometric method.....	118
18	Comparison of the features of the proposed method with those of other reported methods for potassium determination.....	119
19	Summarize of the analytical performances of the four developed methods.....	123



LIST OF FIGURES

Figure		Page
1	Composition of soil.....	5
2	Schematic representation of μ PAD.....	11
3	The process of photolithography and an example of a μ PAD fabricated via photolithography method.....	13
4	Step-by-step fabrication of μ PADs and an example of a μ PAD fabricated via wax printing method.....	14
5	Fabrication process of inkjet printing and images of pattern printed.....	15
6	Schematic of the screen printing method and an example of a μ PAD.....	16
7	Scheme showing the fabrication of μ PADs through 3D pen drawing.....	17
8	Steps involved in the stamping-based fabrication method.....	17
9	The process of cutting method and a final μ PAD.....	19
10	Colorimetric of nitrate through Griess's reaction.....	22
11	Schematic diagrams of the μ PADs.....	23
12	Schematic diagram of the detection assay for nitrite and nitrate in food samples based on colorimetric μ PAD.....	24
13	Schematic assembly of the mixed μ PAD for determination of nitrite and nitrate.....	25
14	Schematic diagram of the colorimetric ammonium assay by 3-nitrophenol or bromothymol blue: A) Proposed gas diffusion μ PAD; B) Photograph of a bromothymol blue μ PAD and a 3-nitrophenol μ PAD.....	27
15	Schematic diagram of the colorimetric ammonium assay by Nessler reagent.....	28
16	Optical images of the ammonia sensor at different concentrations.....	28
17	PAD for the determination of phosphorus.....	30
18	μ PPC for the determination of phosphate.....	30

LIST OF FIGURES (CONT.)

Figure	Page
19 Colorimetric sensor for the detection of phosphate performed on paper-based analytical devices (PADs) based on the anti-aggregation of 2-mercaptoethanesulfonate (MS)-modified silver nanoplates.....	31
20 Colorimetric detection of potassium.....	32
21 The photograph of Au NPs with different concentrations of potassium...	33
22 Quantification of potassium using a distance-based μ PAD.....	33
23 A schematic diagram showing fabrication process of the μ PAD with beeswax using the screen-printing method.....	40
24 Schematic diagram of the nitrate assay using the colorimetric μ PAD.....	42
25 The appearance resulting of the emulsifier CTAB.....	46
26 Evaluating hydrophobicity A) Blue dye dropped onto hydrophobic and hydrophilic zones, B) Magnified border, before blue dye is applied to the hydrophilic zone, C) Magnified border, after blue dye is applied to the hydrophilic zone, D) Various screen-printed beeswax patterns with dye, showing clear hydrophobic barriers...	48
27 Resolution test results of the beeswax screen printing method.....	49
28 Measurement results from the 24 μ PADs.....	50
29 The effect of various chemicals on the integrity of the hydrophobic barrier.....	51
30 The effect of sulfanilic acid concentrations.....	52
31 The effect of NED concentrations.....	52
32 The effect of VCl_3 concentrations.....	53
33 The effect of reaction time on color intensity.....	53
34 The effect of interfering ions on the determination of 40 mg L^{-1} nitrate using μ PAD. The concentrations of interfering ions were 100 mg L^{-1} for Na^+ , K^+ , Ca^{2+} , Cl^- , and SO_4^{2-}	54

LIST OF FIGURES (CONT.)

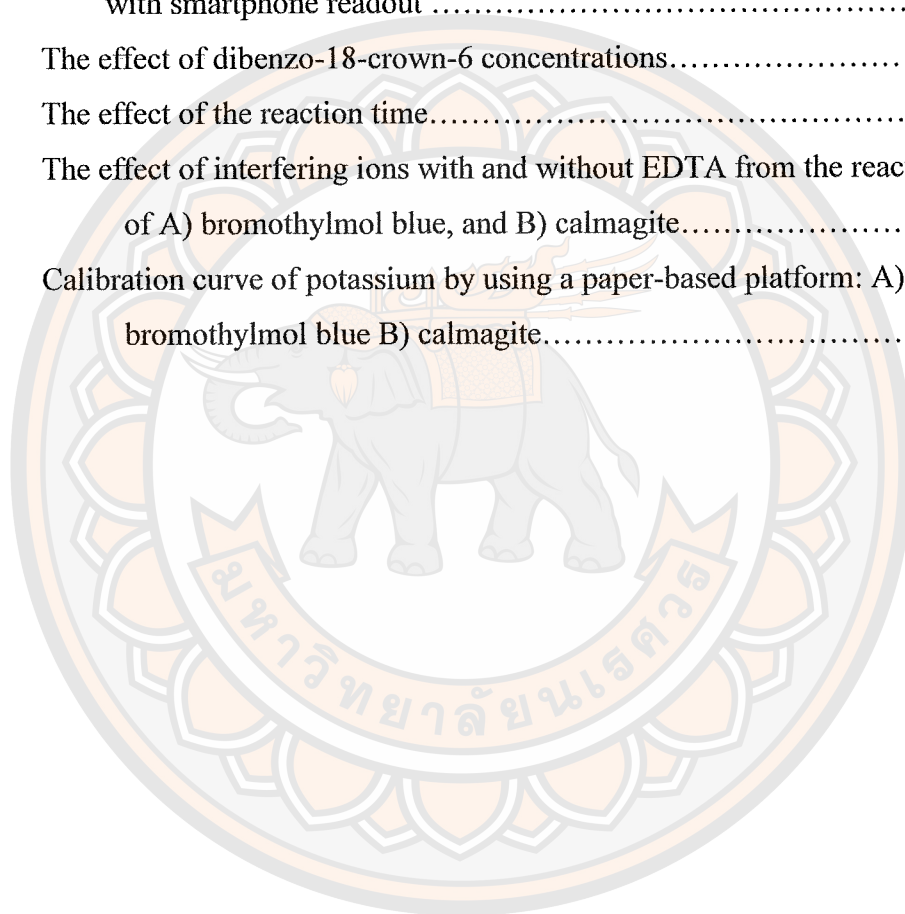
Figure	Page
35 Calibration curve of nitrate.....	55
36 The effect of the stability of the μ PADs stored at 2°C.....	56
37 Image of the μ PAD fabricated by the beeswax screen-printing method and after utilizing for the detection of nitrate.....	56
38 Schematic diagram of UV resin screen-printing for the fabrication of 3D PAD.....	63
39 Schematic diagram of the colorimetric ammonium assay using the 3D PAD.....	65
40 The effect of UV resin concentration.....	68
41 The effect of curing time on the hydrophobic and hydrophilic zone.....	69
42 Filter paper printed with UV resin using the screen printing method: A) contact angle of a water droplet placed on the UV resin coated region, B) the hydrophilic-hydrophobic boundary, as seen under a microscope at 5x magnification, C) various sample patterns created to highlight the versatility of the UV resin screen printing method.....	70
43 The effect of various chemicals on the integrity of the hydrophobic barrier.....	71
44 The effect of sodium salicylate concentrations.....	72
45 The effect of sodium dichloroisocyanurate concentrations.....	72
46 The effect of reaction time on color intensity.....	73
47 The effect of interfering ions on the determination of 100 mg L ⁻¹ ammonium using 3D PAD. The concentrations of interfering ions were 100 mg L ⁻¹ for NO ₃ ⁻ , PO ₄ ³⁻ , K ⁺ , Fe ²⁺ , Mn ²⁺ , and Cu ²⁺	74
48 Calibration curve of ammonium.....	75
49 The color comparison chart for testing soil ammonium content.....	78

LIST OF FIGURES (CONT.)

Figure		Page
50	Schematic diagram of epoxy resin screen-printing for the fabrication of PADS.....	82
51	Step for detection of phosphate on 3D PAD.....	84
52	Hydrophilic–hydrophobic contrast on the paper: A) comparison of hydrophilic and hydrophobic regions of the paper after applying a drop of dye solution and water contact angle on the hydrophobic region, B) a comparison of the hydrophilic and hydrophobic areas imaged with a microscope (5×magnification), C) examples of μ PADs with epoxy resin barriers fabricated using the screen printing method, D) a pattern of hydrophilic lines with different channel widths of 0.1, 0.2, 0.3, 0.4, 0.5, 0.6, 0.7, 0.8, 1.0, 1.2, and 1.4 mm were immersed in a dye solution.....	90
53	Epoxy resin barriers with some surfactants, organic, and inorganic solvents. Images of the circles on the μ PADs after contact with a green dye solution of different solvents.....	91
54	The effect of ammonium molybdate concentrations.....	92
55	The effect of sulfuric acid concentrations.....	93
56	The effect of stannous chloride concentrations.....	94
57	The effect of reaction time on color intensity.....	94
58	The effect of interfering ions on the determination of 40 mg L ⁻¹ phosphate using 3D PADS. The concentrations of interfering ions were 100 mg L ⁻¹ for NO ₃ ⁻ , NH ₄ ⁺ , K ⁺ , Fe ²⁺ , Mn ²⁺ , Cu ²⁺ , and Ca ²⁺	95
59	Calibration curve of phosphate.....	96
60	The effect of the stability of the 3D PADS stored at 2°C.....	97
61	Pattern of paper-based platform.....	105
62	Process for the detection of potassium by using spectrophotometric method.....	106

LIST OF FIGURES (CONT.)

Figure	Page
63 Process for the detection of potassium by using paper-based platform with smartphone readout	108
64 The effect of dibenzo-18-crown-6 concentrations.....	113
65 The effect of the reaction time.....	114
66 The effect of interfering ions with and without EDTA from the reaction of A) bromothymol blue, and B) calmagite.....	115
67 Calibration curve of potassium by using a paper-based platform: A) bromothymol blue B) calmagite.....	117



CHAPTER I

INTRODUCTION

Introduction

Soil is a major source of nutrients for plant growth. It is a complex system which includes minerals, organic matter, water, air, and organisms. The primary macronutrients are nitrogen (N), phosphorus (P), and potassium (K) commonly known as NPK, which are essential elements for crops growth and development (1-3). Nitrogen is an essential nutrient for plant growth. It is present in the form of nitrate (NO_3^-) and ammonium (NH_4^+). Nitrogen promotes growth of leaves and stems (4). The orthophosphates, H_2PO_4^- and HPO_4^{2-} are macro compound of phosphorus that is needed for plants growth. Phosphorus helps transfer energy from sunlight, stimulates early roots, plant growth, and hastens maturity (5). Potassium is always present as K^+ in soils (6). It increases strength of plants and disease resistance, helps form and move starches, sugars and oils in plants, and can improve fruit quality (7). The quantity of NPK varies depending on type of crops and plant growth level. Therefore, the quantity of fertilizer have to be estimated based on the requirements for optimum production at each location in the field (8). However, a deficiency of the macronutrients leads to oxidative stress, which is assessed by markers, such as malondialdehyde, protein oxidation, and the ratio of reductant to oxidant. By alleviating oxidative stress, N, P, and K use efficiency might be improved and plant growth be promoted under the N, P, and K deficiency (9). In addition, excessive use of NPK has created serious impact on the environment which is not only contaminating the land and eventually plants but also threatening human health, as well as it can be just as detrimental as a deficiency, may impair plant growth, contaminate surface and groundwater (10-12). Therefore, the application of sufficient quantities of plant nutrients is essential to increasing agricultural productivity, economic return, reduce negative environmental impact, and reduce production costs. In the effective fertilization of agricultural fields, agriculturists should know the concentration of soil nutrients before adding fertilizer to meet the nutrition requirements of the crops by quantitative nutrients assays in the soil before plant.

Various methods are available for the measurement of nutrients in soil with high sensitivity and accuracy, such as spectrophotometric methods (13), electrochemical method (14), chemiluminescence (15), capillary electrophoresis (16) and chromatography (17). Unfortunately, most detection techniques require expensive laboratory instruments, time consuming, and large amounts of chemicals using. Nowadays, different commercial test kits have been manufactured by several companies under different trade names for soil testing. However, these commercial test kits are expensive, and some have been imported from overseas. This makes is inconvenient or unaffordable for the agriculturist to use these test kits for monitoring the soil nutrients. This work therefore is an attempt to develop a simple low cost device that can lead to be more effective and convenient for detection of soil primary macronutrients.

One revolutionary approach for conducting inexpensive analysis is based on the use of microfluidic paper-based analytical devices (μ PADs) that were first introduced by the Whitesides group in 2007 (18). The μ PADs are miniaturized devices developed with a cellulose paper on which hydrophobic barriers are constructed, creating hydrophilic channels which allows the water to penetrate and/or transport within its hydrophilic zone, by using capillary actions (19-22). It is easy-to-use, disposable, biodegradable, small sample and reagent consumption, low-cost analytical platform, and amenable to use by unskilled operators. The fabrication of the channels on the paper can be performed by modifying some of the hydrophilic zones to become hydrophobic barriers, in order to confine the liquid flow with in the hydrophilic channels in a controlled manner (23). The μ PADs have great potential for analysis applications beyond laboratory settings, such as environmental analysis (24-26), food safety inspection (27-30), biosensing (31-32), pharmaceutical analysis (33-34), and clinical diagnosis (35-38). Therefore, the μ PADs was investigated for determination of primary macronutrients in the soil.

The aims of the thesis were: (i) to design and fabricate the (μ)PADs by using new hydrophobic materials in conjunction with the screen printing method (ii) to develop more convenient devices for the determination of primary macronutrients in the soil, which are nitrogen, phosphorus, and potassium in the forms of nitrate (NO_3^-) and ammonium (NH_4^+), phosphate (PO_4^{3-}), and potassium (K^+) by using the colorimetric detection methods.

Research aim

1. To fabricate (microfluidic) paper-based analytical devices - (μ)PADs - for colorimetric detection of nitrate, ammonium, phosphate, and potassium.
2. To apply (μ)PADs for the detection of primary macronutrients in soil.

The scope of the study

This study consists of four major parts. The first is the fabrication of an environmental friendly μ PAD for the determination of nitrate in the soil samples, by using beeswax to screen print patterns onto the paper. The μ PAD measures the nitrate content using VCl_3 as a reductant for reducing nitrate to nitrite. The reduced nitrate, plus the nitrite originally present in the sample, reacts with the Griess reagent (sulfanilamide and NED) under acidic conditions.

The second is the fabrication of the 3D PAD, using the UV resin screen printing method for the determination of ammonium in soil. The colorimetric detection based on the modified Berthelot reaction was used for rapid determination of ammonium on the 3D PAD. Sodium salicylate and dichloroisocyanurate respectively can be substituted as safer alternatives to toxic phenol and unstable hypochlorite, for the indophenol reaction.

The third is to investigate the 3D PAD which is produced by the one-step epoxy resin screen printing method, for the determination of phosphate in soil. The colorimetric detection of phosphate is based on the molybdenum blue method. The 3D PAD measures the phosphate content using ammonium molybdate, then reduced by stannous chloride.

The fourth will focus on the use of crown ether with counter ion for the determination of potassium on the PAD. The method is based on the extraction of dibenzo-18-crown-6-potassium-counter ion ternary complex in dichloromethane. The pore diameter of the crown ether matches the diameter of the potassium very well, and the colored dye was used as counter ion, which can be used for the qualitative and quantitative analysis of potassium in soil.

Expected outcomes

The fabricated (μ)PADs can be used as devices for the detection of soil primary macronutrients. This information is useful for evaluation of the fertility status of the soil and planning a nutrient management program to reduce cost and increase agricultural production. These (μ)PADs can serve as fast, easy-to-use, low cost, and disposable devices.



CHAPTER II

LITERATURE REVIEWS

All literature reviews, including of soil, soil nutrients, microfluidic paper-based analytical devices (μ PADs), and colorimetric detection of nitrate, ammonium, phosphate and potassium are presented.

Soil

Soil is a dynamic natural body developed as a result of pedogenic processes through weathering of rocks, consisting of mineral and organic constituents, possessing definite chemical, physical, mineralogical and biological properties, having a variable depth over the surface of the earth, and providing a medium for plant growth. The soil consists of four major components: mineral matter, organic matter, soil air and soil water. By volume, the air-dry soil contains about 45% mineral matter, 5% organic matter and 25% each of water and air (Figure 1) (39).

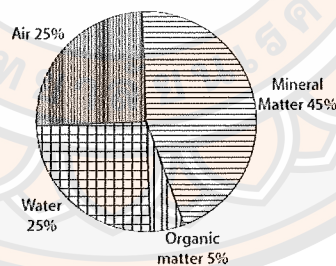


Figure 1 Composition of soil (39)

The arrangement of solid particles and pore space is called the soil matrix. The matrix is a three-phase system of solid (mineral matter and organic matter), liquid (water) and gas (air). The proportion of air and water are subject to rapid and great fluctuations under natural conditions, depending on the weather and other factors. The interactions among these components are of great significance in providing plants with water, air and essential nutrients (39).

Soil nutrients

Nutrients are chemical elements that are essential for growth and fertility. Soil fertility is the capacity to receive, store and transmit energy to support plant growth. It is the component of overall soil productivity that deals with its available nutrient status, and its ability to provide nutrients from its own reserves and through external applications for crop production (40). Soil fertility management is most important for optimizing nutrition for both short and long-term basis to achieve sustainable crop production, because plants require at least 16 elements to complete their life cycle. These nutrients can originate from weathered minerals or from decomposing organic matter. The non-mineral nutrients include carbon (C), hydrogen (H) and oxygen (O) originating from the air and water during photosynthesis (41).

Mineral nutrients are divided into two types: macronutrients and micronutrients. Macronutrients are further divided into primary and secondary, with the primary nutrients being required by plants in relatively large proportions. The three main nutrients are nitrogen (N), phosphorus (P) and potassium (K), which are commonly known as NPK. Secondary nutrients include calcium (Ca) magnesium (Mg) and sulfur (S). Micronutrients are needed in very small amounts and they include boron (B), iron (Fe), manganese (Mn), copper (Cu), zinc (Zn), molybdenum (Mo) and chlorine (Cl) (42). It is important to note that though the soil nutrients are separated into different groups (based on the quantity required by the plant), each nutrient is equally important. A shortage of any nutrient can limit the growth and yield of a plant. Soil pH is also important for maintaining proper fertility, and this affects the availability of the nutrients (43). As shown in Table 1, each nutrient has a different function for plant growth. The role of primary macronutrients in soil, including nitrogen, phosphorus and potassium as follows:

1. Nitrogen

Mineral and organic nitrogen (N) forms undergo a number of changes throughout the N-cycle. Nitrogen is easily transformed among various reduced and oxidized forms and is readily distributed by hydrologic and atmospheric processes. The amount of plant available nitrogen is positively influenced by nitrogen fertilization, mineralization of soil organic matter, biological nitrogen fixation and by precipitation. Negative influences result from immobilization, crop uptake and removal,

denitrification, volatilization, leaching, run-off and erosion (44). Nitrogen is the first fertilizer element of the macronutrients usually applied as commercial fertilizers, which is very important nutrient for plants and it seems to have the quickest and most pronounced effect. Nitrogen is the most important plant nutrient for crop production. It is a constituent of the building blocks of almost all plant structures. It is an essential component of chlorophyll, enzymes, proteins, etc (45). Nitrogen occupies a unique position as a plant nutrient because rather high amounts are required compared to the other essential nutrients. It stimulates root growth and crop development as well as uptake of the other nutrients. Nitrogen tends primarily to encourage above ground vegetative growth and it imparts dark green color to plants. It is a regulator that governs to a considerable degree the utilization of potassium, phosphorus and other constituents. It promotes vegetative growth and improves the quality of produce including fodder, leafy vegetable and food crops. It increases the tillering of cereal crops. Nitrogen occurs in soil as organic and inorganic forms. Inorganic or mineral nitrogen is commonly found in the forms of nitrate (NO_3^-) and ammonium (NH_4^+) (46). Nitrate is the most abundant form of nitrogen available for plant uptake. Ammonium is the first form of nitrogen produced when soil microorganisms convert organic nitrogen into mineral nitrogen. It is also the main form in which fertilizer nitrogen is applied in agriculture (47). However, the ammonium that plants do not take up, is subject to change (conversion to NO_3^-) by the biological transformation occurring within days of its application to the soil system (48). However, if nitrogen is low, growth is stunted, and all plant functions are disturbed. Nitrogen is mobile and when in short supply, will drift from older leaves to younger ones. Deprived of nitrogen, the older leaves will often turn light green, yellow, or in some cases pink. In addition, the excessive use of this element causes serious problems agriculture and environment. This can disrupt the development of many important plants. Over much accumulation of nitrogen in plants may cause toxicity problems for human health like methemoglobinemia, nitrous oxide emissions, and groundwater's nitrate pollution (49).

2. Phosphorus

Phosphorus is the second fertilizer element and it is an essential constituent of every living cells and for the nutrition of plant and animal. It takes active part in all type of metabolism of plant. It is an essential constituent of majority

of enzyme and also structural component of membrane system of cell, the chloroplasts and the mitochondria. It is intimately associated with the life process. It participates in metabolic processes such as photosynthesis, energy transfer, synthesis and the breakdown of carbohydrates. It is also critical in biological energy transfer processes that are vital for life and growth. Adequate phosphorus results in higher grain production, improved crop quality, greater stalk strength, increased root growth, and earlier crop maturity (50). Phosphorus is found in soils both in an organic form and an in-organic (mineral) form and its solubility in soil is low. There is equilibrium between the solid phase phosphorus in soil, and the phosphorus in the soil solution. Plants can only take up phosphorus dissolved in the soil solution, and since most of the soil phosphorus exists in stable chemical compounds, only a small amount of it is available to the plant at any given time. Plants take up phosphorus from the soil solution as orthophosphate (H_2PO_4^- , HPO_4^{2-}), although the uptake of HPO_4^{2-} appears to be slower than the uptake of H_2PO_4^- . The ratio of these two forms is dictated by the pH, with H_2PO_4^- dominant in acid solutions, while HPO_4^{2-} is dominant in alkaline solutions. It is important to note that these ions are negatively charged (anions), so the plant will need a different mechanism to take up phosphorus, than the one used for cations uptake (51). However, without phosphorus, plant growth is retarded, and will have spindly and stunted roots. Deficiency symptoms also include dull greyish-green leaves, red pigment at their bases and dying leaves. Phosphorus deficiency is difficult to diagnose, and by the time it is recognized it may be too late to do anything. If plants are starved of phosphorus as seedlings they may not recover when phosphorus is applied later (52). In addition, higher concentration of phosphorus mostly interferes with uptake of other elements, such as iron, manganese and zinc. Over-fertilization with phosphorus is common and many growers apply unnecessarily high amounts of it, especially when compound NPK fertilizers are used or when irrigation water is acidified using phosphoric acid (53).

3. Potassium

Potassium is the third fertilizer element that is absorbed by plants in the form of K^+ . Potassium in fertilizer is usually defined as K_2O and is used to express the content of various fertilizer materials containing potassium, such as potassium (KCl), sulfate of potassium (K_2SO_4), double sulfate of potassium and magnesium (K_2SO_4 ,

MgSO₄), and nitrate of potassium (KNO₃). Potassium is an essential element for the development of chlorophyll. It is essential for photosynthesis, i.e., converting carbon-dioxide and hydrogen into sugars and for translocation of sugars and also for starch formation. It is, therefore, of special value for crops like sugarcane and potatoes which are rich in sugar and starch (7). It is absolutely necessary for tuber development. Potassium improves the health and vigor of the plant, enabling it to withstand adverse climatic condition. It strengthens the straw of cereals and keeps the plant green and functioning longer than it would otherwise do. Thus it reduces lodging in cereal crops. Potassium improves the quality of crops like tobacco, potatoes, sugarcane, vegetables and fruits. It also increases the crop resistance to certain diseases and counteract the damaging effects of excess nitrogen. It is necessary for the production of best quality of grains and fruits. Potassium plays a key role in production of quality vegetables. In delaying maturity, potassium works against undue ripening influences of phosphorus. In a general way it exerts a balancing effect on both nitrogen and phosphorus and consequently is especially important in a mixed fertilizer. Potassium improves water balance, promotes metabolism and increases the production of carbohydrates. However, potassium deficiency is often called the “hidden hunger” as crop potassium requirements are often large and visual symptoms to a potassium deficiency can be quite difficult to identify during the growing season. Potassium deficiency will be most likely when potassium concentrations in the soil are suboptimal for grass or crop production. In general, potassium deficiency can be evident in older leaves as potassium is mobilised to the stems with the result of the necrosis of the leaf tips (dying). One of the most common signs of potassium deficiency is the yellow scorching, or firing (chlorosis), along the leaf margin. In severe cases, the fired margin of the leaf may fall out. Potassium-deficient crops grow slowly and have poorly developed root systems. Stalks are weak, and lodging of cereal crops such as corn and small grain is common (54). As important as it is, too much potassium can be unhealthy for plants because it affects the way the soil absorbs other critical nutrients.

Table 1 Forms in which plant of nutrients are utilized by plants (55)

Element	Abbreviation	Forms of nutrients used by the plants
Nitrogen	N	NO_3^- (nitrate) and NH_4^+ (ammonium)
Phosphorus	P	H_2PO_4^- and HPO_4^{2-} (orthophosphate)
Potassium	K	K^+

It is useful for agriculturists to know which and how much nutrients are required by analyzing their soil before planting, because each plant requires different kinds and amounts of nutrients. Guidelines for evaluating major nutrients and soil fertility levels are shown in Table 2.

Table 2 Guidelines for interpreting nutrients levels in soil for rice grown (56-57)

Fertility level	Nitrogen (mg kg^{-1})	Phosphorus (mg kg^{-1})	Potassium (mg kg^{-1})
Low	< 10	< 10	< 60
Medium	10 – 20	10 – 20	60 – 90
High	20 – 30	20 – 40	90 – 120
Excessive	> 30	> 40	> 120

This work therefore is an attempt to develop a new and simpler microfluidic paper-based analytical device (μPAD) for the rapid detection of soil primary macronutrients.

Microfluidic paper-based analytical devices (μPADs)

Microfluidic paper-based analytical devices (μPADs) were first described by Martinez, et al., 2007 (18). This method has continued to develop at an exponential rate with notable impacts to academic and industrial communities. Nowadays there is a growing trend to use it as substrate for sensors due to its several inherent advantages including; a small footprint, small reagent volumes generating small waste volumes,

and increased portability and accessibility for detection relative to traditional laboratory testing methods (58). Generally, μ PADs are produced from filter paper (also called cellulose paper) which is a material that can process 0.1 to 100 μ L of liquids using fluidic channels (59). Using μ PADs made from these methods, samples were transported through the hydrophilic flow channel of the paper by capillary forces without external power sources (60). The common detection method is colorimetry, which uses chemical reaction on the hydrophilic area of the paper to fabricate a color change. The resulting color intensity is proportional to the analyte's concentration. To quantify the analytes, a digital camera, cell phone, or scanner is typically used to record the color intensity (61). The use of paper as a substrate for analytical purposes has several advantages because it is readily available and inexpensive. Paper-based devices can be easily patterned into discrete hydrophilic and hydrophobic zones (Figure 2) which is lightweight, easy to transport, disposable and biodegradable (62). In particular, the Whatman filter paper is popular to use as paper-based devices because of the important parameters such as porosity, flow rate and particle retention. Application of μ PADs is particularly favored in point-of-need settings that require rapid analysis with low cost and simple operation. Recently, μ PADs have been used for a variety of analytes, such as environmental analysis (62-63), food safety inspection (64), biosensing (65), pharmaceutical analysis (33-34), and clinical diagnosis (35-38).

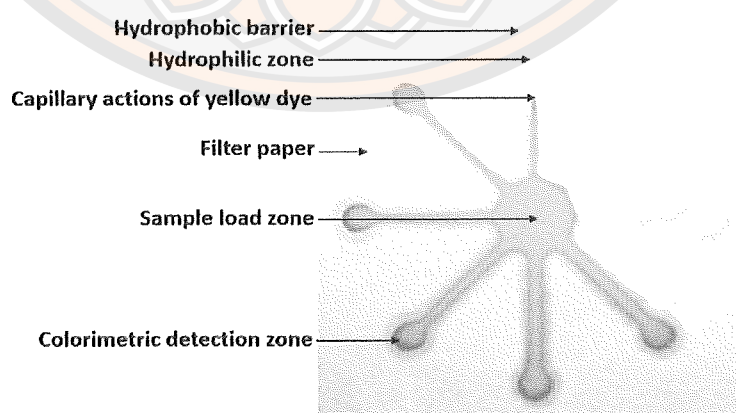


Figure 2 Schematic representation of μ PAD (66)

The hydrophobic barriers and hydrophilic channels of μ PADs can be fabricated using a variety of methods. Described below are the most common methods for fabrication of μ PADs including photolithography (67-68), wax printing (69-72), inkjet printing (73-75), screen-printing (20, 76-78), cutting (79-80), wax dipping (81), and stamping (82-87) method. Pattern principles and hydrophobic material of these methods have also been summarized in Table 3.

1. Photolithography

Production of the paper based plates by patterning sheets of paper into hydrophilic zones bounded by hydrophobic barriers. This method can use low cost formulation photo resistant that permits fast prototyping of paper based plates which around 15 minutes. Martinez, et al. (18) was the first to demonstrate the use of photolithography to fabricate microfluidic channels on paper. The first step of the process is to impregnate the filter paper with photoresist. Then a transparency film is placed on top of the paper and a black paper is placed under the filter paper. Next, the desired pattern is printed onto the transparency film and exposed to UV light. The photoresist will polymerize, forming a hydrophobic barrier in the paper. The paper is then removed from the film and broken to crosslink the exposed portion. Finally, the paper is washed with solvent to remove the unexposed photoresist from the paper. A diagram of the process and a picture of the microfluidic device are shown in Figure 3. However, there are a few drawbacks in photolithography. It is a multistep, and time-consuming process. Moreover, the paper channels are exposed to polymers and solvents which might affect the fluids that flow through the channels and ultimately the assays being performed. Photolithography method was used for multiple detections, such as glucose, protein (88), copper (89), iron (67), and chromium (90).

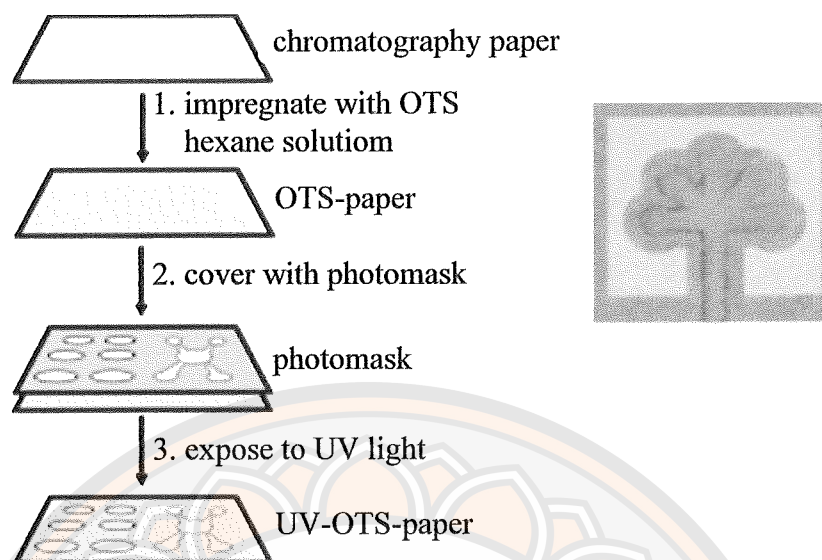


Figure 3 The process of photolithography and an example of a μ PAD fabricated via photolithography method (67, 91)

2. Wax printing

Wax printing was introduced by Carrilho, et al. (71). Hydrophilic patterns can be printed on flexible substrates using a desktop wax printer that uses colored solid wax cubes as ink. The wax printer heats the wax cube to melt and jet out the molten wax to print patterns on a substrate. The printed wax was then melted in an oven or hotplate. Due to the porous structure of the filter paper, the wax penetrates into the paper to form well-defined micro-channels on the paper. Because wax printing is easy to accomplish with a wax printer, it has now become a major method for fabrication of μ PADs. A diagram of the process and an example of paper-based microfluidics fabricated by wax printing is shown in Figure 4. The advantages of this method are high resolution, high throughput, biodegradable and biocompatible barriers. However, these methods still require expensive wax printer (>150\$), extra controlling steps for fabrication and unavailability in developing countries. Wax printed μ PADs was applied to colorimetric detection of copper (92), lead (93), cadmium (93), iron (94), adulterants (70), formaldehyde (95-96), human chorionic gonadotropin (97) etc.

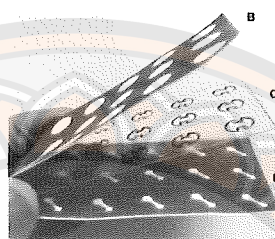
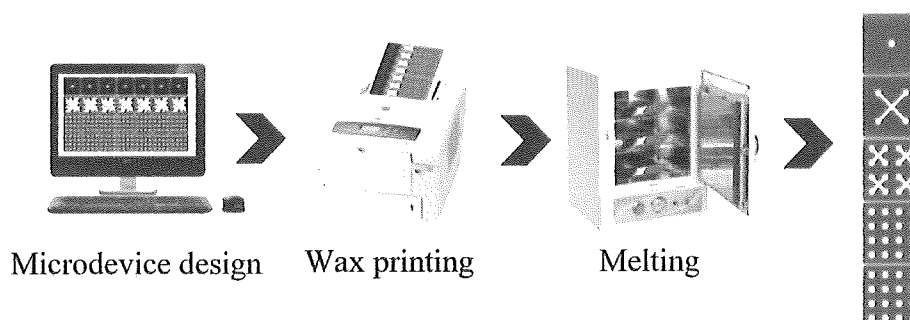


Figure 4 Step-by-step fabrication of μ PADs and an example of a μ PAD fabricated via wax printing method (98-99)

3. Inkjet printing

Inkjet printing method is known as digital writing, which is used to deposit functional materials onto a substrate. It is a cost effective and widely adopted tool for the fabrication of microfluidic devices by depositing hydrophobic materials. One such chemical is alkyl ketene dimer (AKD), which can selectively hydrophobize paper (21). The method involves printing AKD-heptane solution on paper and curing it at 100°C for 8 min to create hydrophobic barriers. Although a simple technique, its disadvantage is the damage caused to the printer, especially to the cartridge, by organic solvents. Abe et al. described the polymer solution using polystyrene with inkjet printing to fabricate paper-based microfluidic devices (74). This method described by Citterio et al. and Maejima et al. used a UV-curable acrylate ink instead of the hazardous organic solvents for printing on paper; further, for curing, the pattern was exposed to UV light for 60 s (75, 100). Moreover, Xu et al. also described a low-cost and rapid method using permanent marker with inkjet printing to fabricate paper-based microfluidic devices. The printed filter paper was allowed to air dry for 15 min, allowing the evaporation of ethanol (101). Therefore, the cartridge and printers are not easily attacked and damaged by the solvent. Recently, Prabhu et al. used a paraffin

wax-heptane solution on paper and curing it at 100°C for 15 min to allow the paraffin to penetrate into the paper pores (102). The hydrophilic-hydrophobic contrast of patterns so created provides an excellent ability to control capillary penetration of aqueous liquids in paper channels. Fabrication of μ PADs by inkjet printing has advantages such as cost-effectiveness, time-savings, ease of mass fabrication, and direct patterning of hydrophilic and hydrophobic barriers on paper. The inkjet printing method has become a common method for the detection of a variety of analytes, such as glucose (101, 103-104), phosphate (105), ammonia (106), uric acid (107), and mercury (108). Figure 5 shows schematic illustration and μ PAD fabricated by inkjet printing.

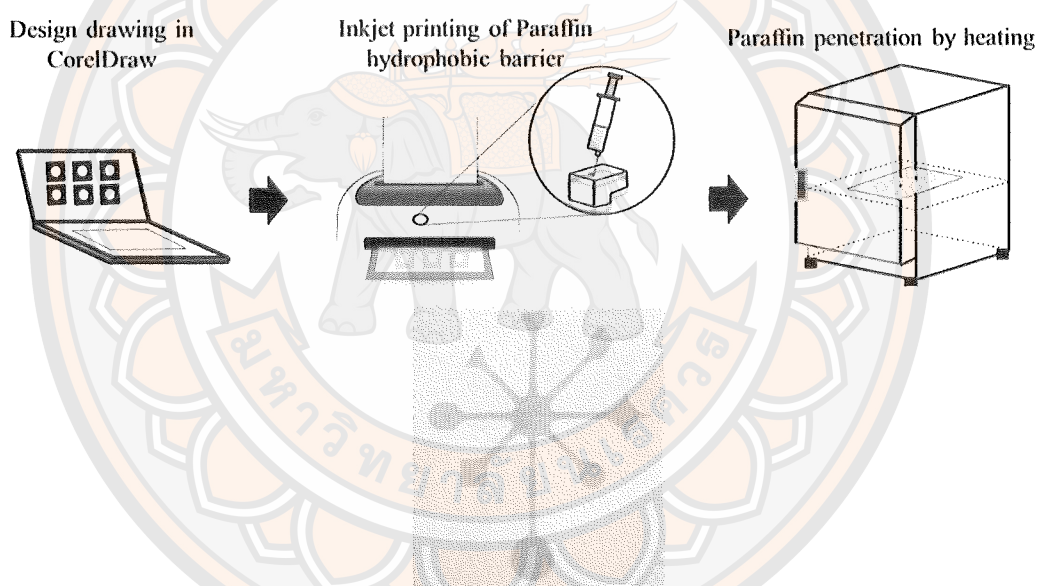


Figure 5 Fabrication process of inkjet printing and images of pattern printed (102, 109)

4. Screen printing

One of the simple fabrication methods is screen printing. Screen printing method was also used to develop hydrophobic barriers and hydrophilic channels on filter paper using hydrophobic materials such as wax (20, 110), polystyrene (77), poly(dimethylsiloxane) (111), polylactic acid (78), and polymeric ink (112) can be screen printed onto the surface of paper (Figure 6). The polymer solution is squeezed

to pass through the screen and penetrate to the bottom of the paper for creating of 3D patterned hydrophobic barrier. The patterned paper is ready to use after drying. This method has the advantages of low cost and simple fabrication steps. However, it demonstrates low resolution of microfluidic channels and rough barriers. Moreover, it is required to produce different designs. The utility of μ PADs fabricated by the screen-printing was demonstrated using colorimetric detection for glucose (112), uric acid (113), nitrite (78) etc.

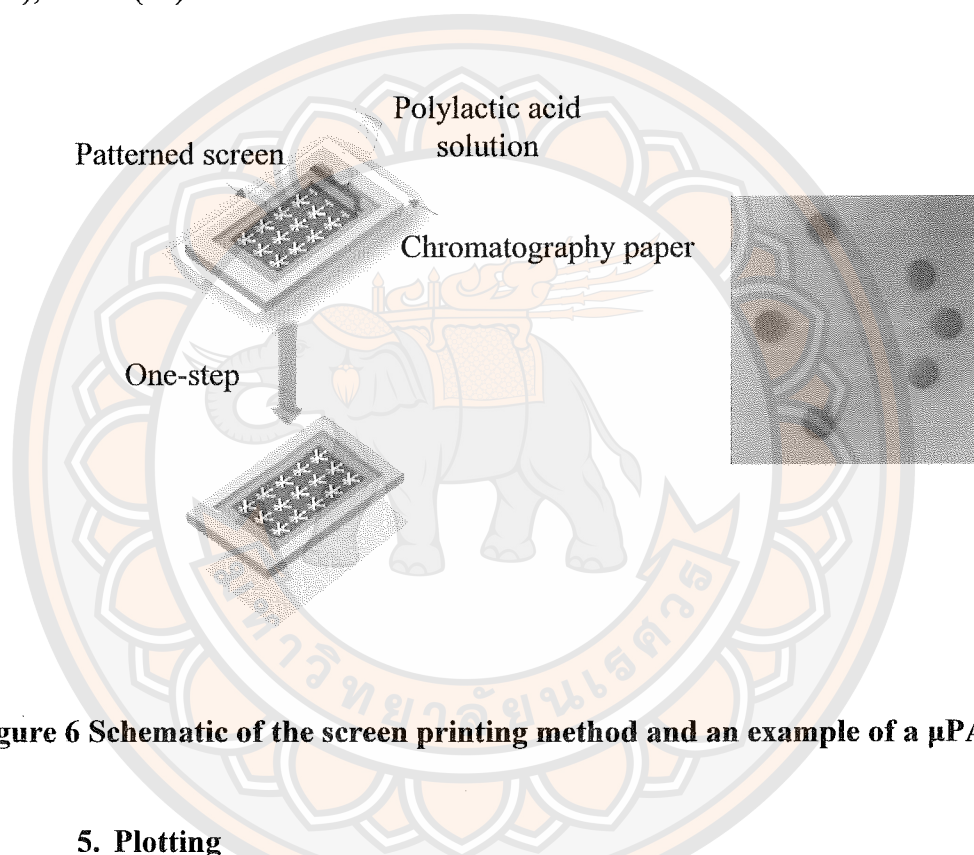


Figure 6 Schematic of the screen printing method and an example of a μ PAD (78)

5. Plotting

Generally, the μ PADs were fabricated through technical drawing pens adapted in a plotter by using difference hydrophobic materials such as permanent marker inks (114), PDMS (115). Moreover, Sousa et al. (116) used 3D pens for fabrication of μ PADs followed by a UV-curing using a portable flashlight. These pens make use of polymer filaments or liquid resins based on acrylate monomer, which are UV-curable. With the liquid polymer filaments or liquid resins, it is possible to create barriers on paper rapidly and in a variety of designs in a highly flexible manner. Considering the time required drawing and curing the hydrophobic barriers, the resulting μ PAD is obtained within 60 s (Figure 7). This method is simple, flexible,

quick and inexpensive. However, the drawbacks of plotting method are very low resolution, and required special pen and plotter. The utility of μ PADs fabricated by the plotting method was used for colorimetric detection of protein (117), glucose (118) nitrite (119) etc.

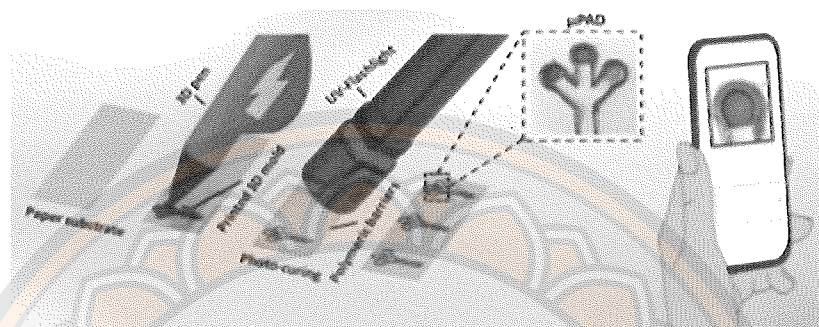


Figure 7 Scheme showing the fabrication of μ PADs through 3D pen drawing (116)

6. Stamping

The general process of stamping is prevalent in common life. Its ease and convenience have prompted of use many researchers to try and fabricate μ PADs using different types of stamps and ink. Garcia et al. have fabricated μ PADs by metal stamping, and it is schematically shown in Figure 8. A paper piece was impregnated with paraffin sheet. The metal stamp was preheated at 150°C and then brought in contact with the paraffin paper to enable the thermal transfer of the paraffin to the paper. This step enables the quick transference of the paraffin from the paraffin to paper, thus forming the hydrophobic barriers. The developed μ PADs can be used for determination of various ions such as nitrite (82), creatinine (83), glucose and uric acid (84).

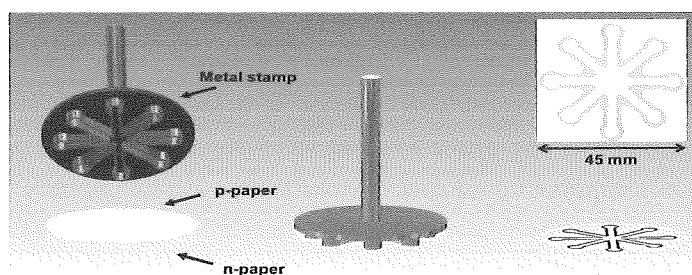


Figure 8 Steps involved in the stamping-based fabrication method (84)

7. Cutting

The fabricating methods, mentioned earlier, always use hydrophobic materials to pattern papers. However, it is equally feasible to simply cut through the paper, allowing the geometric shape of the paper to guide the liquid flow. Therefore, a myriad of cutting approaches have been developed and adopted on the basis of different cutting mechanisms and devices, including laser cutting (80, 120), plotter (121), mechanical cutting (122-123), and any combination of these techniques (124-126). All paper cutting method may have a drawback-difficult to precisely control the channel size. In addition, another limitation is that the assembly process may be only suitable for handle operation and fabricating prototype μ PADs. These advantages have enabled the use of colorimetric μ PADs for the analysis of nitrite, proteins (79), glucose (127), urine (128), and others analytes. Figure 9 shows the process of cutting method and a final μ PAD.

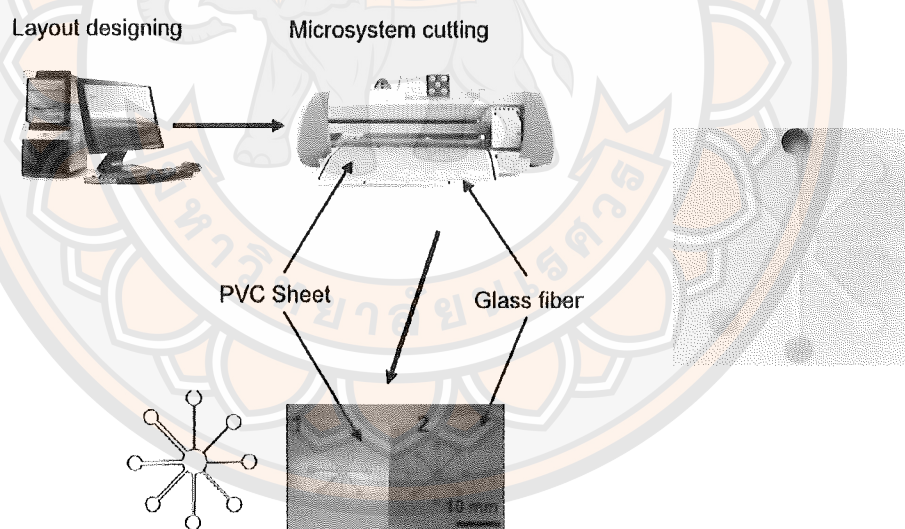


Figure 9 The process of cutting method and a final μ PAD (128)

Table 3 Hydrophobic materials used for the paper's pattern


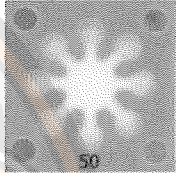
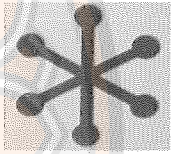

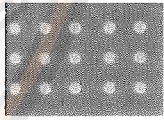
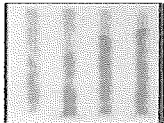
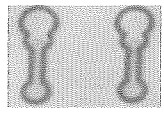
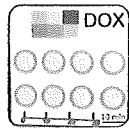
Technology	Hydrophobic material	Pattern principles	Reference
Photolithography	SU-8 photoresist	Physical blocking of pores in paper	(67-68, 129)
Wax printing	Wax	Physical deposition of reagent on fiber surface	(130)
Inkjet printing	Alkyl ketene dimer (AKD), permanent marker ink	Chemical modification of fiber surface	(21, 73, 75, 101)
Screen printing	Wax, polystyrene, poly(dimethylsiloxane)	Physical deposition of reagent on fiber surface	(77, 111)
Plotting	poly(dimethylsiloxane), chemical ink	Physical blocking of pores in paper	(131-132)
Cutting	—	—	(79, 120, 133)
Stamping	Indelible ink, poly(dimethylsiloxane)	Physical deposition of reagent on fiber surface	(84, 134)

A summary of the advantages and disadvantage of these methods is provided in Table 4, with particular attention paid to the resolution and cost of each method. Table 5 shows the summary of colorimetric detection of different ions from various samples. Given their many strong features, μ PADs are a very promising development to investigate for determination of nutrients in soil.

Table 4 Summary of the main advantages and disadvantages of different method for producing paper-based microfluidic devices (60-61, 135-136)

Technology	Advantages	Disadvantages
Photolithography	High resolution of microfluidic channels, the barrier is sharp	Requires expensive equipment, complex steps, expensive reagents
Wax printing	High resolution, high throughput method, biodegradable and biocompatible barriers.	Requires expensive wax printers, requires an extra heating step after wax deposition.
Inkjet printing	Uses very cheap AKD, can mass produce devices quickly, requires only a desktop printer to produce devices	Requires an extra heating step after AKD deposition, requires modified inkjet printers.
Screen printing	Produces devices through a simple process	Low resolution of microfluidic channels (rough barrier), requires different printing screens.
Plotting	Patterning agent (PDMS) is cheap, devices are flexible.	Very low resolution and special pen and plotter is needed
Stamping	Simple and fast production process.	Requires different iron mold for creating different patterns, Low resolution of microfluidic channels
Cutting	Sharp defined features	Requires expensive equipment.

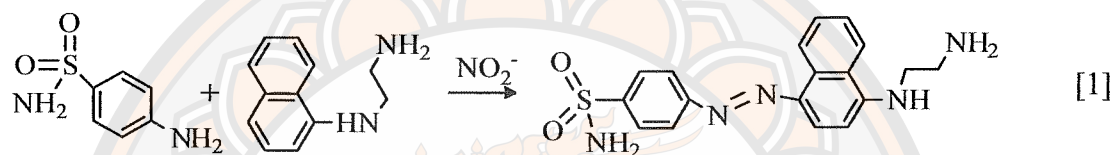
Table 5 Summary of colorimetric detection of different from various samples in μ PADs

Target analyte(s)	Fabrication (design)	Samples	Analytical figures of merit	Device image	Ref.
Glucose, lactate, and uric acid	SU-8 photoresist	Serum and urine	LR 0.5–20 mM glucose, 1–25 mM lactate, and 0.1–7 mM uric acid		(137)
Copper(II)	Wax printing	Water	LOD 4.7 nM LR 0.0079–3.1 μ M		(92)
Glucose	Laser cutting	Fruit	LOD 3.12 mM LR 5–50 mM		(138)
Lead(II)	Inkjet printing	Water	LOD 0.05 μ M LR 0.05–0.5 μ M		(63)
Procaine	Wax printing	Seized cocaine	LR 5–60 μ mol L ⁻¹ LOD 0.9 μ mol L ⁻¹		(139)
Magnesium	Screen-printing	Rubber latex waste	LR 25–200 mg L ⁻¹ LOD 25 mg L ⁻¹		(140)
Dopamine	Wax printing	Serum	LOD 0.37 μ mol L ⁻¹ LR 0.527–4.75 μ mol L ⁻¹		(141)
Doxycycline hyclate	Wax printing	Pharmaceutical	LOD 0.24 mg L ⁻¹ LR 0.5–35 mg L ⁻¹		(142)

Colorimetric detection

1. Nitrate

Griess reaction has been used frequently for the detection of nitrite. This reaction is based on diazo coupling reaction, wherein nitrite ion converts sulphanilamide into diazonium salt that subsequently coupled with naphthylethylenediamine (NED) to extract a highly colored azo dye, the color intensity of which related to the original nitrite concentration. The principle of nitrite measurement using the Griess reaction as shown in equation 1 (143).



A portable test kit for nitrate determination was reported by Murray et al. (144) who used zinc reduction in combination with the Griess assay, for the detection of nitrate in water. Zinc represents an example of a less toxic solid state reductant which can be used to reduce nitrate to nitrite. Nitration of salicylic acid by nitrate occurs under acidic conditions, and the subsequent addition of an alkaline solution results in a yellow complex. Under acidic conditions, nitrite reacts with sulfanilamide and NED, to form a pink azo compound (Figure 10). The linear range for the method was 0.5–45 mg L⁻¹ and the limit of detection (LOD) was 0.5 mg L⁻¹.

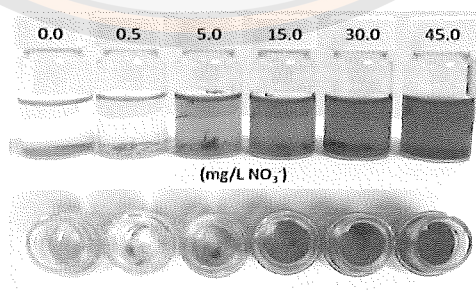


Figure 10 Colorimetric of nitrate through Griess's reaction (144)

Unfortunately, these methods require considerable amounts of reagents, and samples, as well as specialized equipment with skilled operators. The development of

a simpler and less expensive method that requires fewer reagents would be very desirable to overcome these disadvantages. The μ PADs have gained increasing interest as a simple, faster, low cost, disposable method that also requires fewer reagents. The μ PADs is a method which can be used to determine nitrite and nitrate in water, as described by Jayawardane et al. (145). The present paper reports on the development of μ PADs with identical fluidic design which employs the Griess reaction for the determination of nitrite and nitrate in environmental samples (Figure 11). One of the μ PADs is used for the determination of nitrite only, while the other one allows the determination of both nitrite and nitrate after reduction in a hydrophilic channel containing Zn microparticles. The limits of detection and quantification for nitrite are 1.0 and 7.8 μ M, respectively, while the corresponding values for nitrate are 19 and 48 μ M, respectively.

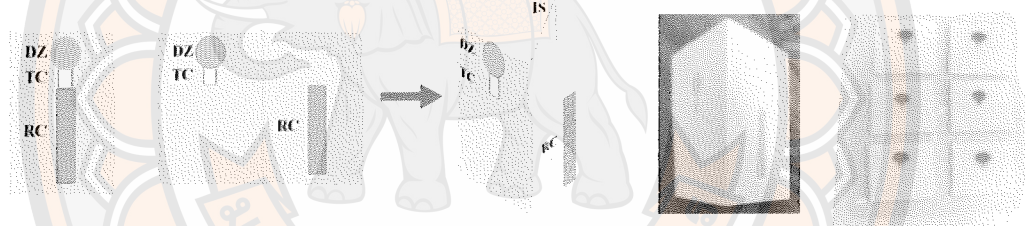


Figure 11 Schematic diagrams of the μ PADs (145)

Next, Teepoo et al. (78) reported on a one-step approach for fabricating screened-printed μ PAD using polylactic acid as a new hydrophobic material. A μ PAD was evaluated for nitrite and nitrate detection in food samples, based on the Griess method (Figure 12). Nitrate to nitrite reduction was attained with zinc followed by derivatization with sulfanilamide and N-1 naphthylethylenediamine dihydrochloride (NED), which resulted in a red-pink azo dye being formed. The detection limits and the linear ranges, respectively, were 1.2 mg L⁻¹ and 2–10 mg L⁻¹ for nitrite and 3.6 mg L⁻¹ and 10–50 mg L⁻¹ for nitrate, and the detection times for both ions were found to be within 12 min.

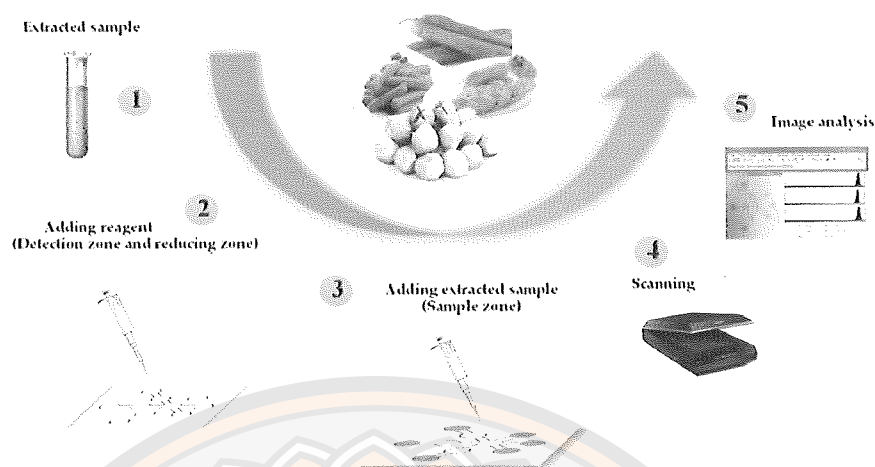


Figure 12 Schematic diagram of the detection assay for nitrite and nitrate in food samples based on colorimetric μ PAD (78)

Recently, Ferreira et al. (72) developed two μ PADs for the quantification of nitrite and nitrate anions in human saliva samples based on the Griess reaction with zinc (Figure 13). These μ PADs allowed a nitrite determination in a range of 5–250 μ M with limits of detection and quantification of 0.05 μ M and 0.17 μ M, respectively, and a nitrate determination in the range 0.2–1.2 mM with limits of detection and quantification of 0.08 mM and 0.27 mM, respectively. As for the stability, both of the μ PADs were stable when stored in vacuum at 4°C (the nitrite μ PAD for at least 60 days and the nitrate μ PAD for at least of 14 days). The idea was for these μ PADs to ultimately be capable of being used as a screening option not only in healthcare facilities, but also to aid in the diagnosis of some diseases and health conditions in remote locations.

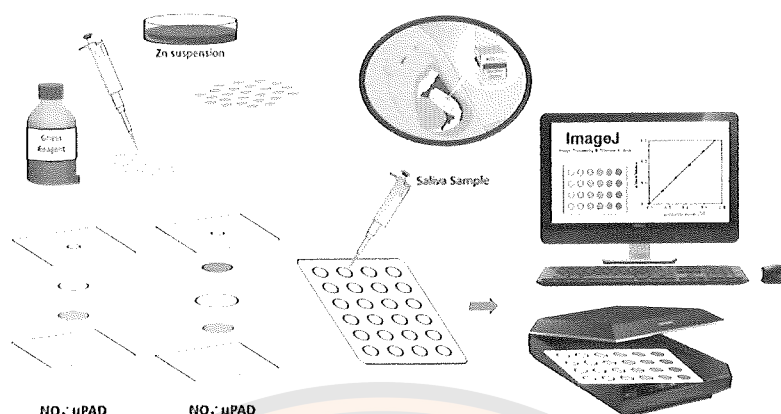
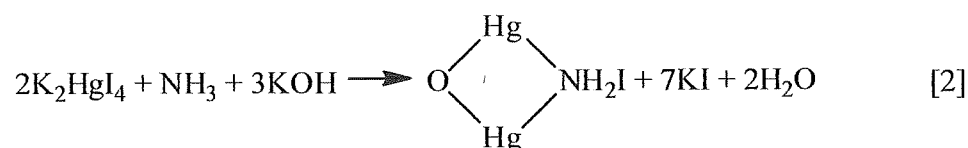


Figure 13 Schematic assembly of the mixed μ PAD for determination of nitrite and nitrate (72)

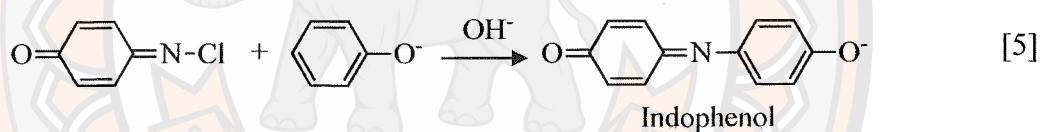
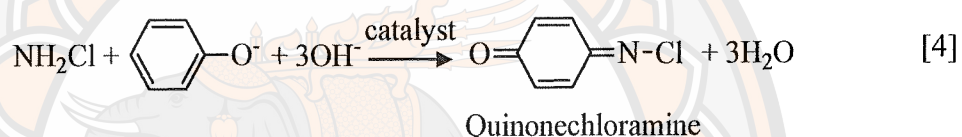
2. Ammonium

Ammonium is usually quantified by spectrophotometric methods. Two reactions of measuring ammonium concentration are used in agriculture and the environment which include standard laboratory colorimeter procedures using Nessler (146-148) and Berthelot reaction (phenol and salicylate methods) (149-151). Nessler's reagent is a solution consisting of mercury (II) iodide and potassium iodide. It is a standard method for the determination of ammonia nitrogen in water. The advantages of this method are easy operation and high sensitivity towards ammonia. It can be observed, that the Nessler reagent (K_2HgI_4) reacts with the ammonia present in the sample under highly alkaline conditions to produce a yellow-brown color complex when assessed colorimetrically (147, 149). The color intensity is in direct proportion to the ammonia concentration. The basic reaction is:



The indophenol bule method is based on the Bethelot reaction in which ammonia reacts with phenol and hypochlorite under alkaline condition. Ammonia is converted to monochloramine at pH 9.7–11.5, which reacts with phenol in the

presence of hydrochlorine, to form blue-colored indophenol under the catalytic influence of a nitroprusside salt (152). Each experimental procedure is easy, rapid, and simple. Afkhami and Norooz-Asl (153) proposed a method for the spectrophotometric determination of ammonia that was based on the color reactions of ammonia with phenol under suitable oxidizing conditions in an alkaline medium, and cloud point extraction of produced indophenol dye. Linearity was obeyed in the range of 2–125 ng mL⁻¹ of ammonia. The detection limit of this method was 1.0 ng mL⁻¹ of ammonia. The reactions of indophenol blue are highlighted in equations 3, 4 and 5.



However, these standard methods require expensive laboratory instruments, which are difficult to be employed in the field, time consuming, and use large amounts of chemicals. Therefore, it is necessary to develop a new method to overcome the disadvantages. μ PADs is a renewable method in research technology, which are disposable, fast and easy to use for sample monitoring, and field analysis.

Given their many strong features, μ PADs are a very promising development for determining the amount of ammonium in the environment. Up to this time, many researches have applied μ PADs for the determination of ammonium. Jayawadance et al. (106) were the first to demonstrate the use of μ PAD for determination of ammonia in wastewater based on gas-diffusion separation (Figure 14). The determination of ammonia in the proposed gas-diffusion μ PAD involves mixing an ammonia sample or standard with excess solid NaOH deposited in a hydrophilic reagent zone, to produce molecular ammonia which then diffuses across a polytetrafluoroethylene (PTFE) hydrophobic microporous membrane into a detection

zone containing an acid–base indicator solution (3-nitrophenol or bromothymol blue). Under optimal conditions, the μ PAD is characterized by a limit of detection of 0.8 and 1.8 mg L⁻¹ and repeatability of 3.1 and 3.7% (20 mg L⁻¹), expressed as relative standard deviation, in the case of 3-nitrophenol or bromothymol blue, respectively.

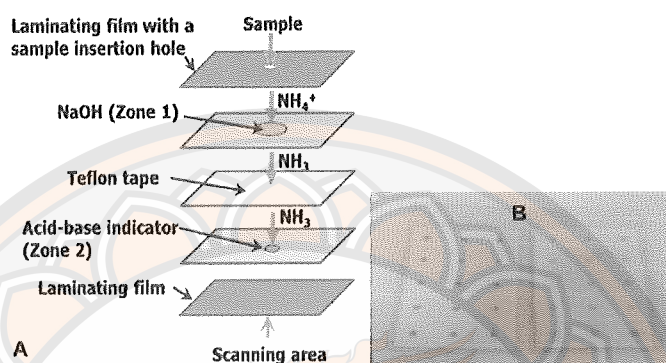


Figure 14 Schematic diagram of the colorimetric ammonium assay by 3-nitrophenol or bromothymol blue: A) Proposed gas diffusion μ PAD; B) Photograph of a bromothymol blue μ PAD and a 3-nitrophenol μ PAD (106)

The second method for determining ammonia was Nessler reagent, which was introduced by Phansi et al. (154). A new concept of gas–liquid separation in μ PAD format that can be employed for direct analysis without pretreatment of the sample (membraneless gas-separation microfluidic paper-based analytical devices, MBL-GS μ PADs) as show in Figure 15. MBL-GS μ PADs offer direct quantitative analysis of volatile and nonvolatile compounds. The detection limit of this method was 3.14 mg L⁻¹ of ammonia. The observed linear range for Nessler reagent is 10–100 mg L⁻¹.

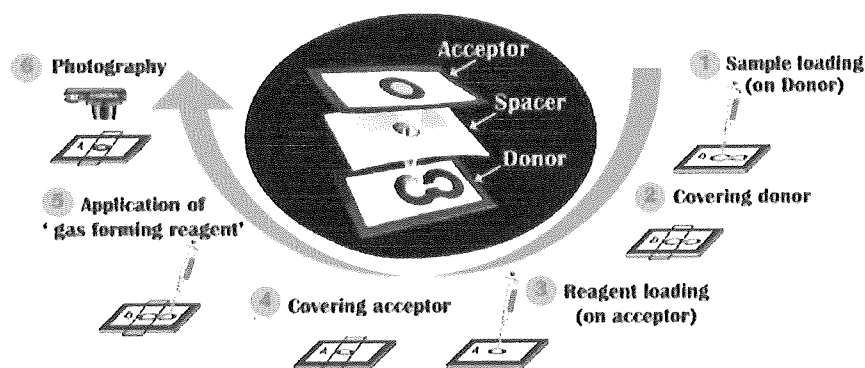


Figure 15 Schematic diagram of the colorimetric ammonium assay by Nessler Reagent (154)

The modified Berthelot's reaction is a method which can be used to determine ammonia, as described by Cho et al. (155). This is a new method for quantifying ammonia in water samples by means of the evaporation of dissolved ammonia into headspace, followed by selective detection using a colorimetric sensor. Gaseous ammonia detection is attained by the selective formation of blue indophenol dye through the modified Berthelot's reaction on porous paper. The colorimetric response of the low-cost paper sensors were saturated within 10 min, and color change was observed by the naked eye for an ammonia solution of 10 mg L^{-1} . These cheap NH_3 paper sensors demonstrated a good colorimetric response to ammonia samples in the concentration range of $10\text{--}1020 \text{ mg L}^{-1}$ (Figure 16).

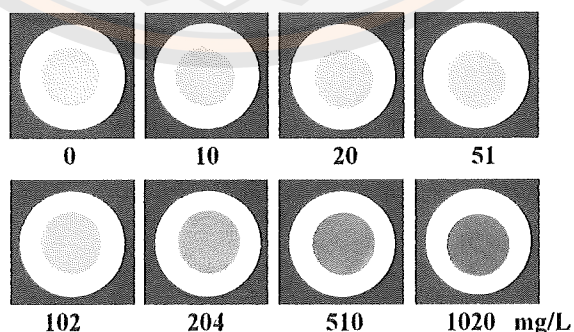


Figure 16 Optical images of the ammonia sensor at different concentrations (155)

3. Phosphate

The method most commonly used for the colorimetric analysis of phosphate is the molybdenum blue. In this method, ammonium molybdate and antimony potassium tartrate react in an acidic medium with dilute solution of orthophosphate to form an intensity colored of antimony-phosphomolybdate complex. The complex is reduced to an intensity blue colored complex by ascorbic, stannous chloride, or hydrazine. The chemical reactions are shown in equation 6 and 7 (156).



The colorimetric analyzer for detection of phosphorus in form of solutions as reported by Moonrungssee et al. (157), who studied the molybdenum blue method, and developed a new colorimetric analyzer application for use with a smartphone, that could be used for the determination of the available phosphorus content in the soil. The calibration graph was created by measuring the blue intensity of a series of standard phosphorus solutions (0–1.0 mg L⁻¹), and the results obtained from this method agreed well with the spectrophotometric method, with a detection limit (LOD) of 0.01 mg L⁻¹. The developed method provided good accuracy (RE < 5%), precision (RSD < 2%, intra and inter-day), fast and cheap analysis, and was especially suitable for analysing the soil in the crop fields for phosphorus nutrient. Although these methods provide low LOD, they are sophisticated, large amount of chemicals, and high-cost. Thus, there is a clear need for a simple, rapid, highly sensitive and selective method for phosphate detection.

μPADs is one of easy to use method, rapidly implemented, inexpensive, and portable, there has been considerable interest of late in using such methods for environmental analysis. Jayawardane et al. (23) also developed a simple PADs for the determination of reactive phosphate in natural and soil waters based on the formation of phosphomolybdenum blue (Figure 17). The molybdate/potassium antimony(III)-tartrate reagent and ascorbic acid reductant merged together from adjacent hydrophilic zones after spotting the liquid sample onto the paper. The color intensity of the phosphoantimonyl molybdenumblue complex was measured using

a flatbed scanner. Under optimal conditions, the PAD is characterized by a working range of $0.2\text{--}10\text{ mg L}^{-1}$, with limits of detection and quantitation of 0.05 and 0.16 mg L^{-1} .

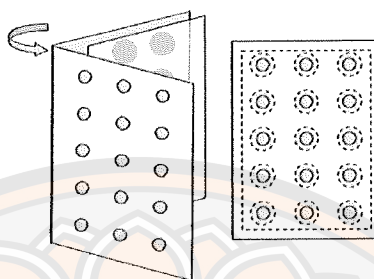


Figure 17 PAD for the determination of phosphorus (23)

Recently, Deng et al. (158) designed a microfluidic paper-based phosphorus detection chip (μ PPC) for the determination of phosphate, as shows in Figure 18. The SU-8 photoresist was used for the fabrication of the μ PPC. In the colorimetric detection, orthophosphate can react with ammonium molybdate and potassium antimony tartrate to form phosphomolybdic acid, which can be reduced by ascorbic acid to form the molybdenum blue complex. The limit of detection was $0.86\text{ }\mu\text{g mL}^{-1}$ for orthophosphate. The μ PPC is a rapid and low-cost orthophosphate detective platform.

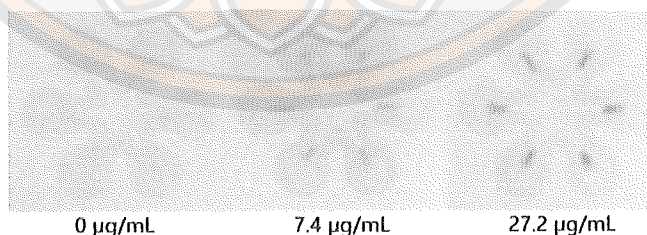


Figure 18 μ PPC for the determination of phosphate (158)

Pinyorosphatum et al. proposed the colorimetric sensor for the detection of phosphate ions performed on paper-based analytical devices (PADs) based on the anti-aggregation of 2-mercaptoethanesulfonate (MS)-modified silver nanoplates (Figure 19). This method can detect phosphate in the range of $1\text{--}30\text{ mg L}^{-1}$, with a detection limit of

0.33 mg L^{-1} and a limit of quantification equal to 1.01 mg L^{-1} . Finally, this method was applied in real samples and showed satisfactory results that agreed with those of the conventional method. This method was performed on PADs for the first time, which comprised the advantages of simple, rapid, and inexpensive instrumentation.

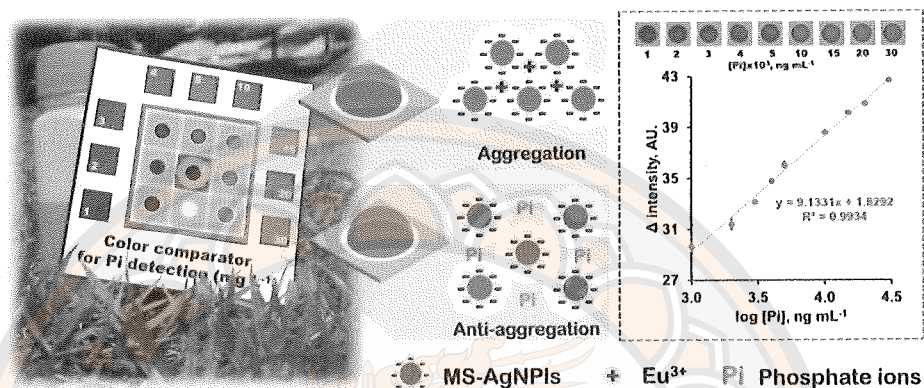
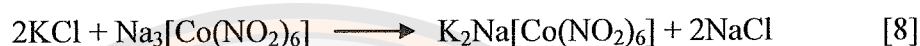


Figure 19 Colorimetric sensor for the detection of phosphate performed on paper-based analytical devices (PADs) based on the anti-aggregation of 2-mercaptoethanesulfonate (MS)-modified silver nanoplates (159)

4. Potassium

A method for the estimation of potassium depends on precipitation as cobaltinitrite (equation 8), and subsequent estimation of one of the constituents of the precipitate. Jacobs (160) described the formation of a green compound from cobalt, choline, and sodium ferrocyanide, gives a method for the colorimetric estimation of cobalt, which may be extended to the estimation of potassium in biological fluids, after precipitation as potassium cobaltinitrite. Moreover, Looney et al. (161) modified the silver cobaltinitrite method for the determination of potassium by the use of sulfanilamide and NED. The reaction is based on the formation of an azo compound by the nitrite radicals of cobaltinitrite. Abdul (162) also reported a method for the estimation of potassium in sera and biological fluids. The method depends on the precipitation of potassium as cobaltinitrite, and the colorimetric estimation of the cobalt in the latter by the reduction of the Folin-Ciocalteu phenol reagent, which gives a stable blue color. The colorimetric method for the determination of potassium in soil

was also studied by Whittles et al. (163). The determination of potassium precipitated involves the diazotization of sulphanilic acid, using the nitrite groups, of the cobaltinitrite precipitate, and subsequent coupling with dimethylaniline to give methyl orange. However, the basic disadvantage of precipitation methods is the production of a large amount of sludge that poses handling and disposal problems, insensitive, and longtime reaction.



In order to overcome some disadvantages of chemical precipitation and to increase the efficiency of the detection method, the colorimetric detection in form of solution was interested. Song et al. (164) reported a colorimetric potassium sensor (KS7) in which a hemicyanine dye was used as a fluorophore and phenylaza-18-crown-6 lariat ether (ACLE) was utilized as a potassium ligand (Figure 20). This sensor exhibited a linear response range to potassium from 1 to 200 mM, indicating its wide detection range for cellular, urinary, and environmental potassium.

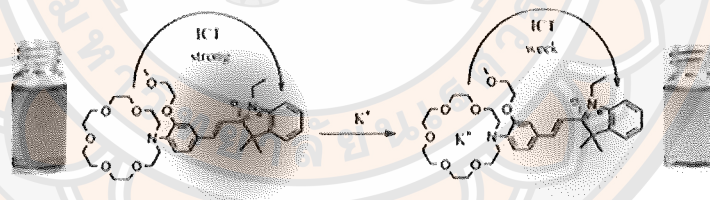


Figure 20 Colorimetric detection of potassium (164)

Next, Qiu et al. (165) developed a detection method for K^+ by using crown-ether-modified Au NPs (Figure 21). The amino group on the crown ether (4-aminobenzo-18-crown-6, ABC) can be modified onto the surface of gold nanoparticle through gold nitrogen bonds. The pore diameter of the crown ether matches with the diameter of K^+ very well, and the sandwich structure between ABC and K^+ can be formed. The detection method is not only simple and convenient to operate, but also has excellent selectivity. It takes only 20 min to achieve on-site inspection. There is a good linear relationship ($R^2=0.9979$) in the range of 0–200 μM

K^+ concentration and this detection method can be successfully applied in the detection of K^+ in real urine samples. However, these methods require expensive instrument and high skilled operators.

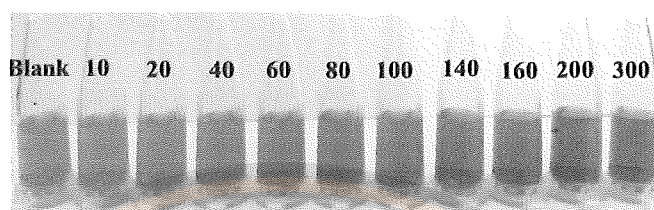


Figure 21 The photograph of Au NPs with different concentrations of potassium (165)

μ PAD has gained recent interest as an analytical platform due to several advantages such as low cost, easy to fabricate, low reagent consumption, without requirement of high skilled operators. The feasibility of the use of lipophilic phase containing potassium ionophore I (valinomycin) as a reagent in the quantitative determination of potassium has been reported from Gerold, Bakker, & Henry (166). In this reach, μ PADs capable of potassium quantification in aqueous samples. The channels are a distinctive blue and change to a reddish-purple color upon the addition of samples containing potassium. The color transition from the region exposed to potassium (reddish-purple) to the region where potassium is no longer present (blue) due to consumption by the lipophilic phase is sharp and easily identified by eye (Figure 22).

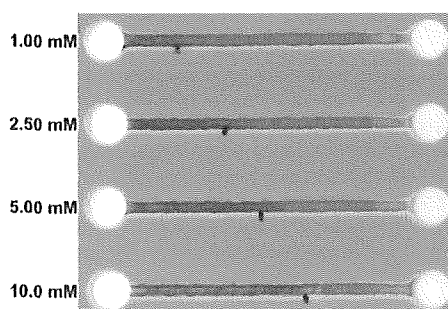


Figure 22 Quantification of potassium using a distance-based μ PAD (166)

CHAPTER III

FABRICATION OF ENVIRONMENTAL FRIENDLY MICROFLUIDIC PAPER-BASED ANALYTICAL DEVICES FOR THE DETERMINATION OF NITRATE

Introduction

Nitrate (NO_3^-) is a critical nitrogen source for plant growth. It is one of the most important compounds in soil fertility, and its measurement in soil materials has received much attention (167). Nitrate is assailable by plants and serve as a basis for the nitrogenous diet of many cultivated plants (168), and can also be assimilated by soil microorganisms in competition with plants. Sources of soil nitrate include decomposing plant residues and animal manure/compost, chemical fertilizers, exudates from living plants, and rainfall. In well-drained soil ammonium (NH_4^+) and ammonia (NH_3) are converted into nitrate by very specific populations of aerobic bacteria, which is known as nitrification. Nitrate is very soluble in water and can be easily transported by runoff and other surface and subsurface flows to rivers and lakes or moved downwards to ground water (169). The amount of nitrate required in the soil for crops should not fall below 10 mg kg^{-1} and should not exceed 40 mg kg^{-1} (170).

The determination of the nitrate that exists in the soil profile and in the plow layer, is critical for regulating the required amounts of nitrogen fertilizer. The goal is to avoid excess application of nitrogen, because it can reduce the levels of nitrate and enter aquifers, as well as negatively affecting crop yield and quality (171). Nitrate is usually quantified by spectrophotometric methods (46, 167, 172) that normally requires time-consuming laboratory procedures using advance instruments, and large quantities of chemicals which are expensive and inconvenient for field work. The development of simpler and less expensive methods to overcome these disadvantages would be very desirable.

Microfluidic paper-based analytical devices (μ PADs) have gained increasing interest as simple, low cost, disposable, and portable analytical tools. The μ PADs are devices developed with a cellulose paper on which hydrophobic barriers are constructed,

creating hydrophilic channels (19-21). Several methods have been used for μ PAD fabrication including photolithography (67, 129), wax printing (19, 69, 71), plasma treatment (173), cutting (79-80), and inkjet printing (174). While these methods provide good precision and reproducibility, they are associated with some drawbacks such as complicated processes and expensive equipment. In addition, a variety of one step fabrication methods have been reported such as plotting using a permanent marker and a metal template (117) contact stamping using indelible ink (134), and writing using a wax pen (175). Although these methods have shown their potential in rapid fabrication, they are less practical for mass production. Wax screen-printing is an alternative method that is simple, inexpensive, and quick because it requires only a screen, wax, and a hot plate (20, 110, 176). One limitation of this method is that it normally utilizes solid paraffin wax rubbed through a mesh screen, which makes it difficult to achieve an even layer on the paper underneath the screen. To overcome this limitation of solid paraffin, this study was conducted to seek an alternative wax material that can be used to consistently fabricate μ PAD repetitively in large quantities with reasonable precision and be more environmentally friendly. Ultimately, beeswax was used as a new hydrophobic material for the fabrication of μ PAD using screen-printing method. This beeswax μ PAD is proposed for green chemical analysis as it uses a natural material and does not require any organic solvent.

The present work developed a method using beeswax to screen print patterns onto paper and fabricated a new μ PAD for determination of nitrate in soil. Beeswax screen printing method is a comparatively quick procedure that results in high resolution, with good repeatability. The μ PAD measures the nitrate content using VCl_3 as a reductant for reducing nitrate to nitrite. The reduced nitrate plus the nitrite originally present in the sample reacts with the Griess reagent (sulfanilamide and NED) under acidic condition. Then by measuring the color intensity of the result using ImageJ software, the concentrations of nitrate can be ascertained. The effectiveness and reliability of the new μ PAD for detection of nitrate was tested and confirmed using a variety of soil samples. This developed device for colorimetric detection of nitrate is easy to use, quick, inexpensive, and environmentally friendly.

Experimental

1. Chemicals

All chemicals used in this study were analytical grade or better, and deionized water (DI water) was used for the preparation of all solutions in the experiments. Potassium nitrate and potassium chloride were purchased from Ajax (Finechem, Australia). Sulfanilamide and N-(1-Naphthyl)ethylenediamine dihydrochloride (NED) were purchased from PanReac AppliChem (Darmstadt, Germany). Hydrochloric acid was purchased from RCI Labscan Ltd. (Bangkok, Thailand). Vanadium (III) chloride was purchased from Merck (Darmstadt, Germany). Cetyltrimethyl ammonium bromide (CTAB) was purchased from LOBA Chemie (Mumbai, India). Beeswax from Germany was purchased from Chemipan (Bangkok, Thailand).

2. Apparatus

Whatman Grade 1 and Grade 5 qualitative filter paper were purchased from Whatman International, Ltd. (Buckinghamshire, UK). The stencil screen, made with polyester fabric on a wooden frame (35 cm x 45 cm) was custom ordered from a local screen-printing shop (Phitsanulok, Thailand). An HP 2135 scanner was used for colorimetric analysis. An OCA20 contact-angle measuring instrument (DataPhysics Instrument GmbH, Germany) was used for contact angle measurement. A shaking water bath (Daihan Scientific, Korea) was used to extract of nitrate from soil. A synergy H1 hybrid multi-mode microplate reader (BioTex, Vermont, USA) was used for the reference spectrophotometric method.

3. Preparation of solutions

3.1 Nitrate stock solution (1000 mg L⁻¹)

The nitrate stock solution was prepared by dissolving 0.7221 g of potassium nitrate to 100 mL using DI water in a volumetric flask.

3.2 Nitrate standard solution (0.5–40 mg L⁻¹)

The nitrate standard solutions with concentration of 0.5, 2.5, 5, 10, 20, 30, and 40 mg L⁻¹ were prepared by added 0.5, 2.5, 5, 10, 20, 30, and 40 mL of 100 mg L⁻¹ nitrate stock solution to 100 mL volumetric flask and adjusted to the volume with DI water, respectively.

3.3 Reagent

Sulfanilic acid solution of 1% w/v was prepared by dissolving sulfanilamide in 2 mol L⁻¹ hydrochloric acid. NED solution of 0.1% w/v was prepared by dissolving 0.1 g of NED in 100 mL of DI water. The reducing reagent of 3% w/v was prepared by dissolving 3.0 g of VCl₃ in 100 mL of 6 mol L⁻¹ hydrochloric acid. It took about 1 h for the solid to be fully dissolved with agitation. The reagent for nitrate detection was prepared by mixing sulfanilic acid solution, NED solution, and VCl₃ in equal volumes (1:1:1 ratio).

3.4 Potassium chloride solution (2 mol L⁻¹)

A 2 mol L⁻¹ potassium chloride solution was prepared by dissolving 74.55 g of potassium chloride to 500 mL using DI water in a volumetric flask.

4. Optimization of the beeswax screen-printing method

The screen-printing method was used to transfer beeswax onto filter paper, thereby creating hydrophobic barriers and hydrophilic analysis zones for the μ PADs. The fabrication of microfluidic paper-based devices has various factors which can affect the efficiency of them. These factors are the CTAB concentration, melting temperature and time, hydrophobicity tests, resolution and reproducibility, and chemical compatibility tests. Therefore, the influences of these variables were verified by the experiment.

4.1 Optimization of CTAB concentration on beeswax emulsion

40 mL portion of 0.1, 0.5, 1, 5, 10, and 15 g L⁻¹ CTAB solution was added to 10.0 g of melted beeswax in an Erlenmeyer flask. The mixture was heated and stirred for 5 min on a hot plate stirrer at 90°C. Then the mixture was thoroughly homogenized at a speed of 21,000 rpm for 2 min using a homogenizer, and the hot wax emulsion was quickly cooled to room temperature in an ice bath. This emulsification process was adapted from that of Zhang, Lu (177).

4.2 Optimization of melting temperature and time on wax diffusion

The screen patterns were designed using Silhouette Studio software (version 4, Silhouette America, Lindon, Utah, USA). The beeswax emulsion is first screen-printed onto the filter paper surface, and the printed paper is then heated in oven (varied at 60, 80, and 100°C), whereas the time on wax diffusion were 1, 2, 5, 10, 15, and 20 min in order to cause the wax to melt and penetrate downward completely

to the bottom of the filter paper. The beeswax emulsion thus forms hydrophobic barriers that delimit the hydrophilic sample zone, reaction zones, and channels. Figure 23 provides an overview of the μ PAD fabrication.

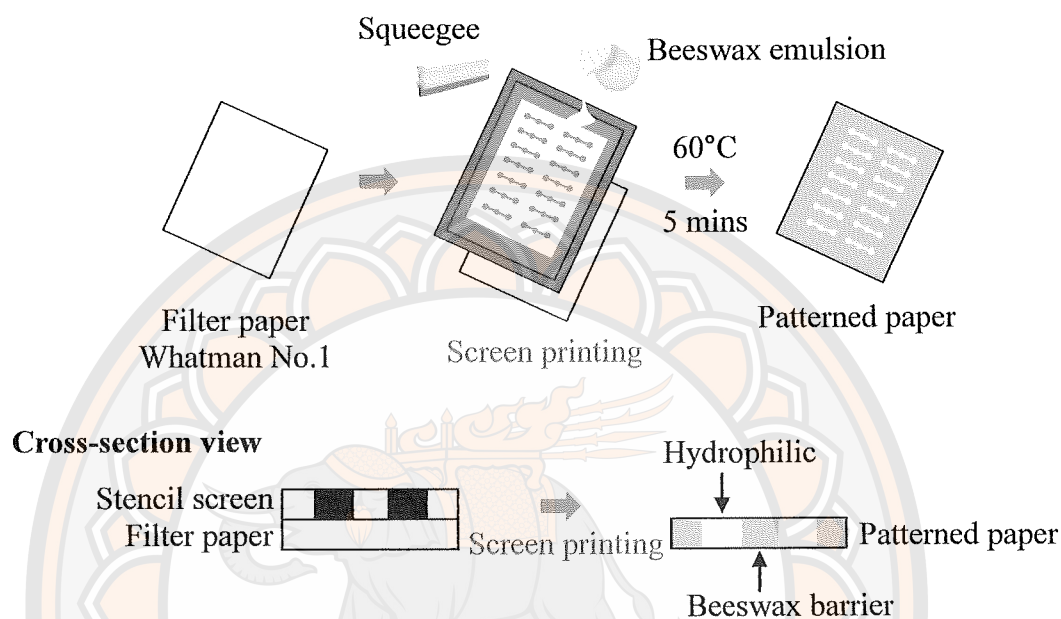


Figure 23 A schematic diagram showing fabrication process of the μ PAD with beeswax using the screen-printing method

4.3 Optimization of hydrophobicity test

The experiment was carried out according to the procedure described in section 4.2 under optimum conditions. After producing the μ PADs, the contact angle of the water on the hydrophobic surface was measured to examine the hydrophobicity of the barrier, and then a drop of blue dye solution was applied to the hydrophilic zone of the plain filter paper. A microscope was also used to examine the border between the hydrophobic and hydrophilic zones, and the application of the blue dye. Examples of other various patterns which could be used for different chemical reactions were also studied.

4.4 Optimization of resolution, and reproducibility

The experiment was carried out according to the procedure described in section 4.2 under optimum conditions. To evaluate the resolution between the hydrophobic and the hydrophilic areas of the fabrication of the hydrophilic channels, a shape mould composed of a 5 mm sample zone, and 0.2, 0.4, 0.6, 0.8, 1, 1.5, 2 mm hydrophilic channel (length 10 cm) detection zones were fabricated. A 10 μL of blue dye solution was applied to the hydrophilic zone (5 mm circular inlet) of the filter paper and stand for 5 minutes. The resolution was evaluated by conducting flow tests of a blue dye solution in each hydrophilic channel.

To evaluate the reproducibility of the fabrication of the hydrophilic channels, 24 pieces of paper with a shape mold composed of a 5 mm sample zone, 6 mm detection zones and a 2 mm hydrophilic channel were fabricated. Pictures of the paper devices were scanned and used to measure the widths of the hydrophilic channel by using ImageJ.

4.5 Chemical compatibility test

The experiment was then carried out according to the procedure as described in a section 4.2 under optimum conditions. To evaluate the beeswax barrier's compatibility with various sorts of reagents, 5 μL of aqueous solutions containing surfactants (1% w/v of Triton X-100, CTAB, and SLS), organic solvents (methanol, ethanol, toluene, hexane, and heptane), salts (2 mol L^{-1} ammonium chloride and ammonium sulphate), acids (2 mol L^{-1} sulfuric, nitric and hydrochloric acids) and a base (2 mol L^{-1} sodium hydroxide, potassium hydroxide, and ammonium hydroxide), were added to the hydrophilic zone, then a drop of blue dye solution was applied to the hydrophilic zone of the filter paper.

5. Optimization of the Griess reaction on μPAD

The objective of this part of the work is to investigate the effect of the variables that impose on the Griess reaction involving in nitrate determination. The concentration of color development reagent (sulfanilic acid, NED, and VCl_3), and the reaction time were optimized to provide the highest values of color intensity.

5.1 Concentration of sulfanilic acid

The first step is the addition of 2 μL of reagent containing sulfanilic acid (varied at 0.05, 0.1, 0.5, 1.0, 1.5, and 2.0% w/v), 0.2% w/v NED, and 2% w/v VCl_3 to the detection zones. The reagents take approximately 5 minutes to dry at room temperature. After that, 20 μL of 40 mg L^{-1} nitrate standard solution was added in the sample zone, and wait for 10 minutes ($n=6$). The resulting colors are digitalized with a scanner, quantified with ImageJ software in RGB mode (Figure 24).

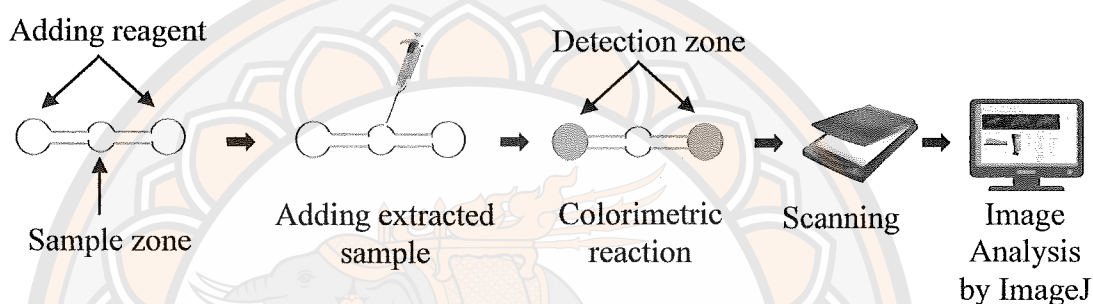


Figure 24 Schematic diagram of the nitrate assay using the colorimetric μPAD

5.2 Concentration of NED

The experiment was carried out according to the procedure as described in a section 5.1, except the concentration of reagents was changed as follow: The concentrations of NED were 0.05, 0.1, 0.2, 0.3, and 0.4% w/v. The sulfanilic acid and VCl_3 were set at 1% w/v and 2% w/v, respectively.

5.3 Concentration of VCl_3

The experiment was carried out according to the procedure as described in a section 5.1, except the concentration of reagents was changed as follow: The concentrations of VCl_3 were 0.1, 0.2, 0.5, 1, 2, 3, and 4% w/v. The sulfanilic acid and NED were set at 1% w/v and 0.1% w/v, respectively.

5.4 Reaction time

The experiment was carried out according to the procedure as described in a section 5.1, with the reaction times of 2, 4, 6, 8, 10, 15, 20, 30, and 40 minutes. The sulfanilic acid, NED, and VCl_3 were set at 1 % w/v, 0.1 % w/v, and 3% w/v, respectively.

6. Interference

A 4 mL of 100 mg L⁻¹ nitrate standard solution and 2 mL of 1000 mg L⁻¹ NaCl, KCl, CaCl₂, and K₂SO₄ stock solution were added into each 10 mL volumetric flask, and adjusted to 10 mL with DI water. After that, the experiment was carried out according to the procedure as described in a section 5 under optimum conditions (n=6).

7. Analytical Method Validation

Validation of the proposed VCl₃ combined with detection by the Griess reaction for nitrate determination in soil samples is performed. The validation parameters included linearity, limit of detection (LOD), limit of quantitation (LOQ), precision, and accuracy of the proposed method were evaluated under a selected condition.

7.1 Linearity

The experiment was carried out according to the procedure as described in a section 5 under optimum conditions (n=3), by using nitrate standard solution in the concentrations of 0.5, 2.5, 5, 10, 20, 30, and 40 mg L⁻¹. A graph plotted between color intensity and concentration of nitrate was constructed to find the linearity.

7.2 LOD and LOQ

The experiment was carried out according to the procedure as described in a section 5 under optimum conditions. The DI water was analyzed by the VCl₃ combined with detection by the Griess reaction in 10 replicates. The SD of the response and the slopes of the concentration of the calibration curves were used to estimate the LOD (3σ/slope) and LOQ (10σ/slope).

7.3 Precision

Evaluation of method repeatability (intraday precision) and reproducibility (interday precision) were performed. The nitrate standard solutions at three different concentrations (2.5, 10, and 40 mg L⁻¹) were analyzed using procedure with optimum conditions in section 5. Intraday precision was determined from six replications within 1 day, and the interday precision was analyzed in six replications on 5 days.

7.4 Accuracy and Recovery

Accuracy was evaluated across the specified range of the analytical procedure by a recovery study. The standard solution of the nitrate was spiked into the soil samples extract in triplicate. The recovery was determined as follows: (total nitrate amount – original nitrate amount in real sample)/nitrate amount of added.

8. Optimization of the stability of the μ PAD

The first step is the addition of 2 μ L of reagent containing 1% w/v sulfanilic acid, 0.1% w/v NED, and 3% w/v VCl_3 to the detection zones of the μ PAD, which take approximately 60 minutes to dry at room temperature. Then, the μ PAD was placed in a plastic bag and vacuum sealed, and stored in a dark ziplock bag in a refrigerator at $\leq 2^\circ\text{C}$. To evaluate the stability of the μ PAD, the 6 pieces of μ PADs were tested by determination the concentration of 40 mg L^{-1} nitrate standard solution every 10 days of storage over 120 days.

9. Application in real samples

The μ PAD was applied to the determination nitrate in soil. Seven soil samples were collected from rice fields in five provinces of Thailand: Phitsanulok, Sukhothai, Khamphaeng Phet, Sa Kaeo, and Ubon Ratchathani. All samples were dried in the open-air to remove the moisture, and then sieved to a particle size of 2 mm.

To validate the accuracy of the proposed method, 5.0 g of the soil sample was added in 7 centrifuge tubes. Then, 6 of the 7 sampled were spiked with 0.125, 0.625, 1.25, 2.50, 5.00, 7.50, and 10.00 mL of 100 mg L^{-1} nitrate standard solution to achieve concentrations of 0.5, 2.5, 5, 10, 20, 30, and 40 mg L^{-1} , respectively. After that, the soil samples were mixed with 25 mL of 2 mol L^{-1} potassium chloride and shaken for 15 min. The mixture was filtered through a filter paper (Whatman#5). The filtrate was then carried out according to the procedure as described in a section 5 under optimum conditions. The results from the μ PADs were compared to spectrophotometry.

10. Spectrophotometric method

The volume of 0.5 mL of filtrate (from section 9) was added into a microcentrifuge tube, then added 0.5 mL of Griess reagent. The solution was shaken, and then allowed to stand for 10 min to ensure complete color development. The absorbance was measured with a spectrophotometry at 540 nm.

Results and discussion

1. The μ PAD fabrication using beeswax screen printing method

1.1 Effect of CTAB concentration on beeswax emulsion

In order to enable the beeswax to pass through the stencil screen, the cationic surfactant CTAB is used to prepare an emulsion of beeswax and water. Changing the concentration of the emulsifying agent, CTAB, affects the viscosity of the emulsion and its behavior as a liquid (178). Therefore, six different concentrations of CTAB (0.1, 0.5, 1, 5, 10, and 15 g L⁻¹) were examined to determine which concentration produced the most effective beeswax emulsion. The appearance of the emulsions from the six investigated CTAB concentrations is shown in Figure 25, and the viscosity and density values of these emulsions are shown in Table 6. Phase separation was obvious after 30 min when the CTAB concentration was 0.1, 0.5, and 1 g L⁻¹ indicating that the emulsification was insufficient. Properly formed emulsion was obtained when the CTAB concentration was 5 g L⁻¹ and above, which is evident from the large increase of viscosity at CTAB concentrations of 5 g L⁻¹ and above. After emulsification was complete, a slight increase of viscosity and density of emulsion were observed for CTAB concentrations of 5, 10, and 15 g L⁻¹, which is due to lowering of water content. However, the CTAB concentration of 5 g L⁻¹ produced too low viscosity for screen-printing method, causing wax to spread horizontally outside of the target area. A practical and dependable beeswax emulsion was obtained when the CTAB concentration reached 10 g L⁻¹. This emulsion passed smoothly through the stencil screen as desired. The highest trialed CTAB concentration of 15 g L⁻¹ produced excessive viscosity, and this emulsion could not pass properly through the stencil screen. So, 10 g L⁻¹ was determined as the optimal CTAB concentration to produce the best beeswax emulsion, without phase separation or stickiness. The shelf life of the prepared emulsion for screen-printing on to the filter paper was determined and it was found that the beeswax emulsion kept acceptable quality for 3 months at room temperature.

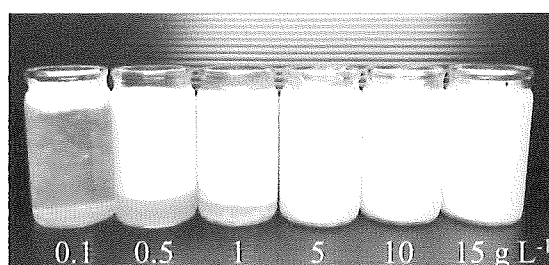


Figure 25 The appearance resulting of the emulsifier CTAB

Table 6 Viscosity and density data of the prepared beeswax emulsion



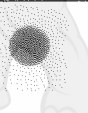


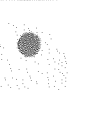



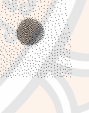




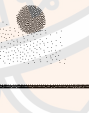

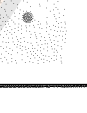

CTAB concentration (g L ⁻¹)	Viscosity (mPa.s) (n=3)	Density (g cm ⁻³) (n=3)
0.1	1040 ± 40	1.028 ± 0.022
0.5	2973 ± 46	1.012 ± 0.008
1.0	13100 ± 361	0.917 ± 0.060
5.0	77467 ± 2479	0.820 ± 0.017
10.0	81800 ± 1453	0.926 ± 0.001
15.0	89033 ± 7057	0.931 ± 0.002

1.2 Effect of melting temperature and time on wax diffusion

It was important to identify the optimal melting temperature and time that would result in the wax penetrating completely to the bottom of the filter paper. Three different melting temperatures (60, 80, and 100°C) were investigated in combination with six different melting times (1, 2, 5, 10, 15, and 20 minutes) in order to find the most effective combination of these two variables. The results were evaluated by dropping a blue dye solution into the finished hydrophilic zones to highlight them and facilitate visual examination and measurement of each diameter. Table 7 shows the wax barriers that resulted from the various combinations of melting temperature and melting time. When the melting time was 1 or 2 minutes, the resulting viscosity of the wax was still too high, regardless of which temperature was used, and the wax could not penetrate the paper sufficiently to correctly form the barriers needed. The result was shown that hydrophilic zones were too large and had a

smudged appearance, as the unbridled blue dye overstepped its intended bounds. The opposite danger is that if either the melting temperature or time is too high, then the viscosity of the wax will become too low, and the wax will spread out excessively within the filter paper. The further the wax spreads beyond the intended target area, the smaller the resulting hydrophilic zone will be. This experiment revealed that the optimal degree of viscosity was achieved by heating the wax-printed paper at 60°C for 5 min. This particular combination of melting temperature and time produced a tidy circular hydrophilic zone with the desired 6 mm diameter, the same diameter as the stencil. Thus, the melting temperature of 60°C and melting time of 5 minutes were used to create the hydrophobic barrier.

Table 7 Effect of melting temperature and time on wax barrier formation

Temperature (°C)	Melting time (min)					
	1	2	5	10	15	20
60						
80						
100						

1.3 Evaluating hydrophobicity of the finished beeswax barriers

A drop of blue dye solution was applied to a finished beeswax coated region (hydrophobic zone) and another drop was applied to plain filter paper (hydrophilic zone) in order to evaluate barrier hydrophobicity and compare this to the behavior of unprinted filter paper. Figure 26A shows that the drop of dye placed on the hydrophobic zone maintained its expected position faithfully without entering the filter paper, while the drop placed on the filter paper immediately entered the paper as expected. The degree of hydrophobicity of the beeswax coated region was also evaluated by measuring the contact angle of the water droplet on the beeswax surface. The measured contact angle was 129.1°, indicating a reliably hydrophobic barrier.

When the contact angle determined in this experiment is above 90° , the surface is considered hydrophobic (179). Figure 26B and 26C show the magnified border between hydrophobic and hydrophilic zones, before and after (respectively) application of the blue dye to the hydrophilic zone. These microscope images reveal a distinct border, which the dye was not able to breach.

A variety of screen-printed beeswax patterns were produced in order to test the robustness and versatility of the new method, and to confirm hydrophobicity of the finished beeswax barriers. Figure 26D shows five different screen-printed beeswax patterns that were produced in order to apply and test this new method in a variety of ways. Dyes added to the hydrophilic zones indicate well-defined hydrophobic barriers.

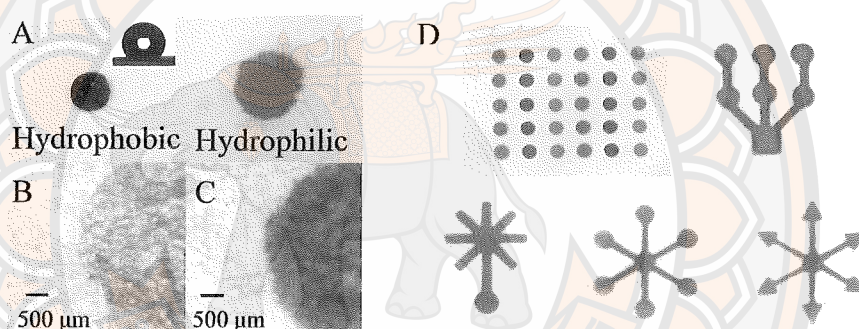


Figure 26 Evaluating hydrophobicity A) Blue dye dropped onto hydrophobic and hydrophilic zones, B) Magnified border, before blue dye is applied to the hydrophilic zone, C) Magnified border, after blue dye is applied to the hydrophilic zone, D) Various screen-printed beeswax patterns with dye, showing clear hydrophobic barriers

1.4 Resolution, reproducibility, and stability of the μ PAD

In order to determine the resolution that the beeswax screen printing method can produce, channels of seven different widths, ranging from 0.2 mm to 2 mm, were evaluated by conducting flow tests with a blue dye solution. Each channel is 10 mm long, with a 5 mm circular inlet at one end, and a 10 μ L portion of dye was dropped into the inlets. A successful test result is defined as the dye entering the channel and traveling completely to the other end, which indicates a correctly functioning hydrophilic channel. Figure 27 shows the results of testing the resolution

of the new device. The channel widths of 0.2, 0.4, and 0.6 mm prevented the dye from flowing into the channel, while the flow in channel width of 0.8 mm was incomplete. Although these unusually narrow channels are beyond the capability of this new method because these very narrow widths cannot prevent the wax from reaching under the stencil, the channel widths of 1.0 mm and wider have a 100% success rate.

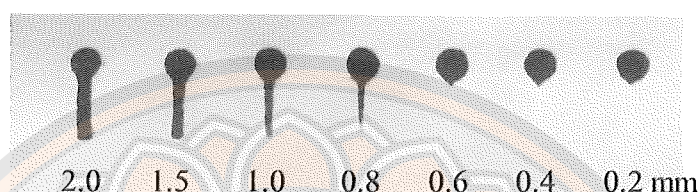


Figure 27 Resolution test results of the beeswax screen printing method

Reproducibility of the μ PAD fabrication method was evaluated by dyeing the hydrophilic zone, and then taking three measurements from each device: 1) the sample zone diameter, 2) the averaged diameters of the left and right detection zones, and 3) the averaged widths of the left and right channels. All measurements were carried out using ImageJ software and subsequently analyzed. Figure 28 shows the measurements of the stencil pattern, as they are intended to appear on each finished μ PAD. The results of measuring the 24 finished μ PADs yielded an average sample zone diameter of 4.95 ± 0.07 mm and an average detection zone diameter of 5.94 ± 0.08 mm, with relative standard deviation (RSD) of 1.39 and 1.33%, respectively. The mean channel width was 1.95 ± 0.07 mm, with an RSD of 3.38%. Thus, all RSDs were below 5%, indicating good fabrication reproducibility of the beeswax screen printing method. The results of the stability test after 12 months showed that all the stored devices remained stable, with their hydrophobic barriers and hydrophilic zones intact and unchanged, indicating reliable stability of the beeswax printed μ PADs.

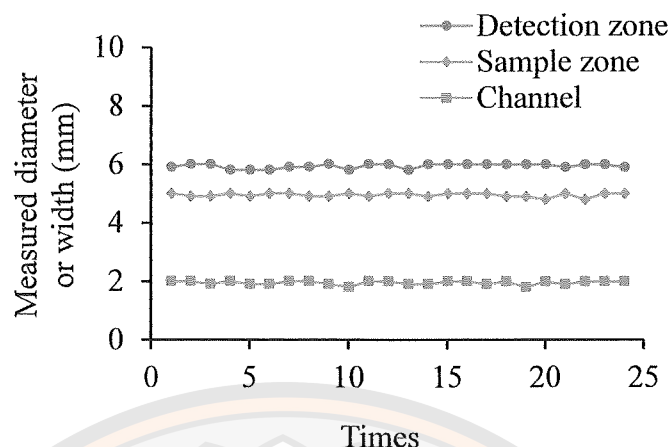


Figure 28 Measurement results from the 24 μ PADs

1.5 Chemical compatibility

In order to employ this μ PAD fabrication method for analytical chemistry, it was important to test the beeswax barrier's compatibility with various sorts of reagents that the barrier could potentially contact. The proposed beeswax barrier was tested by exposing it to 16 common reagents including aqueous solutions containing surfactants (1% w/v of Triton X-100, CTAB, and SLS), organic solvents (methanol, ethanol, toluene, hexane, and heptane), salts (2 mol L⁻¹ ammonium chloride and ammonium sulphate), acids (2 mol L⁻¹ sulfuric, nitric and hydrochloric acids) and a base (2 mol L⁻¹ sodium hydroxide, potassium hydroxide, and ammonium hydroxide), and their compatibility with the barrier was evaluated by visual inspection of the hydrophilic circles to see if barrier remained effective. The results showed that the beeswax formed solid hydrophobic barriers which performed well in containing all eight of the tested inorganic solutions (Figure 29). However, the beeswax was not resilient to either of the three surfactants (Triton X-100, CTAB, and SLS), and five organic solvents (methanol, ethanol, toluene, hexane, and heptane) that were tested.

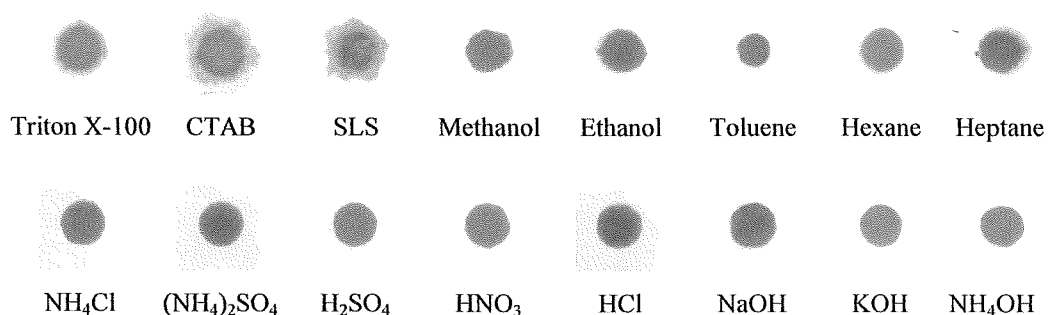
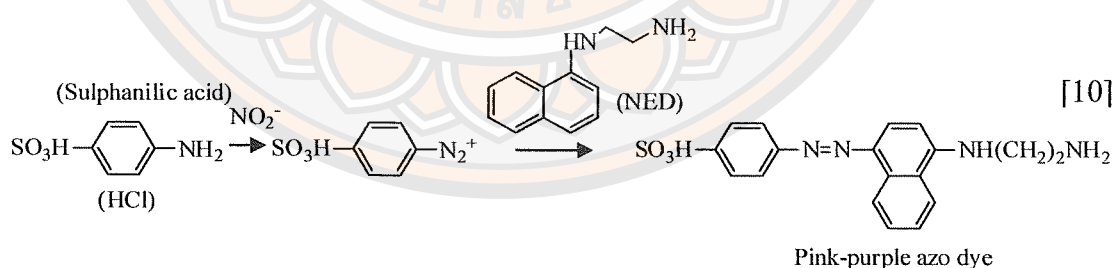


Figure 29 The effect of various chemicals on the integrity of the hydrophobic barrier

2. Effect of colorimetric detection of nitrate

The μ PAD measures the nitrate content using VCl_3 as a reductant for reducing nitrate to nitrite. The reduced nitrate plus the nitrite originally present in the sample reacts with the Griess reagent (sulfanilamide and NED) under acidic condition (equation 9–10). In order to determine the optimum conditions of colorimetric detection on the μ PAD, various concentrations of the three critical chemicals in the reaction were evaluated, along with various reaction times. The goal is to obtain high color intensity when the nitrate concentration is 40 mg L^{-1} , which was the concentration of the test sample used.



2.1 Effect of sulfanilic acid concentrations

The color intensity initially also increased, up to 1% w/v for nitrate determination, after which point the color intensity decreased at higher sulfanilic acid concentrations. Thus 1% w/v sulfanilic acid was used for nitrate determination, as seen in Figure 30.

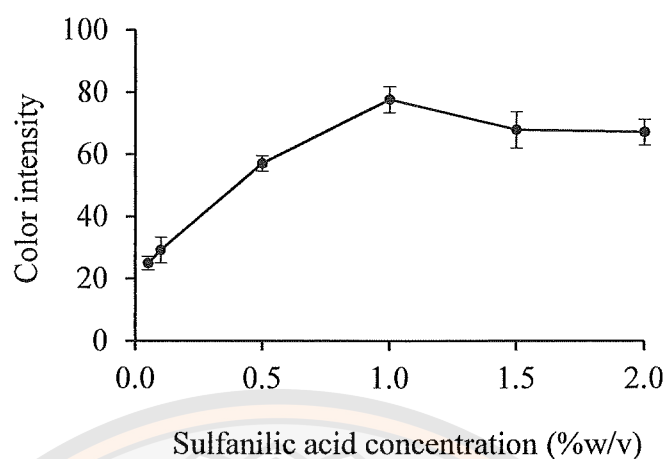


Figure 30 The effect of sulfanilic acid concentrations

2.2 Effect of NED concentrations

As NED concentrations increased in Figure 31, the color intensity initially also increased, up to 0.1% w/v, after which point the color intensity decreased at higher NED concentrations for nitrate determination. Thus 0.1% w/v NED was used for nitrate determination.

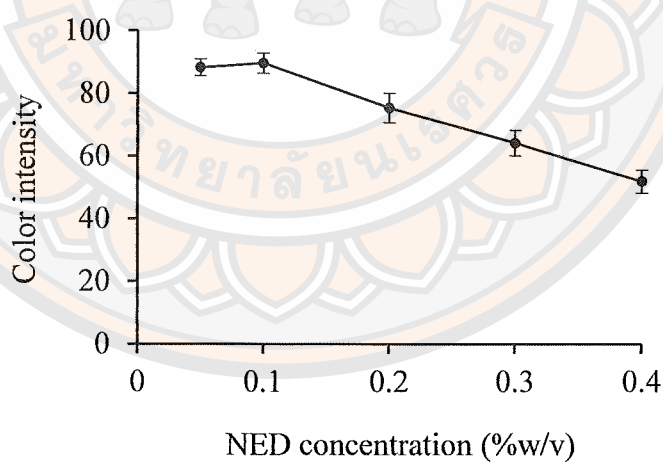


Figure 31 The effect of NED concentrations

2.3 Effect of VCl_3 concentrations

Figure 32 shows how increasing VCl_3 concentration caused increasing color intensity up to 3% w/v, but the increase plateaued at that concentration, so 3% w/v VCl_3 was used to convert nitrate to nitrite.

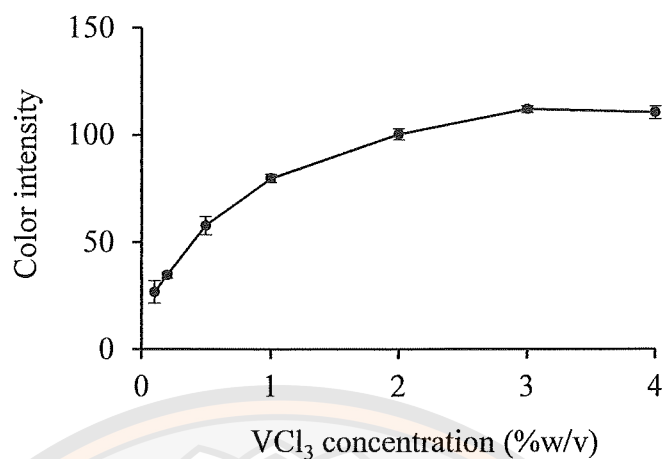


Figure 32 The effect of VCl₃ concentrations

2.4 Effect of reaction time

The effect of reaction time was also investigated, as shown in Figure 33. The color intensity of nitrate detection was observed to stabilize in about 10 min, and then leveled off above 15 min. Therefore, the optimized reaction time selected was 10 min for nitrate determination.

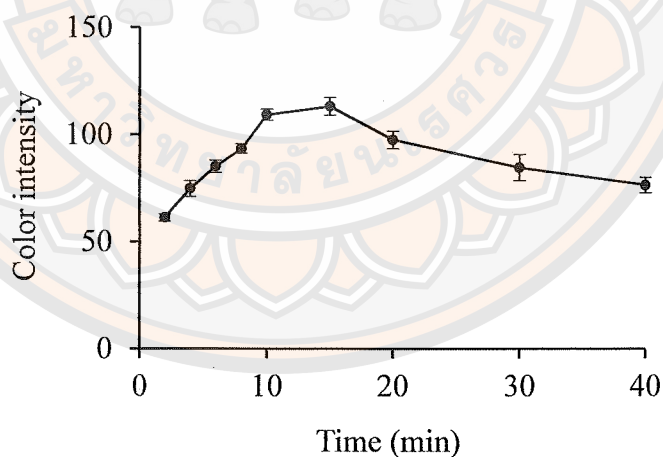


Figure 33 The effect of reaction time on color intensity

The optimum concentration of sulfanilic acid, NED, and VCl₃ were found to be 1% w/v, 0.1% w/v, and 3% w/v for nitrate determination, respectively. The analysis of the reaction using this method was obtained in 10 min.

3. Effect of interference

Soil are usually complex mixtures of various ions, which could be naturally occurring or added. Therefore, it is important to find out if some kinds of ions could interfere with the soil nitrate testing. Various ions were added to nitrate solutions then each of these solutions was tested for nitrate with the μ PAD. The resulting color intensity was compared against the corresponding control solution that had no ion added, in order to see if the added ion affected the color intensity result. The interference effect of the various common ions (at 100 mg L^{-1}) such as Na^+ , K^+ , Ca^{2+} , Cl^- , SO_4^{2-} on the determination of nitrate (at 40 mg L^{-1}) were studied. Figure 34 shows that no significant change in the color intensity resulted from any of the ions. All interference recovery deviations were smaller than 5% for nitrate (2.57–4.25%). This indicates that there is negligible interference from any of these ions in the determination of nitrate by the μ PAD.

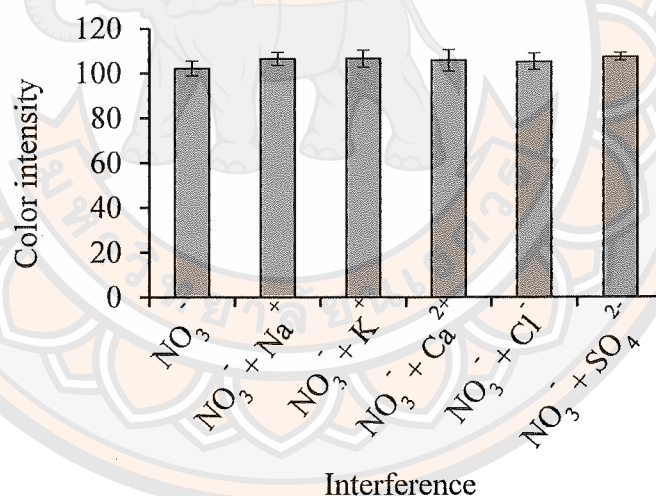


Figure 34 The effect of interfering ions on the determination of 40 mg L^{-1} nitrate using μ PAD. The concentrations of interfering ions were 100 mg L^{-1} for Na^+ , K^+ , Ca^{2+} , Cl^- , and SO_4^{2-} .

4. Analytical performance

Calibration curve was established by plotting the color intensity against seven different concentrations of nitrate ($0.5\text{--}40\text{ mg L}^{-1}$), as shown in Figure 35. The response fitted to a linear model with $r^2 = 0.9924$. The precision of the μ PAD was evaluated by studying inter-day and intra-day result variations. Each of the three nitrate solutions (2.5 , 10 , and 40 mg L^{-1}) were tested with the μ PAD for nitrate content in sixuplicate in one day, and then the same procedure was carried out every day for five days. The RSD values was $1.15\text{--}2.24\%$ (inter-day precision), and $1.50\text{--}2.16\%$ (intra-day precision). The RSD values obtained indicated good precision of the analytical method. The limit of detection (LOD) values was 0.41 mg L^{-1} , and the limit of qualification (LOQ) values was 1.35 mg L^{-1} .

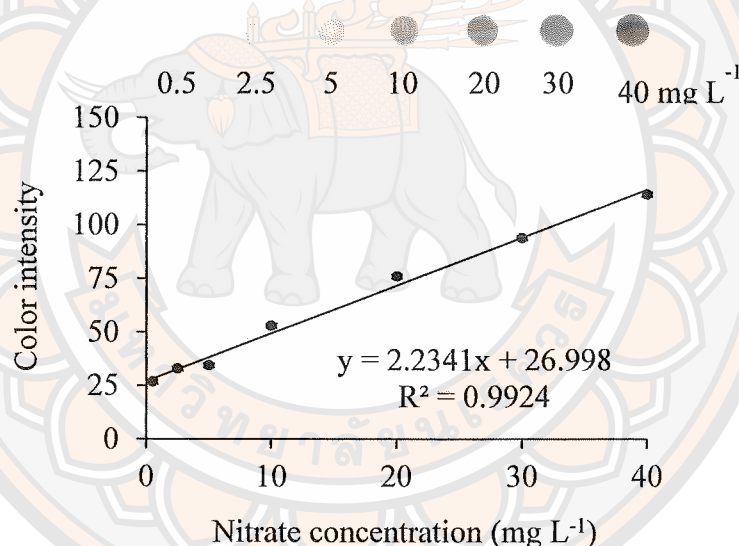


Figure 35 Calibration curve of nitrate

5. Stability of the μ PAD

The proposed μ PADs were individually kept in vacuum sealed bags up to 120 days at temperatures $\leq 2^\circ\text{C}$. The stability of the μ PAD, was evaluated by determining the amount of nitrate every 10 days. The color intensity of nitrate detection was observed to stabilize in about 40 days, and then leveled off after that (Figure 36). The one-way ANOVA showed that there were no statistically significant difference over 40 days of storage ($F = 2.22$, $F_{\text{critical}} = 2.76$). Therefore, the devices can be stored for 40 days.

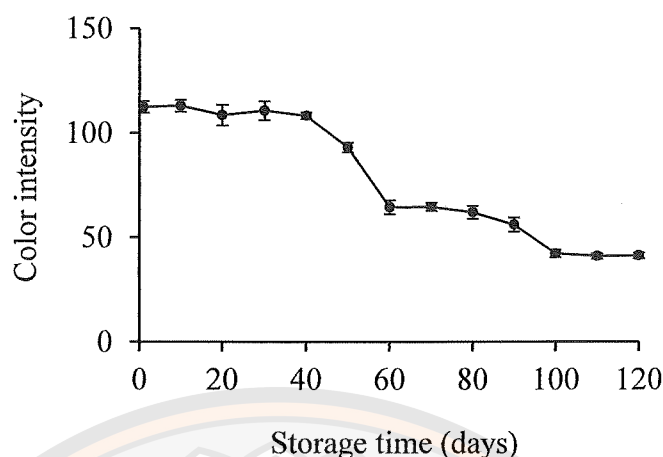


Figure 36 The effect of the stability of the μ PADs stored at 2°C

6. Sample analysis

The intended functionality of the proposed μ PAD was tested by applying the device to determine nitrate in soil. Images of the colorimetric reaction of nitrate on the μ PAD is shown in Figure 37. Six soil samples were analyzed for determination of nitrate in actual samples, and the results were compared with the results of a spectrophotometric method according to the procedure described by García-Robledo et al. and Miranda et al. (180-181). The analysis results are shown in Table 8. The pair t-test at 95% confidence level showed that there were no statistically significant differences between two method ($t_{\text{stat}} = 1.30$, $t_{\text{critical}} = 2.20$). The accuracy of the μ PAD was further evaluated by measuring the recovery of nitrate in the ten spiked samples at 40 mg L⁻¹ concentration. Excellent percentage recoveries of 88.4–99.8% was obtained for nitrate (n=6). It can therefore be concluded that the μ PAD fabricated by the beeswax screen-printing method can be used for quantitative assays in the soil.



Figure 37 Image of the fabricated μ PAD before and after reaction with nitrate

Table 8 Comparison of nitrate detection results in soil using the μ PAD versus the spectrophotometric method.

Sample	Added (mg kg ⁻¹)	μ PAD		Spectrophotometric method	
		Found (mg kg ⁻¹)	Recovery (%)	Found (mg kg ⁻¹)	Recovery (%)
Soil 1	0.0	2.9 \pm 1.3	—	3.1 \pm 1.3	—
	200.0	194.5 \pm 5.0	95.8 \pm 3.0	194.6 \pm 2.2	95.8 \pm 1.8
Soil 2	0.0	2.6 \pm 0.9	—	3.4 \pm 2.5	—
	200.0	194.9 \pm 1.2	96.4 \pm 1.0	199.6 \pm 7.4	98.1 \pm 3.8
Soil 3	0.0	12.1 \pm 1.5	—	10.1 \pm 3.9	—
	200.0	200.7 \pm 2.1	94.3 \pm 0.8	205.3 \pm 7.9	97.6 \pm 1.3
Soil 4	0.0	19.5 \pm 4.1	—	15.4 \pm 7.5	—
	200.0	196.7 \pm 4.1	88.4 \pm 4.0	198.5 \pm 0.7	91.6 \pm 3.6
Soil 5	0.0	3.7 \pm 0.7	—	3.5 \pm 0.8	—
	200.0	198.0 \pm 2.1	97.1 \pm 1.1	202.6 \pm 9.1	99.51 \pm 4.4
Soil 6	0.0	7.5 \pm 2.2	—	7.0 \pm 3.9	—
	200.0	207.0 \pm 2.5	99.8 \pm 2.2	209.3 \pm 3.9	101.1 \pm 1.4

Table 9 compares the features of the proposed μ PAD with those of other reported methods used for detection of nitrate in various samples. Most of the features of the μ PADs are comparable or preferable to other existing methods, affirming the effectiveness of this new device. The LOD for nitrate detection is lower than in other existing methods. The μ PAD is easy to make, easy to use, inexpensive, and environmental friendly.

Table 9 Comparison of the features of the proposed μ PADs with those of other reported methods for nitrate determination

Colorimetric assay	Sample	Linear range	LOD	Reaction time (min)	Reference
Zinc combined with Griess reaction	Water	50–1000 μ M	19 μ M	5	(182)
Zinc combined with Griess reaction	Food product	10–50 mg L ⁻¹	3.6 mg L ⁻¹	12	(78)
Zinc combined with Griess reaction	Human saliva	0.2–1.2 mM	0.08 mM	35	(27)
VCl ₃ combined with Griess reaction	Soil	0.5–40 mg L ⁻¹	0.41 mg L ⁻¹	10	This work

Conclusions

A paper-based microfluidic device fabrication method using beeswax as a new environmentally friendly hydrophobic material with a screen-printing method was developed. Under the optimal condition, the method provides a well-defined hydrophobic barrier with an efficient resolution, good reproducibility, and high stability without requiring organic solvent or complicated instruments. The μ PAD was successfully applied to determination of nitrate content in soil using Griess reaction as the colorimetric assay. The analytical results obtained by the μ PAD were in good agreement with those obtained by the spectrophotometric method. The cost of the paper-based devices with the reagents for assay of nitrate was approximately 1.25 baht. The developed μ PAD using the beeswax screen-printing method exhibited simplicity, low-cost, reliability, and environmental friendliness suitable for highly limited regions.

CHAPTER IV

FABRICATION OF 3D PAPER-BASED ANALYTICAL DEVICES BY USING THE UV RESIN SCREEN PRINTING METHOD FOR THE DETERMINATION OF AMMONIUM

Introduction

Ammonium (NH_4^+) is one of the preferential N forms taken up by rice and may account for up to 60 % of the crop demand (183). Ammonium in soil serves not only as a major source of N for plant growth, but also as an important product or reactant in the N transformation processes in soil, and is also the main form in which fertilizer N is applied in agriculture (184). It occurs chiefly in amino acids, proteins, and sugars (185). The positive charged ammonium is held by the negative charges of the soil, which prevents ammonium leaching, except in low cation exchange capacity soil (186). Ammonium concentrations in soil are common 2–10 ppm. Too much ammonium can cause acidification of soil from excess aqueous acid production. Plants cannot use ammonium directly, therefore, large quantities of it may actually impair the health of the soil. The ability to accurately determine ammonium levels in soil is of vital importance in agriculture. The main purpose of nitrogen soil testing is to assess current soil fertility and thereby know the optimal amount of nitrogen to supplement in the form of fertilizer. This information allows farmers to both maximize crop productivity and minimize fertilizer costs (148).

Conventional methods that are used in the field of agriculture and environmental sciences to measure ammonium concentration include common laboratory colorimeter procedures using the Nessler reaction (146, 148) and the Berthelot reaction (indophenol method) (149, 151). Nessler's reagent is a solution consisting of mercury (II) iodide and potassium iodide in a highly alkaline solution. In the presence of ammonium, Nessler's reagent will react to form a yellow color (187). Unfortunately, the use of Nessler's reagent for testing has two disadvantages. First, the method has low sensitivity, and second, mercury (II) iodide is a toxic substance (188). The Berthelot method is based on the formation of indophenol blue dye when ammonia reacts with

phenol, hypochlorite, and the catalyst sodium nitroprusside in an alkaline solution (153, 189-191). There is a modified version of the Berthelot method in which sodium salicylate and dichloroisocyanurate are used instead of toxic phenol and unstable hypochlorite, respectively (149). Both the Nessler Method and Berthelot Method normally require time-consuming laboratory procedures, expensive instruments, and large quantities of chemicals, which is inconvenient for field work (192). The current study, therefore, find out a better alternative method, one that is simpler, faster, cheaper, and requires fewer reagents.

The purpose of this study was to develop a new and simple 3D paper-based analytical device (3D PAD) for the rapid detection of ammonium in soil. The fabrication method consisted of using a simple, inexpensive screen-printing method together with a commonly available commercial UV resin dissolved in ethyl acetate. The advantages of using the UV resin are that it cures quickly at a low temperature. Initially, optimization of the UV resin concentrations and curing times were studied to obtain well-defined hydrophobic barriers on the paper. The hydrophobic barrier's chemical compatibility with commonly used aqueous solutions and organic solvents were also studied. In order to use colorimetric detection based on the modified Berthelot reaction, salicylate was substituted for phenol. This modification eliminates the production of phenol which is toxic and highly volatile. The tri-sodium citrate is included as a complexing agent to prevent the possible interference by metals. The various concentrations of salicylate and dichloroisocyanurate were investigated. After these investigations and completing the fabrication of a suitable 3D PAD, their performance were tested and evaluated for multiple parameters. Finally, the fabricated 3D PAD was applied to ammonium determination in soil samples.

Experimental

1. Chemicals

All the chemicals used in this study were analytical reagent grade. Ammonium chloride was purchased from Carlo Erba Reagents (Val-de-Reuil, France). Sodium salicylate, sodium nitroprusside, tri-sodium citrate, sodium hydroxide, and potassium chloride were purchased from Ajax (Finechem, Australia). Sodium dichloroisocyanurate was purchased from Sigma-Aldrich (Castle Hill, NSW, Australia). Ethyl acetate was purchased from RCI Labscan Ltd (Bangkok, Thailand). UV resin (epoxy acrylate) was purchased from Qiaoqiao Brand (China).

2. Apparatus

Whatman Grade 1 and Grade 5 qualitative filter paper were purchased from Whatman International, Ltd. (Buckinghamshire, UK). The stencil screen, made with polyester fabric on a wooden frame (35 cm x 45 cm) was custom ordered from a local screen-printing shop (Phitsanulok, Thailand). An HP 2135 scanner was used for colorimetric analysis. The UV curing box was made from wood (15 x 20 x 15 cm) in conjunction with 10W UV-A lamp. An OCA20 contact-angle measuring instrument (DataPhysics Instrument GmbH, Germany) was used for contact angle measurement. A shaking water bath (Daihan Scientific, Switzerland) was used to extract of nitrate from soil. A synergy H1 hybrid multi-mode microplate reader (BioTex, Vermont, USA) was used for the reference spectrophotometric method.

3. Preparation of solutions

3.1 Ammonium stock solution (1000 mg L⁻¹)

The ammonium stock solution was prepared by dissolving 0.3821 g of ammonium chloride to 100 mL using DI water in a volumetric flask.

3.2 Ammonium standard solution (10–100 mg L⁻¹)

The ammonium standard solution with concentration of 10, 20, 40, 60, 80, and 100 mg L⁻¹ were prepared by adding 1, 2, 4, 6, 8, and 10 mL of 1000 mg L⁻¹ ammonium stock solution to 100 mL using DI water in a volumetric flask, respectively.

3.3 Reagent A

Reagent A was prepared by dissolving 10.0 g of sodium salicylate and 0.5 g of sodium nitroprusside dehydrate to 100 mL using DI water in a volumetric flask.

3.4 Reagent B

A 1% w/v sodium dichloroisocyanurate solution was prepared by dissolving 1.0 g of sodium dichloroisocyanurate, 2.0 g of sodium hydroxide, and 20 g of tri-sodium citrate dihydrate to 100 mL using DI water in a volumetric flask.

3.5 Potassium chloride solution (2 mol L^{-1})

A 2 mol L^{-1} potassium chloride solution was prepared by dissolving 74.55 g of potassium chloride to 500 mL using DI water in a volumetric flask.

4. Optimization of the UV resin screen-printing method

The screen-printing method was used to transfer UV resin onto filter paper, thereby creating hydrophobic barriers and hydrophilic analysis zones for the PADs. The fabrication of paper-based devices has various factors which can affect the efficiency of them. These factors are the UV resin concentrations, curing times, chemical compatibility tests, and hydrophobicity tests. Therefore, the influences of these variables were verified by the experiment.

4.1 UV resin concentration optimization

A blocking stencil, with a pattern of 6 mm diam. circles arranged in rows were designed using the Silhouette Studio software. The filter paper was placed under the blocking stencil, and then 20 mL of the solution of UV resin in ethyl acetate (varied at 1:1, 2:1, 3:1, and 4:1 by volume) was poured onto the stencil and distributed using a squeegee (Figure 38). The resin solution needed to penetrate to the bottom of the filter paper. The circles (6 mm diam.) on the blocking stencil prevented the resin solution from reaching the portions of the filter paper directly below them. The printing of the circular hydrophilic pattern onto the filter paper, was followed by careful removal of the stencil. The patterned paper was then put under a 10W UV-A backlight for 30 min to cure the UV resin. After curing, the patterned paper was ready to use. A drop of pink dye solution was applied to the finished hydrophilic zones to highlight them and facilitate visual examination.

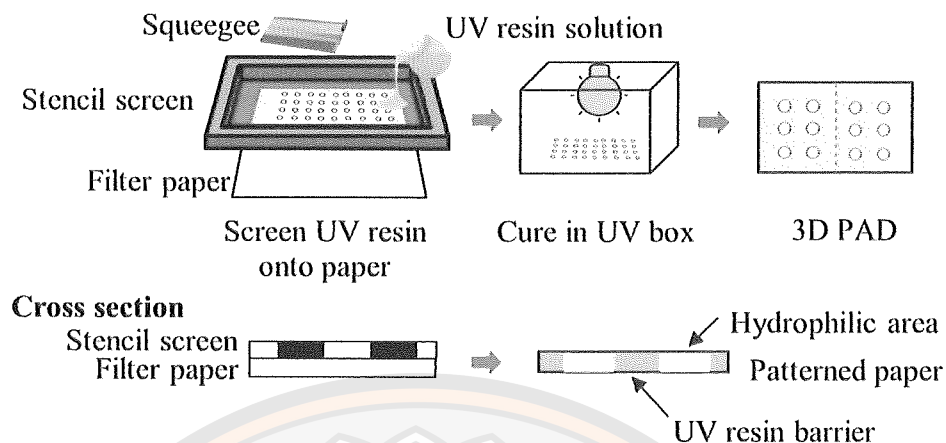


Figure 38 Schematic diagram of UV resin screen-printing for the fabrication of 3D PAD

4.2 UV resin curing time optimization

The experiment was carried out according to the procedure as described in a section 4.1, whereas the curing times of UV resin in ethyl acetate were 5, 10, 15, 20, and 30 minutes, with a ratio of 4:1 by volume.

4.3 Chemical compatibility test

The experiment was carried out according to the procedure as described in a section 4.1 under optimum conditions. To evaluate the UV resin barrier's compatibility with various shorts of reagent, 5 μL of aqueous solutions containing surfactants (1% w/v of Triton X-100, CTAB, and SLS), organic solvents (methanol, ethanol, toluene, hexane, and heptane), salts (2 mol L^{-1} ammonium chloride and ammonium sulphate), acids (2 mol L^{-1} sulfuric, nitric and hydrochloric acids) and bases (2 mol L^{-1} sodium hydroxide, potassium hydroxide, and ammonium hydroxide), were added to the hydrophilic zone.

4.4 Hydrophobicity test and applicability of the method to various patterns

The experiment was carried out according to the procedure described in section 4.1 under optimum conditions. After producing the PADs, the contact angle of the water on the hydrophobic surface was measured to examine the hydrophobicity of the barrier, and then a drop of pink dye solution was applied to the hydrophilic zone of the plain filter paper. A microscope was also used to examine the border between

the hydrophobic and hydrophilic zones, and the application of the pink dye. Examples of other various patterns could be used for different chemical reactions.

5. Optimization of the modified Berthelot's reaction on 3D PAD

The objective of this part of the work is to investigate the effect of the variables that impose on the Berthelot's reaction involving in ammonium determination. The concentration of color development reagents (sodium salicylate and sodium dichloroisocyanurate solution), and the reaction time were optimized to provide the highest values of color intensity.

5.1 Concentration of sodium salicylate

Using a micropipette, each circular area in region 1 received 5 μL of reagent A containing sodium salicylate (varied at 1, 5, 10, 15, and 20% w/v), and 0.5% w/v sodium nitroprusside. Similarly, each circular area in region 2 received 5 μL of reagent B containing 1% w/v sodium dichloroisocyanurate, 2% w/v sodium hydroxide, and 20% w/v tri-sodium citrate. The solutions applied to the two regions were allowed to dry at room temperature. The filter paper was then folded down the middle so that region 1 is on top, region 2 is on the bottom, and both sets of circular wells were aligned. After folding, the paper was inserted into a rectangular plastic holder with a plastic sheet on each side of the filter paper resulting in both layers being attached. Both the top (T) and bottom (B) plastic sheets have six holes, or "windows", that align with the circular areas of the paper inside. The 3D PAD was now ready to use (Figure 39).

A test sample, 10 μL of 100 mg L^{-1} ammonium was deposited through each of the windows of the top plastic sheet to the hydrophilic areas inside on the top layer, and then the sample and reagent A in region 1 would flow toward the detection zones in the bottom layer. The 3D PAD was then left for 10 min while the chemical reactions occurred. During the reaction period, a green color appeared in the windows of the bottom plastic sheet. The color that appeared in the detection zones was scanned by an image scanner, and the intensity was analyzed using ImageJ software ($n=6$). The obtained RGB values were used for the analytical study. It was found that R parameter showed a linear response to concentration. Therefore, the R parameter was taken as the analytical response for the detection of ammonium.

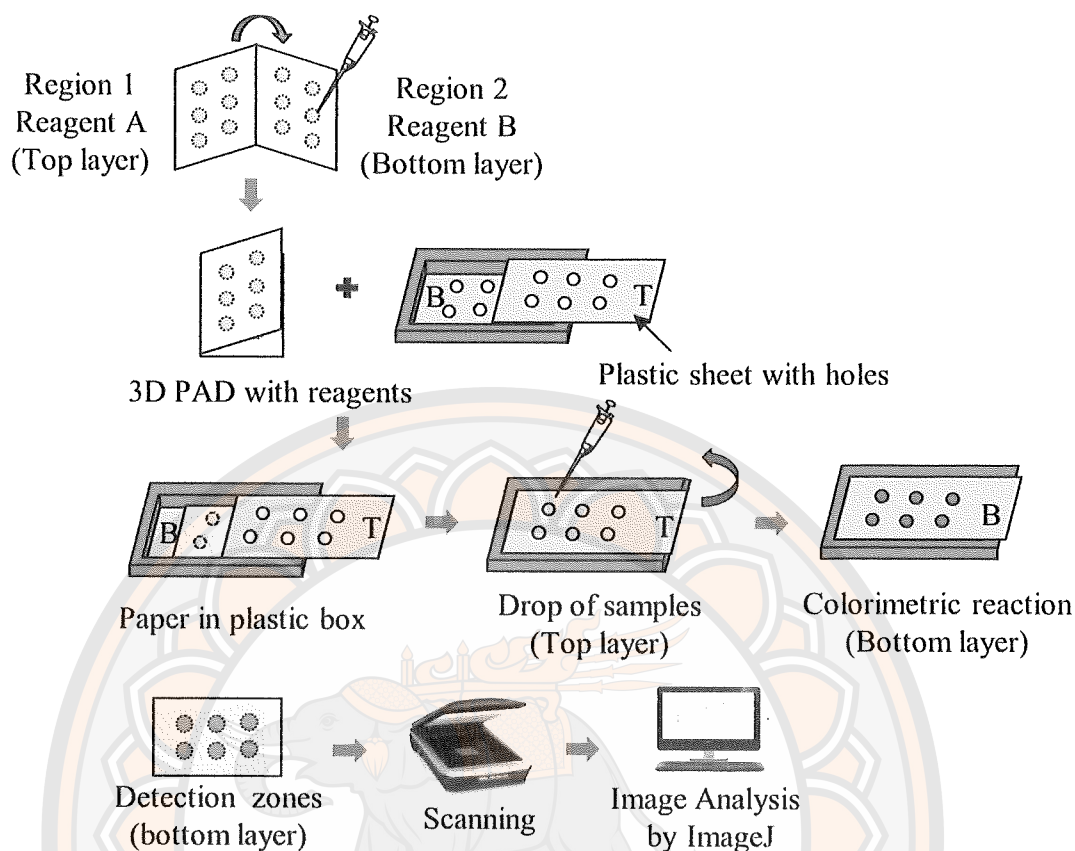


Figure 39 Schematic diagram of the colorimetric ammonium assay using the 3D PAD

5.2 Concentration of sodium dichloroisocyanurate

The experiment was carried out according to the procedure as described in a section 5.1, except the concentration of reagents was changed as follow: The concentrations of sodium dichloroisocyanurate were 0.05, 0.10, 0.50, 1.0, and 2.0% w/v (n=6). The sodium salicylate was set at 10% w/v.

5.3 Reaction time

The experiment was carried out according to the procedure as described in a section 5.1, with the reaction times of 5, 10, 15, 20, and 30 minutes (n=6). The sodium salicylate and sodium dichloroisocyanurate were set at 10% w/v and 1% w/v, respectively.

6. Interference

1 mL of 1000 mg L⁻¹ ammonium stock solution and 1 mL of 1000 mg L⁻¹ KNO₃, NaH₂PO₄, KCl, Fe(NO₃)₂, Mn(NO₃)₂, and Cu(NO₃)₂ stock solution were added into each 10 mL volumetric flask, and adjusted to 10 mL with DI water. After that, the experiment was carried out according to the procedure as described in a section 5.1 under optimum conditions (n=6).

7. Analytical Method Validation

Validation of the proposed modified Berthelot's reaction for ammonium determination in soil samples is performed. The validation parameters included linearity, limit of detection (LOD), limit of quantitation (LOQ), precision, and accuracy of the proposed method were evaluated under a selected condition.

7.1 Linearity

The experiment was carried out according to the procedure as described in a section 5 under optimum conditions (n=3), by using ammonium standard solution in the concentrations of 10, 20, 40, 60, 80, and 100 mg L⁻¹. A graph plotted between color intensity and concentration of ammonium were constructed to find the linearity.

7.2 LOD and LOQ

The experiment was carried out according to the procedure as described in a section 5 under optimum conditions. The DI water was analyzed by the modified Berthelot's reaction in 10 replicates. The SD of the response and the slopes of the concentration curves of the calibration curves were used to estimate the LOD ($3\sigma/\text{slope}$) and LOQ ($10\sigma/\text{slope}$).

7.3 Precision

Evaluation of method repeatability (intraday precision) and reproducibility (interday precision) were performed. The ammonium standard solutions at three different concentrations (20, 60, 100 mg L⁻¹) were analyzed using procedure with optimum conditions in section 5. Intraday precision was determined from six replications within 1 day, and the interday precision was analyzed in six replications on 5 days.

7.4 Accuracy and Recovery

Accuracy was evaluated across the specified range of the analytical procedure by a recovery study. The standard solution of the ammonium was spiked into the soil samples extract in triplicate. The recovery was determined as follows: (total ammonium amount – original ammonium amount in real sample)/ammonium amount of added.

8. Application in real samples

The 3D PAD was applied to the determination ammonium in soil. Potassium chloride is used to extract ammonium from the soil samples. Seven soil samples were collected from rice fields in five provinces of Thailand: Phitsanulok, Sukhothai, Khamphaeng Phet, Sa Kaeo, and Ubon Ratchathani. All soil samples were dried in the open-air to remove the moisture, and then sieved to a particle size of 2 mm.

To validate the accuracy of the proposed method, 5.0 g of the soil sample was added in 7 centrifuge tubes. Then, 6 of the 7 samples were spiked with 0.25, 0.50, 1.00, 1.50, 2.0, and 2.50 mL of ammonium stock solution to achieve the concentrations of 10, 20, 40, 60, 80, and 100 mg L⁻¹, respectively. After that, the soil samples were mixed with 25 mL of 2 mol L⁻¹ potassium chloride and shaken for 15 min. The mixture was filtered through a filter paper (Whatman #5). The filtrate was then carried out according to the procedure as described in a section 5 under optimum conditions. The results from the 3D PAD were compared to the results from spectrophotometry.

9. Spectrophotometric method

The volume of 200 µL of filtrate (from section 8) was added into a microcentrifuge tube, then added 200 µL reagent A, and 200 µL of the reagent B (oxidizing solution). The solution was shaken, and then allowed to stand for 10 min to ensure complete color development. The absorbance was measured with a spectrophotometry at 670 nm.

Results and discussion

1. Effect of the UV resin screen-printing method

An ideal hydrophobic barrier will result in circular hydrophilic zones with a clear, crisp perimeter. The resin must penetrate vertically from the top side of the paper through to the bottom side and must not spread horizontally outside of the target area. The results of hydrophobic barrier optimization experiments were examined by dropping a pink dye solution into the hydrophilic zone, followed by visual inspection.

1.1 Effect of UV resin concentration

In order to enable the UV resin to pass through the stencil screen, the ethyl acetate is used to dilute UV resin. Decreasing the concentration of UV resin, ethyl acetate in this case, affects the viscosity of UV resin. Thus four different ratios of UV resin with ethyl acetate (1:1, 2:1, 3:1, and 4:1 by volume) were trialed to determine which concentration produced the most effective UV resin barrier. The first three ratios (1:1, 2:1, and 3:1 by volume) all resulted in hydrophilic regions that were measurably smaller than the stencil pattern (Figure 40). The images were recorded on the inverted side of the paper. This indicates that viscosity of the resin was too low, causing the resin to spread beyond the stencil pattern. In contrast, the fourth ratio (4:1) resulted in the correct 6 mm size of the hydrophilic region with a very clear perimeter. The 4:1 ratio was, therefore, chosen to create the hydrophobic barrier.

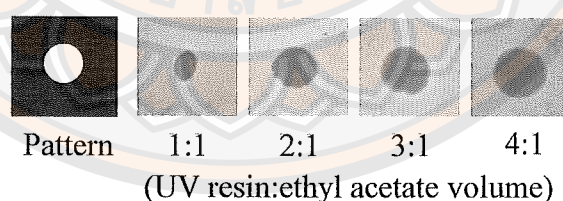


Figure 40 The effect of UV resin concentration

1.2 Effect of UV resin curing time

It was important to identify the optimal curing time that would cause the UV resin to crosslink on the filter paper. Five different curing times (5, 10, 15, 20, and 30 minutes) were tested using the optimum UV resin concentration. At 5 min, the resin is not sufficiently rigid to block the dye correctly, so the resulting hydrophilic

area was too large and it had a smudged appearance (Figure 41). A 10 min curing time was better, but the resin was still wet in appearance and the resulting hydrophilic area was not consistently reliable. When the curing time was increased to 15 min or longer, the hydrophilic zone was reliably formed into a 6 mm circle. Since no benefit was gained by waiting longer than 15 min, this time was selected as optimal.

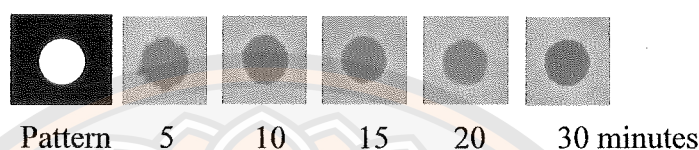


Figure 41 The effect of curing time on the hydrophobic and hydrophilic zone

1.3 Effect of hydrophobicity test

The contact angle of water on the hydrophobic surface was measured to examine the hydrophobicity of the barrier. If the water contact angle is larger than 90° , then the surface is considered hydrophobic (193, 194). The test revealed that the contact angle of the water droplet was 113.2° , as seen in Figure 42A, indicating that there were well-formed hydrophobic surfaces produced by the UV resin. The effectiveness of the optimized hydrophobic barrier was also verified by dropping dye solution onto the hydrophilic area and inspecting the results under a microscope. Figure 42B shows that the border between the filter paper's hydrophobic and hydrophilic regions is distinct. The optimized UV resin screen-printing method was further tested by applying it to produce four different sample patterns, the first being the intended pattern for use in the current study, and the other four being examples of other various patterns that could be used for other chemical reactions, as shown in Figure 42C.

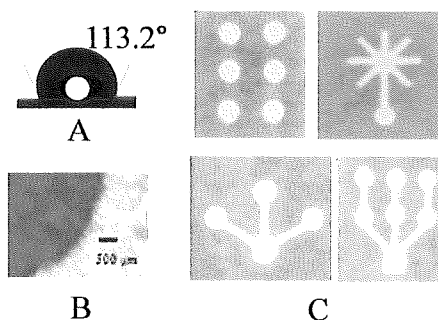


Figure 42 Filter paper printed with UV resin using the screen printing method: A) contact angle of a water droplet placed on the UV resin coated region, B) the hydrophilic-hydrophobic boundary, as seen under a microscope at 5x magnification, C) various sample patterns created to highlight the versatility of the UV resin screen printing method

1.4 Chemical compatibility

In order to employ this 3D PAD fabrication method for analytical chemistry, it was important to test the UV resin barrier's compatibility with various sorts of reagents that the barrier could potentially contact. The proposed UV resin barrier was tested by exposing it to 16 common reagents including aqueous solutions containing surfactants (1% w/v of Triton X-100, CTAB, and SLS), organic solvents (methanol, ethanol, toluene, hexane, and heptane), salts (2 mol L⁻¹ ammonium chloride and ammonium sulphate), acids (2 mol L⁻¹ sulfuric, nitric and hydrochloric acids) and bases (2 mol L⁻¹ sodium hydroxide, potassium hydroxide, and ammonium hydroxide), and their compatibility with the barrier was evaluated by visual inspection of the hydrophilic circles to see if barrier remained effective. The results showed that the UV resin formed solid hydrophobic barriers which performed well in containing all eight of the tested inorganic solutions (Figure 43). However, the UV resin was not resilient to either of the three organic solvents (methanol, ethanol, and toluene), and three surfactants (Triton X-100, CTAB, and SLS) that were tested.

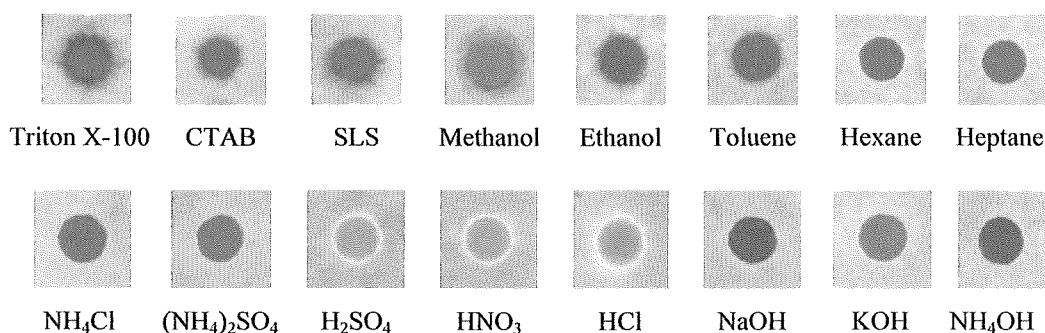
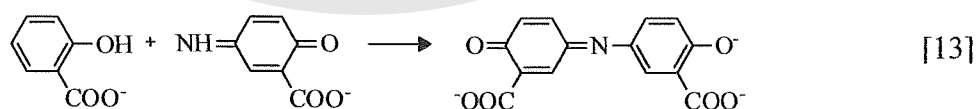
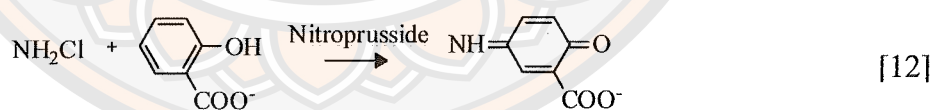
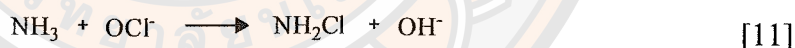


Figure 43 The effect of various chemicals on the integrity of the hydrophobic barrier

2. Effect of modified Berthelot's reaction on 3D PAD

The ammonium is converted to uncharged ammonia in the presence of the alkaline solution. The actual modified Berthelot reaction then causes the formation of the green color of 2-2 dicarboxy indophenol, as shown in the equation 11–13 (149, 155, 195-197). In order to determine the optimum conditions conducive to the modified Berthelot's reaction on the 3D PAD, various concentrations of the two critical chemicals in the reaction were evaluated, along with various reaction times. The goal is to obtain high color intensity when the ammonium concentration is 100 mg L^{-1} , which was the concentration of the test sample used.



2.1 Effect of sodium salicylate concentrations

The color intensity was increased when the concentrations of sodium salicylate was increased up to 10 % w/v, and then decreased at higher concentrations. The color intensity increase was probably due to a higher yield of the colored product. Therefore, a 10% w/v sodium salicylate concentration was used as the optimal concentrations (Figure 44).

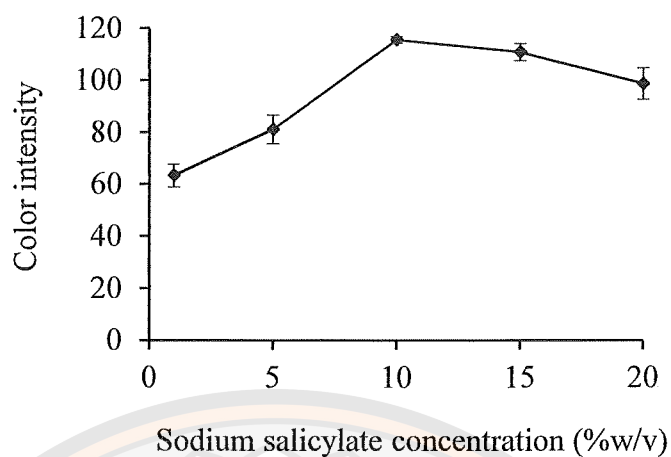


Figure 44 The effect of sodium salicylate concentrations

2.2 Effect of sodium dichloroisocyanurate concentrations

The color intensity was increased when the concentrations of sodium dichloroisocyanurate were increased up to 1.0 % w/v, and then decreased at higher concentrations. The color intensity increase was probably due to a higher yield of the colored product. Therefore, a 1.0% w/v sodium dichloroisocyanurate concentration was used as the optimal concentrations (Figure 45).

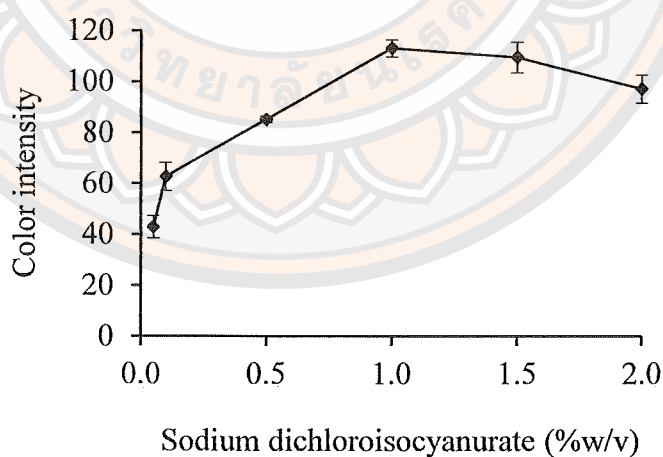


Figure 45 The effect of sodium dichloroisocyanurate concentrations

2.3 Effect of reaction time

The results in Figure 46 show that color intensity reached a maximum at 5 min then remained constant up to 10 min and decreased after that. Therefore, a reaction time at 5 min was selected in this method because it was sufficient to complete the reaction.

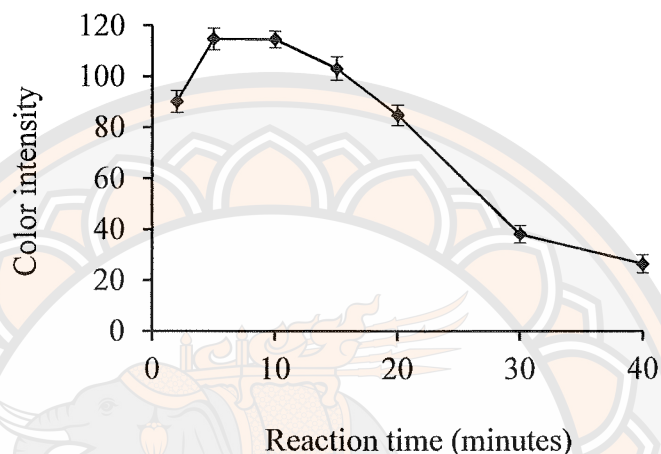


Figure 46 The effect of reaction time on color intensity

The optimum concentration of sodium salicylate, and sodium dichloroisocyanurate were found to be 10% w/v, and 1% w/v for ammonium determination, respectively. The analysis of the reaction using this method was obtained in 10 min.

3. Effect of interference

Soil samples are known to contain other various ions which can interfere with colorimetric detection by the Berthelot reaction (198-199). The green indophenol compound is generated in a strong alkaline solution. This high alkaline condition promotes precipitation of metal hydroxides, which can interfere with proper color formation. The tri-sodium citrate added as a complexing reagent prevents the formation of metal hydroxides during testing of the soil samples. Six ions were tested (at 100 mg L⁻¹) for possible interference in the modified Berthelot's reaction on the 3D PAD and, no significant change in the color intensity was observed for any of these ions, as can be seen in Figure 47. This indicates that there is negligible interference from any of these ions in the formation of 2-2 dicarboxyindophenol.

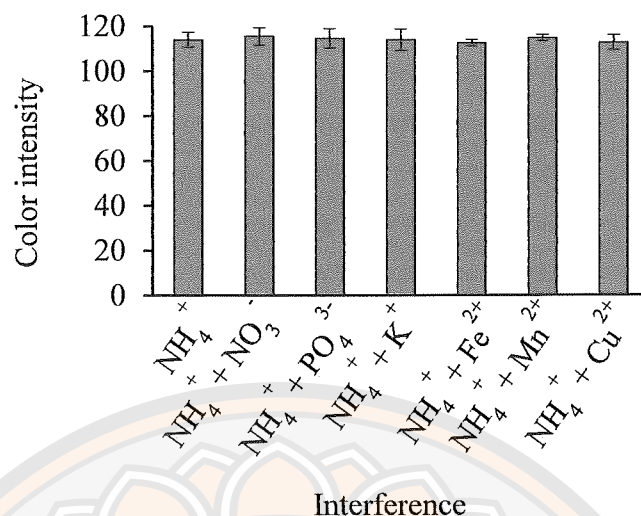


Figure 47 The effect of interfering ions on the determination of 100 mg L^{-1} ammonium using 3D PAD. The concentrations of interfering ions were 100 mg L^{-1} for NO_3^- , PO_4^{3-} , K^+ , Fe^{2+} , Mn^{2+} , and Cu^{2+} .

4. Analytical Performance

The completed 3D PAD exhibited a linear response over the range of $10\text{--}100 \text{ mg L}^{-1}$ (Figure 48). The linear regression equation was $y = 0.8343x + 32.691$ with a correlation coefficient of 0.9963 ($n=6$). The lower limit of detection was determined to be 0.49 mg L^{-1} , and the limit of quantification was found to be 1.65 mg L^{-1} , based respectively on three times and ten times the standard deviation of the color intensity of blank samples as described by Apilux et al. (200). These two limits are comfortably low and easily accommodate the typical ammonium levels in soils, which are $10\text{--}90 \text{ mg kg}^{-1}$ in coarse-textured soils, $60\text{--}270 \text{ mg kg}^{-1}$ in medium-textured soils, and $90\text{--}460 \text{ mg kg}^{-1}$ in fine-textured soils (201). The precision of 3D PAD was calculated in terms of the repeatability (intra-day precision, $n = 6$) and reproducibility (inter-day precision, 5 days) using 20, 60 and 100 mg L^{-1} concentration levels for ammonium. The repeatability of the method evaluated as the relative standard deviation (%RSD) ranged from 1.57–2.58%, and the reproducibility was in the range 1.86–3.81%, indicating good precision.

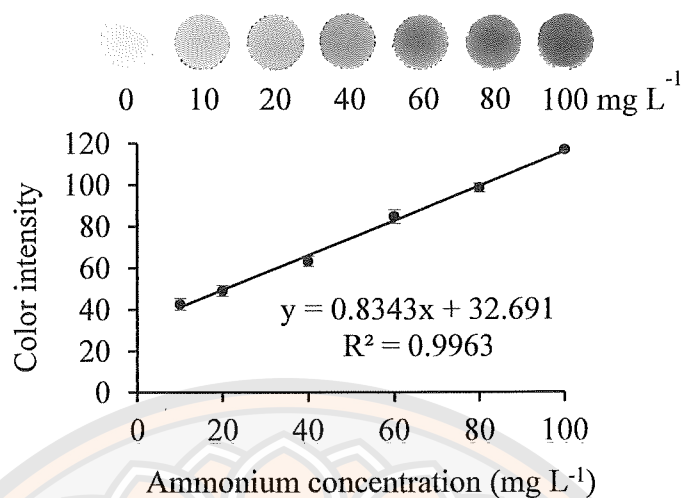


Figure 48 Calibration curve of ammonium

5. Sample analysis

To evaluate the actual application of the 3D PAD, seven soil and five pound samples were used to test the accuracy of ammonium detection. Recovery values in the ranged between 95.5 to 107.5% (Table 10), indicating good accuracy of the developed 3D PAD. These results showed the capability of the 3D PAD to detect ammonium in actual soil samples. The analytical results were compared with a previously established UV-Vis spectrophotometric reference method (196) using a statistic paired t -test. It was found that t_{stat} is lower than t_{critical} at the 95% confidence level. This indicates that there is no evidence of systematic error in the proposed method.

Table 10 Comparison of ammonium detection results and recovery rate in various soil samples using the 3D PAD versus the spectrophotometric method.

Samples	Added (mg kg ⁻¹)	3D PAD		Spectrophotometric method	
		Found (mg kg ⁻¹)	Recovery (%)	Found (mg kg ⁻¹)	Recovery (%)
Soil 1	0.0	24.7 ± 2.0	—	25.0 ± 1.8	—
	50.0	76.1 ± 2.6	102.9 ± 1.7	77.8 ± 2.4	105.5 ± 4.7
Soil 2	0.0	24.3 ± 2.7	—	23.5 ± 0.8	—
	50.0	74.0 ± 2.6	99.5 ± 4.8	77.8 ± 1.3	108.6 ± 1.1
Soil 3	0.0	18.5 ± 2.1	—	19.8 ± 3.1	—
	50.0	69.6 ± 4.3	102.2 ± 4.4	66.7 ± 2.3	93.8 ± 1.6
Soil 4	0.0	18.8 ± 1.5	—	18.5 ± 0.6	—
	50.0	68.4 ± 3.0	99.2 ± 3.7	69.9 ± 1.3	102.9 ± 2.1
Soil 5	0.0	10.7 ± 1.3	—	10.5 ± 2.8	—
	50.0	61.3 ± 2.5	101.2 ± 3.0	60.8 ± 0.6	100.6 ± 4.6
Soil 6	0.0	8.5 ± 5.0	—	9.4 ± 1.7	—
	50.0	62.3 ± 1.7	107.5 ± 4.0	60.9 ± 1.3	103.2 ± 1.0
Soil 7	0.0	9.5 ± 4.0	—	13.9 ± 1.4	—
	50.0	57.2 ± 4.2	95.5 ± 4.2	59.2 ± 1.6	90.4 ± 2.9

Table 11 compares the features of the proposed μ PAD with those of other various methods used for detection of ammonia/ammonium in environmental samples. Most of the features of the PAD are comparable or preferable to other existing methods, affirming the effectiveness of this new device. The PAD is easy to make, easy to use, and inexpensive. The only materials needed are filter paper, a plastic holder, a stencil screen, and a UV lamp.

Table 11 A comparison of the features of the proposed μ PAD with those of other reported methods for ammonia/ammonium determination

Method	Colorimetric assay	Sample	Linear range (mg L ⁻¹)	LOD (mg L ⁻¹)	Reaction time (min)	Reference
Gas-diffusion μ PAD	3-nitrophenol	Ammonia in wastewater	10–100	0.8	2–4	(106)
	Bromothymol blue		10–50	1.8	2–6	
Membraneless Gas-Separation μ PAD	Nessler's reaction	Ammonium in wastewater & fertilizer	10–100	3.14	6	(154)
Solid sensing on paper	Modified Berthelot's reaction	Ammonia in water	10–200	10	10	(155)
Micro-distillation μ PAD	Nitrazine yellow	Ammonia in freshwaters	0.5–3.0	0.32	5	(99)
	Bromothymol blue		2.0–10	0.47	1	
Microplate with gas pervaporation and diffusion	Natural indicator (butterfly pea flower extract)	Ammonia in wastewater and fertilizer samples	10–100	4	15	(202)
3D PAD	Modified Berthelot's reaction	Ammonium in soil	10–100	0.5	5	This work

6. Creation of convenient paper color comparison chart

A convenient color comparison chart was successfully created on paper to enable the user to interpret the color results and find the ammonium concentration without the need for a color scanner or imaging software. The chart is shown in Figure 49. An opening at middle of the chart, corresponding to the size of the detection zone, allows the user to conveniently compare the color result to all the chart's shades simultaneously.

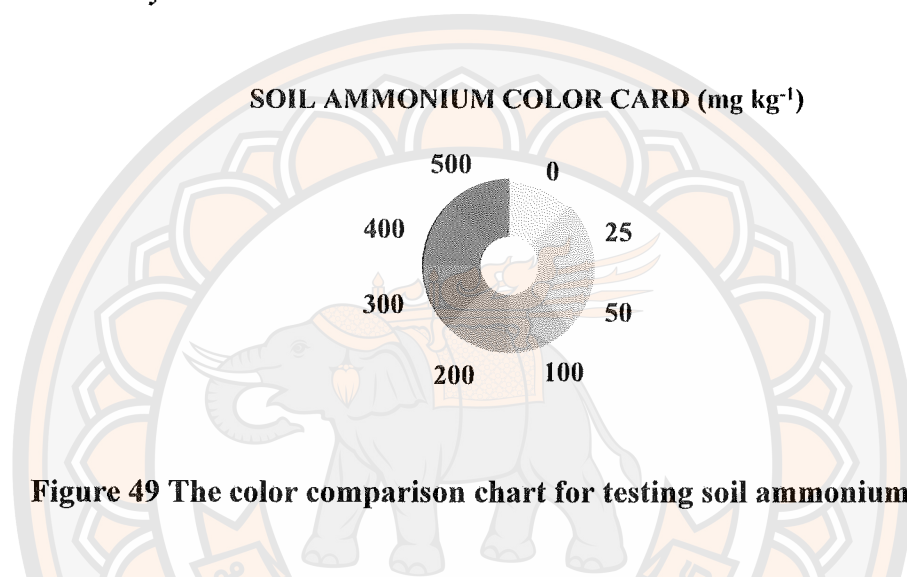


Figure 49 The color comparison chart for testing soil ammonium content

Conclusion

This study has introduced the use of UV resin solution as a new efficient hydrophobic material for the fabrication of PAD. This UV resin screen-printing method creates well-defined hydrophobic barriers that enable efficient measurement of ammonium without any need for expensive instruments. The use of a PAD for the colorimetric detection of ammonium in soil samples has been demonstrated herein by carrying out the modified Berthelot reaction. The multiple validation tests in this study have established that the proposed PAD can analyse ammonium content of actual soil samples with good accuracy and reliability. Therefore, the developed modified Berthelot reaction for the determination of ammonium, can be used as an alternative method to the existing one for ammonium. A convenient color comparison chart was successfully created on paper to eliminate the need for a scanner. The cost of materials per device is approximately 1 baht. The PAD developed here has numerous desirable qualities. They are simple and inexpensive method of production, quick and easy use, portability, and being environmentally friendly.

CHAPTER V

FABRICATION OF 3D PAPER-BASED ANALYTICAL DEVICES BY USING ONE-STEP EPOXY RESIN SCREEN PRINTING METHOD FOR THE DETERMINATION OF PHOSPHATE

Introduction

Phosphorus (P) is a major element in soil which has both organic and inorganic forms. It is known terrestrial minerals are orthophosphates and is often the primary limiting nutrient in freshwater ecosystems (203). The simplest of this is orthophosphate, has the chemical formula of PO_4^{3-} . Plants can only take up phosphorus dissolved in the soil solution, and since most of the soil phosphorus exists in stable chemical compounds, only a small amount of it is available to the plant at any given time. When plant roots remove phosphorus from the soil solution, some of it gets adsorbed into the solid phase in order to maintain equilibrium. Phosphorus is an essential element for plant growth, and plays an important role in a variety of processes (e.g., nucleic acid synthesis, photosynthesis, glycolysis, respiration, enzyme activation/deactivation, carbohydrate metabolisms, and nitrogen fixation) (204). Excess amounts of phosphorus mostly interfere with the uptake of other elements, such as iron, manganese and zinc. Over-fertilization with phosphorus is common and many growers apply unnecessarily high amounts of it, especially when NPK fertilizers are used or when irrigation water is acidified using phosphoric acid. Nutrient pollution causes excess algae growth over large bodies of water, resulting in a significant impact on the environment, human health, and the economy (205). The amount of phosphorus required in the soil for crops should not fall below 10 mg kg^{-1} and should not exceed 40 mg kg^{-1} .

Conventional methods that are used in agriculture and environmental sciences to measure phosphate concentrations, include common laboratory colorimeter procedures using the molybdenum blue and vanadomolybdate methods. In molybdenum blue, a solution consisting of ammonium molybdate, and reductant (ascorbic acid or stannous chloride), which are reacts with the phosphate to produce a blue colored phosphomolybdate

complex (156, 206, 207). For the vanadomolybdate methods, a solution that consists of ammonium molybdate, and ammonium metavanadate in hydrochloric acid solution, which reacts with the phosphate to a yellow colored complex (208). However, the molybdenum blue method became broadly used due to its higher sensitivity and lower susceptibility to interferences than the vanadomolybdate method.

The aims of the research were: (i) to fabricate paper-based devices using one-step epoxy resin in conjunction with the screen-printing method (ii) to apply 3D PADs for the determination of phosphate in the soil. The colorimetric detection of phosphate was based on the molybdenum blue method. These were reduced by stannous chloride which formed the molybdenum blue complex. The stannous chloride was used as a reducing agent for phosphate in the solution because its reaction was rapid and the absorptivity was greater than that of ascorbic acid. The molybdenum blue method that involved ascorbic acid had limitations associated with its stability (23, 209).

Experimental

1. Chemicals

Potassium dihydrogen orthophosphate (KH_2PO_4) was purchased from Ajax (Finechem, Australia). Ammonium molybdate ($(\text{NH}_4)_6\text{Mo}_7\text{O}_{24} \cdot 4\text{H}_2\text{O}$) was purchased from Carlo Erba (Italy). Sulfuric acid (H_2SO_4) and hydrochloric acid (HCl) were purchased from RCI Labscan Ltd. (Bangkok, Thailand). Stannous chloride ($\text{SnCl}_2 \cdot 2\text{H}_2\text{O}$) was purchased from Acros (USA). Ammonium fluoride (NH_4F) was purchased from Chemicals (Belgium). Epoxy resin YD127 and Curing agent TH7301 was supported by Aditya Birla Chemicals (Bangkok, Thailand).

2. Apparatus

Whatman Grade 1 and Grade 5 qualitative filter paper were purchased from Whatman International, Ltd. (Buckinghamshire, UK). The stencil screen, made with polyester fabric on a wooden frame (35 cm x 45 cm) was custom ordered from a local screen-printing shop (Phitsanulok, Thailand). An HP 2135 scanner was used for colorimetric analysis. An OCA20 contact-angle measuring instrument (DataPhysics Instrument GmbH, Germany) was used for contact angle measurement. A shaking water bath (Daihan Scientific, Switzerland) was used to extract of phosphate from soil.

A synergy H1 hybrid multi-mode microplate reader (BioTex, Vermont, USA) was used for the reference spectrophotometric method.

3. Preparation of solutions

3.1 Phosphate stock solution (1000 mg L^{-1})

The phosphate stock solution was prepared by dissolving 0.4404 g of potassium dihydrogen orthophosphate to 100 mL using DI water in a volumetric flask.

3.2 Phosphate standard solution (100 mg L^{-1})

The phosphate standard solution with concentration of 100 mg L^{-1} were prepared by added 10 mL of 1000 mg L^{-1} phosphate stock solution to 100 mL using DI water in a volumetric flask, respectively.

3.3 Phosphate standard solution ($0.5\text{--}40 \text{ mg L}^{-1}$)

The phosphate standard solution with concentration of 0.5, 2.5, 5, 10, 20, 30, and 40 mg L^{-1} were prepared by added 0.5, 2.5, 5, 10, 20, 30, and 40 mL of 100 mg L^{-1} phosphate standard solution to 100 mL using DI water in a volumetric flask, respectively.

3.4 Reagent A

Reagent A was prepared by dissolving 4.0 g of ammonium molybdate in 25 mL of DI water, and then adjusted to 100 mL using 4 mol L^{-1} sulfuric acid in a volumetric flask.

3.5 Reagent B (reducing agent)

A 0.2% w/v stannous chloride was prepared by dissolving 0.2 g of stannous chloride to 100 mL using DI water in a volumetric flask.

3.6 Bray II solution ($0.03 \text{ mol L}^{-1} \text{ NH}_4\text{F}$ and $0.1 \text{ mol L}^{-1} \text{ HCl}$)

A Bray II solution was prepared by 15.0 mL of 1.0 mol L^{-1} ammonium fluoride and 100 mL 0.5 mol L^{-1} hydrochloric acid to 500 mL using DI water in a volumetric flask.

4. Optimization of the epoxy resin screen-printing method

The screen-printing method was used to transfer epoxy resin onto filter paper, thereby creating hydrophobic barriers and hydrophilic analysis zones for the PADs. The fabrication of paper-based devices has various factors which can affect the efficiency of them. These factors are the epoxy resin concentrations, curing times and temperature. Therefore, the influences of these variables were verified by the

experiment. Chemical compatibility and hydrophobicity of epoxy resin barrier were also evaluated.

4.1 Epoxy resin concentration and curing temperature optimization

The pattern was first designed using the Silhouette Studio software. The filter paper was placed under the blocking stencil, and then 20 mL of the solution of epoxy resin in curing agent (varied at 3:1, 2:1, 1:1, 1:2, and 1:3 by volume) was poured onto the stencil and distributed using a squeegee (Figure 50). The epoxy resin solution needed to penetrate to the bottom of the filter paper. The patterned papers were then curing at room temperature for 3 hours. After curing, the patterned papers were ready to use. A drop of green dye solution was applied to the finished hydrophilic zones to highlight them and facilitate visual examination.

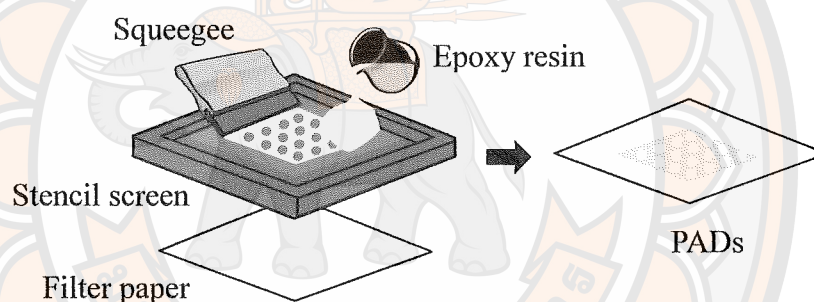


Figure 50 Schematic diagram of epoxy resin screen-printing for the fabrication of PADs

4.2 Hydrophobicity test and applicability of the method to various patterns

The experiment was carried out according to the procedure described in section 4.1 under optimum conditions. After producing the PADs, the contact angle of the water on the hydrophobic surface was measured to examine the hydrophobicity of the barrier, and then a drop of green dye solution was applied to the hydrophilic zone of the plain filter paper. A microscope was also used to examine the border between the hydrophobic and hydrophilic zones, and the application of the green dye. Examples of other various patterns could be used for different chemical reactions.

To evaluate the resolution between the hydrophobic and the hydrophilic areas of the fabrication of the hydrophilic channels, a shape mould

composed of a 5 mm circular inlet, and 0.2, 0.4, 0.6, 0.8, 1, 1.5, 2 mm (length 10 mm) hydrophilic channel. A 10 μL of green dye solution was applied to the inlet zone and stand for 5 minutes.

To examine the reproducibility of the fabrication of the hydrophilic circular, 24 pieces of paper and a shape mold composed of a 5 mm and 6 mm circular hydrophilic zones. Pictures of the paper devices were scanned and used to measure the widths of the hydrophilic circular by using ImageJ.

4.3 Chemical compatibility test

The experiment was carried out according to the procedure as described in a section 4.1 under optimum conditions. To evaluate the epoxy resin barrier's compatibility with various sorts of reagent, 5 μL of aqueous solutions containing surfactants (1% w/v of Triton X-100, CTAB, and SLS), organic solvents (methanol, ethanol, toluene, hexane, and heptane), salts (2 mol L^{-1} ammonium chloride and ammonium sulphate), acids (2 mol L^{-1} sulfuric, nitric and hydrochloric acids) and bases (2 mol L^{-1} sodium hydroxide, potassium hydroxide, and ammonium hydroxide), were added to the hydrophilic zone.

5. Optimization of the molybdenum blue reaction on 3D PAD

The objective of this part of the work is to investigate the effect of the variables that impose on the molybdenum blue involving in phosphate determination. The concentration of color development reagent (ammonium molybdate, sulfuric acid, and stannous chloride solution), and the reaction time were optimized to provide the highest values of color intensity.

5.1 Concentration of ammonium molybdate

Using a micropipette, each circular area in region 1 received 5 μL of reagent A containing ammonium molybdate (varied at 2, 3, 4, 5, 6, 7, and 8% w/v), and 4 mol L^{-1} sulfuric acid. Similarly, each circular area in region 2 received 5 μL of reagent B containing 0.2% w/v stannous chloride. The solutions applied to the two regions were allowed to dry at room temperature. The 3D PAD was now ready to use (Figure 51).

The 3D PAD was folded in half and placed on rubber magnetic sheet (3x3 cm) with a 7 mm window, then another rubber magnetic sheet was placed on top of the first one. To determine the amount of phosphate, 10 μL of a 40 mg L^{-1}

phosphate was dropped onto the sample zone of the 3D PAD via the window of the top rubber magnetic sheet, then the solution would seep through to the detection zone on the bottom layer. The 3D PAD was then left for 10 min while the chemical reactions occurred. During the reaction period, the rubber magnetic sheets are inverted, which enabled the observation of the intensity of the blue on the detection zone of the 3D PAD, which was then scanned and processed by using ImageJ software. The obtained RGB values were used for the analytical study. It was found that R parameter showed a linear response to concentration. Therefore, the R parameter was taken as the analytical response for the detection of phosphate.

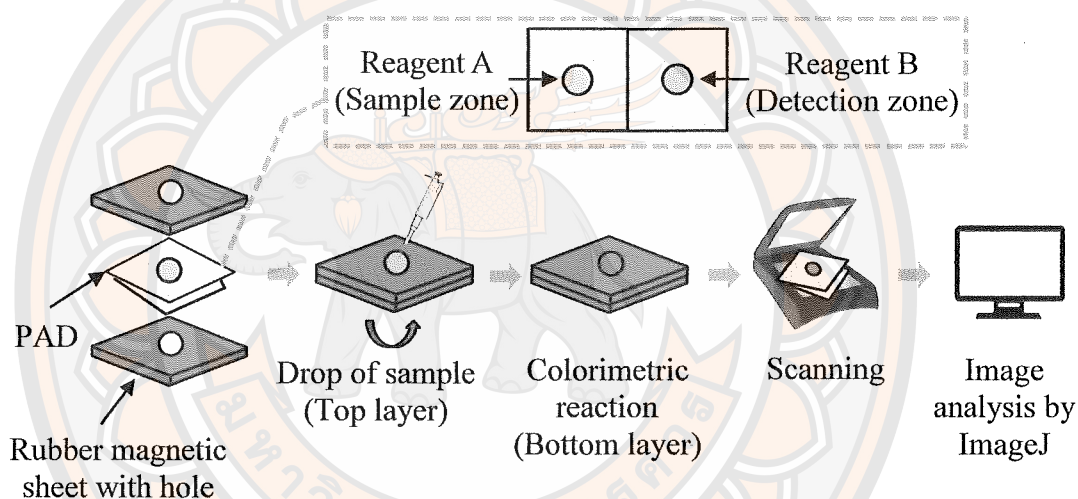


Figure 51 Step for detection of phosphate on 3D PAD

5.2 Concentration of sulfuric acid

The experiment was carried out according to the procedure as described in a section 5.1, except the concentration of reagents was changed as follow: The concentrations of sulfuric acid were 0.5, 2.0, 3.0, 4.0, 5.0, 6.0, and 8.0 mol L⁻¹. The ammonium molybdate and stannous chloride were set at 4.0% w/v and 0.2% w/v, respectively.

5.3 Concentration of stannous chloride

The experiment was carried out according to the procedure as described in a section 5.1, except the concentration of reagents was changed as follow:

The concentrations of stannous chloride were 0.05, 0.1, 0.2, 0.3, 0.4, 0.5, and 0.6% w/v. The ammonium molybdate and sulfuric acid were set at 4.0% w/v and 4.0 mol L⁻¹, respectively.

5.4 Reaction time

The experiment was carried out according to the procedure as described in a section 5.1, with the reaction times of 3, 5, 10, 15, 20, 30 and 40 minutes. The ammonium molybdate, sulfuric acid, and stannous chloride were set at 4% w/v, 4 mol L⁻¹ and 0.2% w/v, respectively.

6. Interference

A 4 mL of 100 mg L⁻¹ phosphate standard solution and 1 mL of 1000 mg L⁻¹ KNO₃, NH₄Cl, KCl, Fe(NO₃)₂, Mn(NO₃)₂, Cu(NO₃)₂, and CaCl₂ stock solution were added into each 10 mL volumetric flask, and adjusted to 10 mL with DI water. After that, the experiment was carried out according to the procedure as described in a section 5.1 under optimum conditions (n=6).

7. Analytical Method Validation

Validation of the proposed molybdenum blue reaction for phosphorus determination in soil samples is performed. The validation parameters included linearity, limit of detection (LOD), limit of quantitation (LOQ), precision, and accuracy of the proposed method were evaluated under a selected condition.

7.1 Linearity

The experiment was carried out according to the procedure as described in a section 5 under optimum conditions (n=3), by using phosphate standard solution in the concentrations of 0.5, 2.5, 5, 10, 20, 30, and 40 mg L⁻¹. A graph plotted between color intensity and concentration of phosphate were constructed to find the linearity.

7.2 LOD and LOQ

The experiment was carried out according to the procedure as described in a section 5 under optimum conditions. The DI water was analyzed by the molybdenum blue reaction in 10 replicates. The SD of the response and the slopes of the concentration curves of the calibration curves were used to estimate the LOD (3σ/slope) and LOQ (10σ/slope).

7.3 Precision

Evaluation of method repeatability (intraday precision) and reproducibility (interday precision) were performed. The phosphate standard solution at the concentrations of 10, 20, and 40 mg L⁻¹ was analyzed using procedure with optimum conditions in section 5. Intraday precision was determined from six replications within 1 day, and the interday precision was analyzed in six replications on 5 days.

7.4 Accuracy and Recovery

Accuracy was evaluated across the specified range of the analytical procedure by a recovery study. The standard solution of the phosphorus was spiked into the soil samples extract in triplicate. The recovery was determined as follows: (total phosphate amount–original phosphate amount in real sample)/phosphate amount of added.

8. Stability of the μ PAD

The first step is the addition of 5 μ L of reagent A and B to each circular area in region 1 and 2 of the 3D PAD, respectively, which take approximately 60 minutes to dry at room temperature. Then, the 3D PAD was placed in a plastic bag and vacuum sealed, and stored in a black ziplock bag in a refrigerator at $\leq 2^{\circ}\text{C}$. To evaluate the stability of the 3D PAD, the 6 pieces of 3D PADs were tested by determination the concentration of 40 mg L⁻¹ phosphate standard solution every 10 days of storage over 120 days.

9. Application in real samples

The 3D PAD was applied to the determination phosphate in soil. Seven soil samples were collected from rice fields in five provinces of Thailand: Phitsanulok, Sukhothai, Khamphaeng Phet, Sa Kaeo, and Ubon Ratchathani. All soil samples were dried in the open-air to remove the moisture, and then sieved to a particle size of 2 mm.

To validate the accuracy of the proposed method, 2.0 g of the soil sample was added in 6 centrifuge tubes. Then 5 of the 6 samples were spiked with 1.25, 2.50, 5.00, 7.50, and 10.00 mL of phosphate standard solution to achieve the concentrations of 5, 10, 20, 30, and 40 mg L⁻¹, respectively. After that, the soil samples were added to 25 mL of Bray II solution and shaken for 5 min. The mixture was filtered through a filter paper (Whatman #5). The filtrate was then carried out according to the procedure

as described in a section 5.1 under optimum conditions. The results from the 3D PAD were compared to the results from spectrophotometry.

10. Spectrophotometric method

The volume of 200 μL of filtrate (from section 9) was added into a microcentrifuge tube, then added 200 μL of reagent A, and 200 μL of reagent B (reducing agent). The solution was shaken, and then allowed to stand for 10 min to ensure complete color development. The absorbance was measured with a spectrophotometry at 650 nm.

Results and discussion

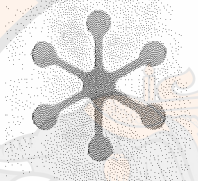
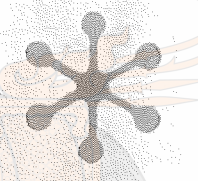
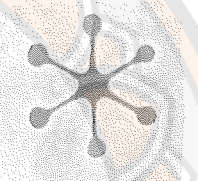
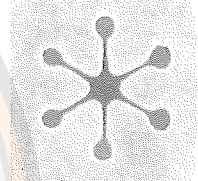
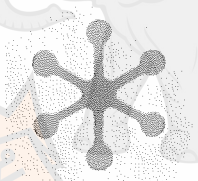
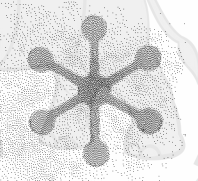
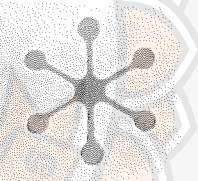
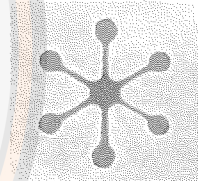
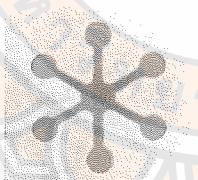
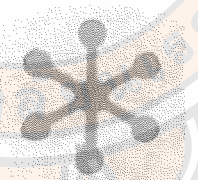
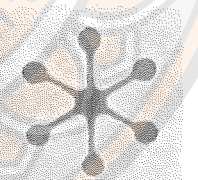
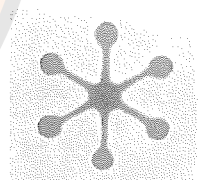
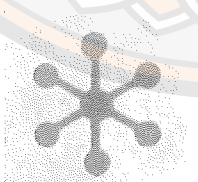
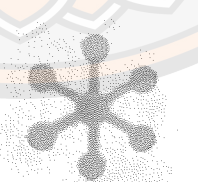
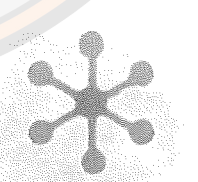
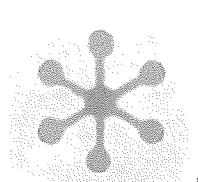
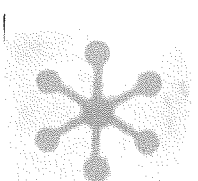
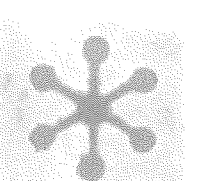
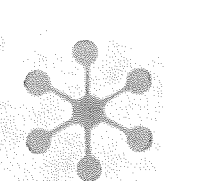
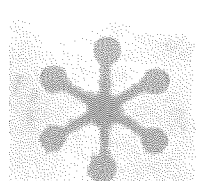
1. Effect of the epoxy resin screen-printing method

1.1 Effect of epoxy resin concentrations and temperatures

To verify the best conditions for the fabrication of microfluidic paper-based device, the effects of the ratios between the epoxy resin and the curing agent, and the temperatures required for curing the resin on the paper were investigated, with the aim of producing hydrophobic barrier. The epoxy resin and the curing agent were combined together in ratios of 3:1, 2:1, 1:1, 1:2, and 1:3. The curing temperatures were studied at room temperature (30°C), and 60°C. As shown in Table 12, the epoxy resin screen-printing effects were dependent to a certain extent on the ratios of epoxy resin/curing agent, and curing temperatures. The results of the hydrophobic barrier optimization experiments were examined by dropping a green dye solution into the hydrophilic zone, followed by a visual inspection. At room temperature, the first two ratios (3:1, and 2:1 by volume) resulted in hydrophilic regions that were the correct sizes and had very clear perimeters. However, the 3:1 ratio was difficult to pass through the stencil screen because it produced a higher viscosity than the 2:1 ratio. The last three ratios (1:1, 1:2, and 1:3 by volume) all resulted in the hydrophilic regions not separating correctly due to the spread of excessive molten epoxy resin, and at the same time the dye solution leaked from the printed pattern. A possible reason for this phenomenon, was that the last three ratios did not contain enough polymer to set correctly on the paper. As stated above, the curing temperature of the epoxy resin had an impact on the formation of the μPADs . At 60°C, all the ratios resulted in hydrophilic regions that were measurably smaller than the stencil pattern, because at

this temperature the epoxy resin was diffused. Therefore, room temperature (30°C) and the epoxy resin/curing agent mixture at a ratio of 2:1 were chosen to create the hydrophobic barrier.

Table 12 Optimization of the mixing ratios between the epoxy resin and the curing agent, and the effects of the curing temperatures

Epoxy resin: Curing agent	Temperature			
	Room temperature (30°C)		60°C	
	Front	Back	Front	Back
3:1				
2:1				
1:1				
1:2				
1:3				

1.2 Hydrophobicity test, applicability of the method for various patterns, resolution and reproducibility of the μ PADs fabrication

The contact angle of water on the hydrophobic surface was measured to examine the hydrophobicity of the barrier. If the water contact angle was greater than 90° , then the surface was considered to be hydrophobic (193, 194). The test revealed that the contact angle of the water droplet was 107.4° , indicating that hydrophobic properties were formed on the paper, as shown in Figure 52A. Hydrophobicity of the paper was further confirmed by the comparison of both the hydrophobic and hydrophilic regions images that were obtained using a microscope ($5\times$ magnification). As shown in Figure 52B, the investigation showed that the dye solution could not penetrate into the hydrophobic region because of the epoxy resin barrier. Figure 52C shows examples of the optical images of the μ PADs, and observed that the epoxy resin hydrophobic barriers allowed the dye solution to flow without any leakage. Furthermore, μ PAD pattern was constructed with well-defined hydrophobic barriers, and their resolutions were also studied. To determine the minimum resolution of the epoxy resin screen-printing method, the patterns were designed to include different channel widths for sample transfer (Figure 52D). After fabrication, 8 μ L of dye solution was dropped onto the paper to allow the observation of the hydrophobic and hydrophilic zones. The parallel lines with increasing thickness represent the epoxy resin hydrophobic barriers (0.1 to 1.4 mm). As shown, the hydrophilic channels from 0.1–0.5 mm were observed but the solvent could not flow all the way through the lines. Thus, the narrowest hydrophobic barrier by the epoxy resin screen printing method to deliver an aqueous sample, was 0.6 mm. To evaluate the reproducibility of the fabrication of the hydrophilic channels, 20 pieces of paper ($n = 20$) with circular hydrophilic diameters of 5 and 6 mm, were fabricated by the epoxy resin screen-printing method under optimal conditions. The mean diameter of the circles were 5.13 ± 0.11 mm (%RSD 2.09), and 6.13 ± 0.10 mm (% RSD = 1.67), respectively. These results indicated that the epoxy resin screen-printing method has good reproducibility.

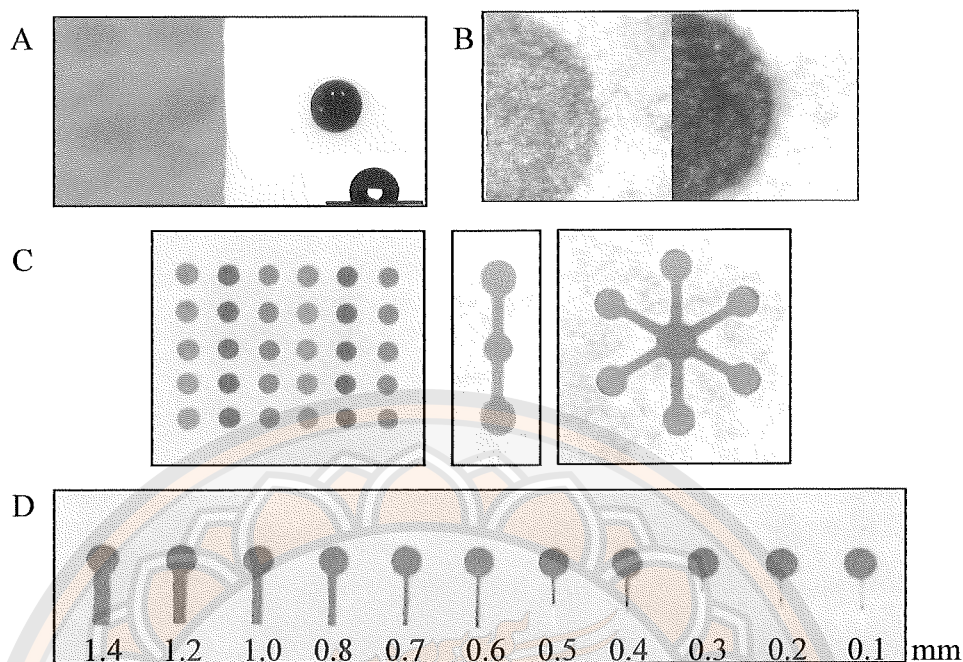


Figure 52 Hydrophilic-hydrophobic contrast on the paper: A) comparison of hydrophilic and hydrophobic regions of the paper after applying a drop of dye solution and water contact angle on the hydrophobic region, B) a comparison of the hydrophilic and hydrophobic areas imaged with a microscope (5×magnification), C) examples of μ PADs with epoxy resin barriers fabricated using the screen printing method, D) a pattern of hydrophilic lines with different channel widths of 0.1, 0.2, 0.3, 0.4, 0.5, 0.6, 0.7, 0.8, 1.0, 1.2, and 1.4 mm were immersed in a dye solution.

1.3 Chemical compatibility

Chemical compatibility is an important parameter that needs to be defined when a new hydrophobic barrier is proposed for the μ PADs. The proposed epoxy resin barrier was tested by exposing it to 16 common reagents that were aqueous solutions containing surfactants (1% w/v of Triton X-100, CTAB, and SLS), organic solvents (methanol, ethanol, toluene, hexane, and heptane), salts (2 mol L⁻¹ ammonium chloride and sodium chloride), acids (2 mol L⁻¹ sulfuric, nitric and hydrochloric acids) and bases (2 mol L⁻¹ sodium hydroxide, potassium hydroxide, and ammonium hydroxide), and their compatibility with the barrier was evaluated by

visual inspection of the hydrophilic circles, to see if it remained effective. The results in Figure 53 showed that the epoxy resin formed solid hydrophobic barriers which performed well in containing all of the tested organic and inorganic solvents, but was not resilient to any of the three surfactants (Triton X-100, CTAB, and SLS) that were tested. These findings are particularly interesting given that acid, base and neutral solutions are the most utilized inorganic aqueous solutions for colorimetric detection, while organic solvents are also commonly used in extraction experiments. The μ PAD that was fabricated from epoxy resin are better than the beeswax and UV resin ones shown in chapter III, and IV, as well as solid wax (20, 70, 81, 210) that was proposed by many researchers.

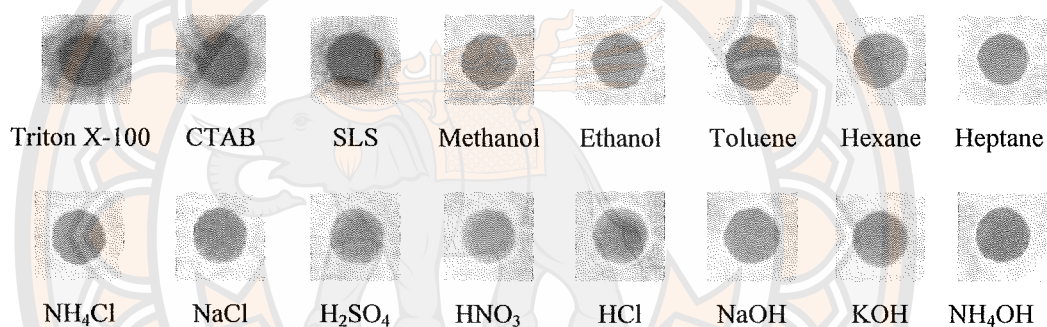
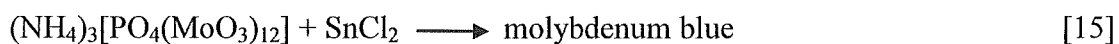
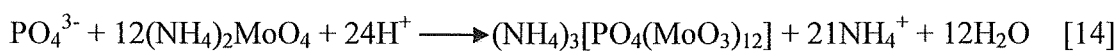


Figure 53 Epoxy resin barriers with some surfactants, organic, and inorganic solvents. Images of the circles on the μ PADs after contact with a green dye solution of different solvents.

2. Effect of the molybdenum blue method on 3D PADs

The colorimetric detection of phosphate was based on the molybdenum blue method. While the molybdenum blue reaction was occurring, the phosphate reacted with the ammonium molybdate and formed the phosphomolybdenum complexes. These were then reduced by stannous chloride which formed the molybdenum blue complex (equation 14–15). In order to determine the optimum conditions conducive to the molybdenum blue method on the 3D PAD, various concentrations of the three critical chemicals in the reaction were evaluated, along with various reaction times. The goal is to obtain high color intensity when the phosphate concentration is 40 mg L^{-1} , which was the concentration of the test sample used.



2.1 Effect of ammonium molybdate concentrations

The ammonium molybdate concentrations play a significant role in the formation of the phosphomolybdenum blue complex. In order to determine the effect of ammonium molybdate, various concentrations of it ranging from 2–8 % w/v were applied onto the paper-based devices. The results showed that the color intensity of the phosphate was increased when the concentrations of ammonium molybdate were raised to 4% w/v, and then started to decline (Figure 54). Therefore, a concentration of 4% w/v of ammonium molybdate was selected for the determination of phosphate.

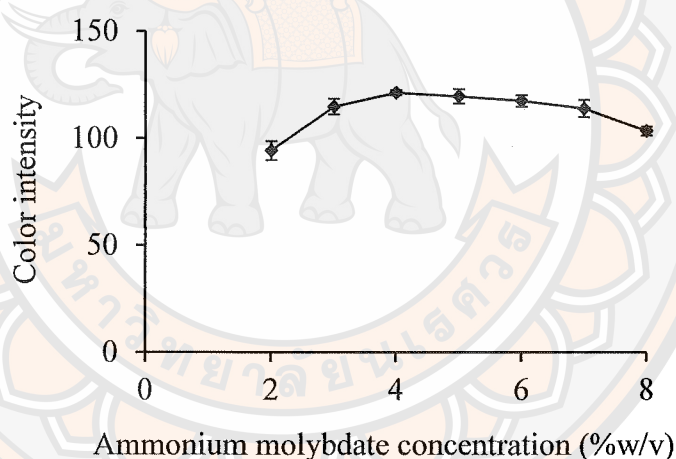


Figure 54 The effect of ammonium molybdate concentrations

2.2 Effect of sulfuric acid concentrations

The effect of sulfuric acid concentrations at 0.5–8.0 mol L⁻¹ were studied. As can be observed in Figure 55, the color intensity of the phosphate increased when the sulfuric acid concentration was set to 4 mol L⁻¹, and then rapidly decreased at higher levels of acidity. This was mainly due to the fact that at high acidity the formation of phosphomolybdenum blue complex decreased. Therefore, 4 mol L⁻¹ of sulfuric acid was used as the optimal concentration.

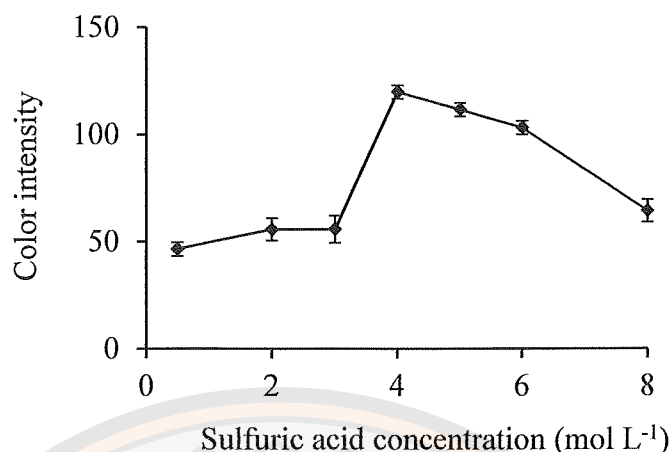


Figure 55 The effect of sulfuric acid concentrations

2.3 Effect of stannous chloride concentrations

In the molybdenum blue method, the reducing agent reduced the phosphormolybdic acid thereby forming the phosphormolybdenum blue. Hence the formation of the phosphormolybdenum was also dependent on the concentration of the reducing agent. Stannous chloride has been used as a reductant, especially for the determination of phosphate in soil, because of its rapid reaction, high sensitivity and its absorptivity is greater than that of ascorbic acid (23, 209). The effect of stannous concentrations in the range of 0.05–0.6 % w/v were also studied. As shown in Figure 56, the color intensity of the phosphate increased by raising the stannous chloride concentration to 0.2% w/v and remained almost constant at higher amounts. Therefore, 0.2% w/v of stannous chloride was used as the optimal concentration for complete color development.

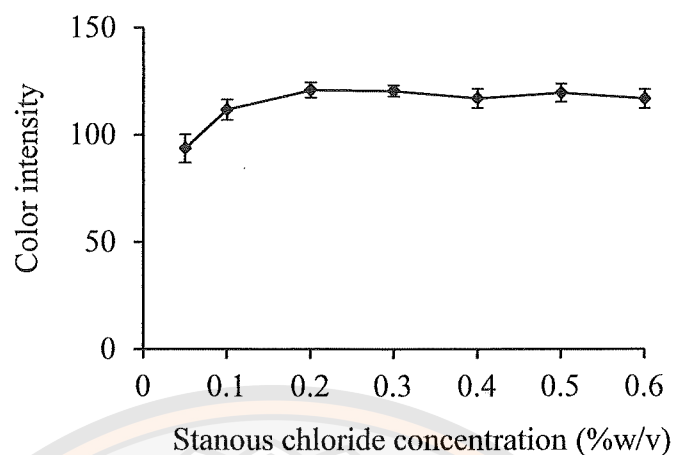


Figure 56 The effect of stannous chloride concentrations

2.4. Effect of the reaction time

The effect of the reaction time was studied in the range of 3–40 min. As shown in Figure 57, the rate of the blue formation gradually increased until the maximum intensity was observed at 10–15 minutes, after which it started to decrease. This may be due to the dissociation of the phosphor molybdenum blue complex. Therefore, 10 minutes was chosen as the optimal reaction time for the phosphate analysis.

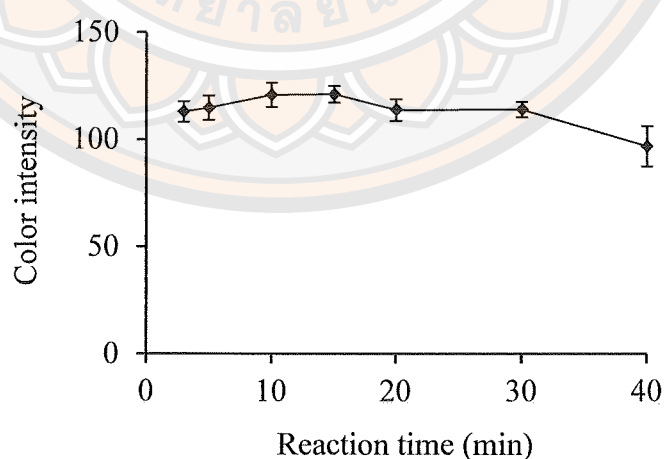


Figure 57 The effect of reaction time on color intensity

The optimum concentration of ammonium molybdate, sulfuric acid, and stannous chloride were found to be 4% w/v, 4 mol L⁻¹, and 0.2% w/v for phosphate determination, respectively. The analysis of the reaction using this method was obtained in 10 min.

3. Effect of interference

The influence of interferences was investigated by combining a standard phosphate solution with the six interfering compounds. It was therefore important to study these interferences to ensure that the autonomous platform could achieve successful analytical results in varying sample matrices. The constituents of soil that are commonly found include nitrate, ammonium, potassium, iron, manganese, copper, and calcium were examined throughout their range of concentrations, while the phosphate was fixed at 40 mg L⁻¹. The interference effects of various common ions at 100 mg L⁻¹ were studied, and the results obtained are shown in Figure 58. The results showed that no significant change in the color intensity resulted for any of the ions. All interference recovery deviations were smaller than 5% (0.75–2.75%), and indicated that all the ions did not interfere with the determination of the phosphate.

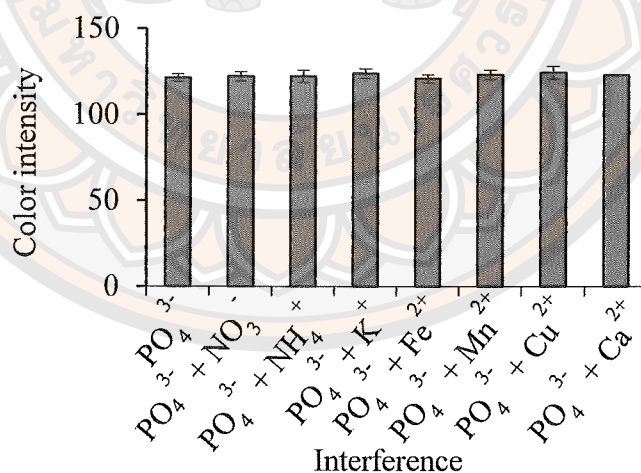


Figure 58 The effect of interfering ions on the determination of 40 mg L⁻¹ phosphate using 3D PADs. The concentrations of interfering ions were 100 mg L⁻¹ for NO₃⁻, NH₄⁺, K⁺, Fe²⁺, Mn²⁺, Cu²⁺, and Ca²⁺.

4. Analytical performance

The analytical features of the 3D PAD including the linear range of the calibration curve, limit of detection, precision, and accuracy were investigated. The linearity of the calibration curve was found to be 0.5–40 mg L⁻¹ with a correlation coefficient of 0.9920 (Figure 59). The detection limit was determined to be 0.25 mg L⁻¹, and the limit of quantification was found to be 0.83 mg L⁻¹. To evaluate the precision of the 3D PADs, intra-repeatability (n = 6) and inter-reproducibility (5 days) were measured, both using a phosphate concentration of 10, 20, and 40 mg L⁻¹, and expressed as %RSD. The % values of RSD for repeatability and reproducibility were 1.52–2.46 and 1.89–2.74, respectively, indicating high precision.

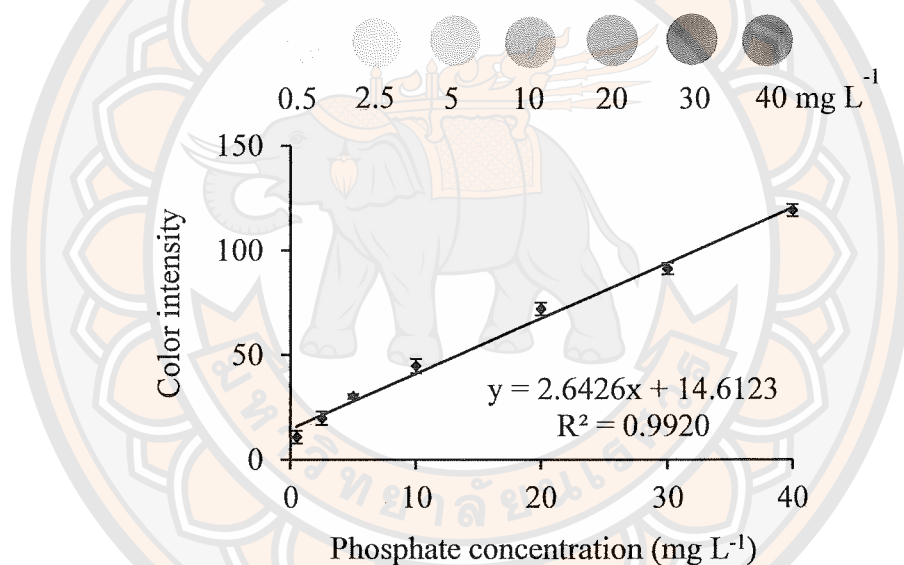


Figure 59 Calibration curve of phosphate

5. Stability of the μ PAD

The proposed μ PADs were individually kept in vacuum sealed bags up to 30 days at temperatures $\leq 2^\circ\text{C}$. The stability of the 3D PAD was evaluated by determining the amount of phosphate every 3 days. The color intensity of phosphate detection was observed to stabilize in about 15 days, and then leveled off after that (Figure 60). The one-way ANOVA showed that there were no statistically significant difference over 30 days of storage ($F = 2.53$, $F_{\text{critical}} = 3.35$). Therefore, the devices can be stored for 15 days.

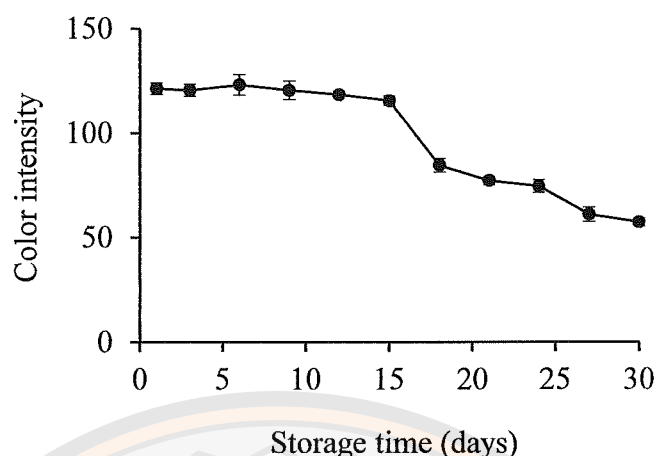


Figure 60 The effect of the stability of the 3D PADs stored at 2°C

6. Sample analysis

The accuracy of the proposed 3D PADs was checked by using the spiked standard, which was then validated by employing the spectrophotometric method. The soil samples were pretreated according to the published method (171), and then the developed device was applied for the determination of phosphate in these samples, and the results are summarized in Table 13. These samples were spiked with 40 mg L⁻¹ of phosphate, and the analytical recoveries were in the acceptable range of 88.8–101.0% and exhibited precisions of RSD in the range of 0.9–3.1%, which indicated that the proposed method was reliable. To demonstrate the accuracy of the proposed method, the concentrations of phosphate found in the soil samples were compared to those obtained from the spectrophotometric method. Therefore, in order to validate the proposed method, a comparison between both the methods was carried out, by using the paired t-test. Statistical analysis of the data showed no significant difference between the two methods ($t_{\text{stat}} = 2.11$, $t_{\text{critical}} = 2.23$), with a confidence level of 95%. Thus, the fabrication of the 3D PAD by the proposed method, demonstrated enormous potential for the determination of phosphate in the soil samples.

Table 13 Comparison of phosphate detection results from soil samples using the 3D PAD versus the spectrophotometric method

Sample	Added (mg kg ⁻¹)	3D PAD		Spectrophotometric method	
		Found (mg kg ⁻¹)	Recovery (%)	Found (mg kg ⁻¹)	Recovery (%)
Soil 1	0.0	42.1 ± 4.1	—	34.1 ± 8.8	—
	500.0	489.8 ± 8.1	89.5 ± 1.0	497.8 ± 6.9	92.7 ± 3.1
Soil 2	0.0	28.3 ± 9.0	—	27.8 ± 8.9	—
	500.0	496.8 ± 10.6	97.4 ± 3.5	503.1 ± 5.8	95.1 ± 1.5
Soil 3	0.0	ND	—	5.0 ± 4.3	—
	500.0	500.1 ± 6.6	101.0 ± 1.3	506.3 ± 2.4	102.8 ± 1.9
Soil 4	0.0	38.4 ± 2.1	—	42.3 ± 22.6	—
	500.0	491.4 ± 13.0	90.6 ± 2.6	500.6 ± 6.9	91.1 ± 5.9
Soil 5	0.0	47.6 ± 9.5	—	48.9 ± 11.3	—
	500.0	491.6 ± 15.3	88.8 ± 3.3	496.3 ± 8.5	89.5 ± 4.0
Soil 6	0.0	31.5 ± 3.3	—	33.4 ± 5.9	—
	500.0	490.9 ± 9.4	93.2 ± 2.4	491.5 ± 4.8	91.6 ± 2.0

ND = Not detected

A comparative study of different μ PADs from the literature is presented in Table 14, showing that the molybdenum blue method combined with stannous chloride described here has advantages such as: 1) a wide range and good detection limit; 2) a shorter reaction time (10 min); 3) a stability better than ascorbic acid in the reducing layer (23); and 4) more simple, cost-effective, and rapid.

Table 14 Comparison of the features of the proposed μ PADs with those of other reported methods for phosphate determination

Colorimetric assay	Sample	Linear range	LOD	Reaction time (min)	Reference
Molybdenum blue method combined with ascorbic acid	Water	0.2–10 mg L ⁻¹	0.05 mg L ⁻¹	40	(23)
Molybdenum blue method combined with ascorbic acid	Vegetable	—	0.86 μ g mL ⁻¹	30	(158)
Molybdenum yellow method	Water	1–20 mg mL ⁻¹	—	—	(211)
Molybdenum blue method combined with ascorbic acid	Seawater	1–10 mg kg ⁻¹	1.3 and 2.8 mg kg ⁻¹	4	(212)
MS-AgNPIS	Soil and water	1–30 mg L ⁻¹	0.33 mg L ⁻¹	3	(159)
Molybdenum blue method combined with stannous chloride	Soil	0.5–40 mg L ⁻¹	0.25 mg L ⁻¹	10	This work

Conclusions

A novel hydrophobic material for the fabrication of a 3D PAD was proposed by using epoxy resin, in conjunction with the screen-printing method. The fabrication was performed by using a single process at room temperature, which did not require complicated and expensive instruments. This method was simple, fast, solvent free, inexpensive, and had a high production rate. The use of a 3D PAD for the colorimetric detection of phosphate in soil samples has been demonstrated herein by carrying out the molybdenum blue method. The results of the 3D PAD were compared to the spectrophotometric method and good agreement was observed. Therefore, the

developed molybdenum blue method with reducing agent stannous chloride can be used as an alternative method to the existing one for phosphate determination involving reducing agent, ascorbic acid (23). The developed 3D PAD is simple, fast, portable, and disposable.



CHAPTER VI

INDIRECT DETERMINATION OF POTASSIUM BY EXTRACTION WITH DIBENZO-18-CROWN-6 AND CALMAGITE USING PAPER-BASED PLATFORM IN CONJUNCTION WITH SMARTPHONE

Introduction

Potassium (K) is an essential nutrient for healthy growth, development of plants, and one of the three main macronutrients together with nitrogen and phosphorus (213-215). It plays a vital role in plant physiological and metabolic processes including photosynthesis, plant growth, metabolism, rate of assimilation, accumulation of sugars, and provides resistance against biotic and abiotic stresses (216-217). Potassium exists in soil in different forms, which are water-soluble, exchangeable, nonexchangeable, and mineral (218). These four forms of potassium give a general representation of the potential sources for plant available potassium, but no distinct boundaries exist among them. The soil solution potassium is readily taken up by the plants root system, which is readily replenished by soil exchangeable potassium (219, 220). Non-exchangeable potassium become exchangeable when solution and exchangeable potassium are depleted by plant removal, leaching, or exchange reactions with other cations. However, mineral potassium is the major proportion of total potassium in soils, is regarded as slowly available to plants via long-term soil weathering (221). Distribution of potassium among mineral forms also occurs when it is added to the soil as fertilizer, manure, or crop residues. The requirement of available potassium for most field crops, range from 60 to 120 ppm. The high level of potassium affects the germination of seeds, and inhibit uptake of other useful minerals, whereas potassium deficiency causes plants to be more sensitive to drought, frost, high salt content, restricted growth, spotting, curling of leaves, reduced flowering, low yields and poor quality products (214, 222). Continuous planting, depletes the soils potassium and requires fertilizers to obtain crop yields of good quality. The application of sufficient quantities of plant nutrients is essential to

increase agricultural productivity, economic return, and reduce negative environmental impact. In the effective fertilization of agricultural fields, agriculturists should know the concentration of soil nutrients before adding fertilizer to meet the nutrition requirements of the crops. Considering the level of potassium for different crops, monitoring its content in the soil is necessary to optimize the use of fertilizers. Therefore, the development of a highly selective test for potassium is extremely important for soil analysis.

To date, a variety of techniques have been employed to detect potassium, such as atomic absorption spectroscopy (AAS), inductively coupled plasma mass spectroscopy (ICP-MS), ion chromatography, UV-Vis spectrometry, and electrochemistry. However, these conventional methods are complex, time consuming, requires expensive instrumentation, generally large in size and elaborate laboratory setup. Therefore, it is necessary to develop new device for potassium detection. The colorimetric detection method for analytes of potassium has been extensively used, including the counter ion (223-224), gold nanoparticles (AuNPs) (165, 225-229) and ionophore (166, 230-232) reaction. For example, Escobar et al. 1989, and Dadfarnia et al. 1992 (223-224) reported the methods for determination of potassium by using spectrophotometric method. This method using dibenzo-18-crown-6, and counter ion (bromothymol blue and camagite) for determination of potassium and its application for fruits and beverage, and biological fluids, respectively. Next, Naderi et al., 2018 (229) developed AuNPs and a cationic dye in an aptasensor system for the colorimetric detection of potassium, was distinguishable by different colors (between orange and green) appeared after reaction. Cationic dye acts as a new aggregator for AuNP based sensors which changes the aggregated AuNP solution color from blue-purple to green. In the presence of potassium, the aptamer dissociated from the surface of the AuNP so that free AuNPs and cationic dye make the solution green. The aptasensor has a wide linear range from 10 nM to 50 mM. Recently, Qiu et al., 2019 (165) developed a detection method for potassium by using crown ether (4-aminobenzo-18-crown-6, ABC) modified AuNPs. The sensor exhibited a linear response to potassium from 0 to 200 μ M. Although the colorimetric detection has the advantage being simple, rapid, and high sensitivity, it has the disadvantages of requiring synthesis enzymes, complicated operation, and large amount of chemicals.

Therefore, the development of enzyme-free colorimetric method that use small amounts of chemicals volume for easy detection of potassium, is still preferred for field applications.

The purpose of this study was to develop a new and simple colorimetric assay using a paper-based platform coupled with smartphone for determination of potassium in soil. The method for the indirect determination of potassium based upon the ion-pair extraction of potassium ion into dichloromethane by using dibenzo-18-crown-6 and an excess amount of calmagite as counter ion. When the extraction was complete, the remaining calmagite in aqueous phase was examined on a paper-based platform and digitized with a smartphone, without the need of expensive analytical instruments. A decrease in color intensity for dyes was proportional to the amount of potassium present. The proposed method is novel, simple, rapid, and require only small volume of chemicals.

Experimental

1. Chemicals

All chemicals used in the study were analytical grade or better, and deionized water (DI water) was used in the preparation of all solutions in the experiments. Potassium chloride was purchased from Ajax (Finechem, Australia). Dibenzo-18-crown-6 was purchased from Sigma-Aldrich (Castle Hill, NSW, Australia). Ethylenediaminetetraacetic acid (EDTA) and lithium hydroxide were purchased from Loba Chemie (India). Acetic acid, glacial was purchased from Macron chemicals (China). Congo red, malachite, methyl orange, bromophenol blue, bromothymol blue, calmagite were purchased from Carlo Erba (Italy).

2. Apparatus

Whatman Grade 1 and Grade 5 qualitative filter paper were purchased from Whatman International, Ltd. (Buckinghamshire, UK). The stencil screen, made with polyester fabric on a wooden frame (35 cm x 45 cm) was custom ordered from a local screen-printing shop (Phitsanulok, Thailand). An Apple iPhone 7S plus with RGB color value application was used for colorimetric analysis. A photo light box was made from wood with LED lights (15x15x15 cm; width x length x height). A shaking water bath (Daihan Scientific, Switzerland) was used to extract phosphate from soil.

A synergy H1 hybrid multi-mode microplate reader (BioTex, Vermont, USA) was used for the reference spectrophotometric method.

3. Preparation of solutions

3.1 Potassium stock solution (1000 mg L⁻¹)

The potassium stock solution was prepared by dissolving 0.1912 g of potassium chloride to 100 mL using DI water in a volumetric flask.

3.2 Potassium standard solution (20–120 mg L⁻¹)

The potassium standard solution with concentrations of 20, 40, 60, 80, 100, and 120 mg L⁻¹ were prepared by 2, 4, 6, 8, 10, and 12 mL of 100 mg L⁻¹ potassium standard solution to 100 mL using DI water in a volumetric flask, respectively.

3.3 Dibenzo-18-crown-6 (0.1–0.8% w/v)

The dibenzo-18-crown-6 with the concentrations of 0.1, 0.2, 0.4, 0.6, 0.8, 1.0% w/v were prepared by dissolving 0.10, 0.20, 0.40, 0.60, 0.80, 1.00 g of dibenzo-18-crown-6 in 100 mL of dichloromethane.

3.4 Bromothymol blue (0.04% w/v)

The bromothymol blue with the concentration of 0.04% w/v was prepared by dissolving 0.04 g of bromothymol blue in 10 mL of ethanol and diluting to 100 mL with DI water.

3.5 Calmagite (0.02% w/v)

The calmagite with the concentration of 0.02% w/v was prepared by dissolving 0.02 g of calmagite in 10 mL of ethanol and diluting to 100 mL with DI water.

3.6 Buffer pH 3.5

Buffer with a pH of 3.5 was prepared by mixing EDTA (0.20 g), lithium hydroxide (0.22 g) and glacial acetic acid (1.80 ml) in 100 mL DI water.

3.7 Buffer pH 5

Buffer with a pH of 5 was prepared by mixing EDTA (0.20 g), lithium hydroxide (0.48 g) and glacial acetic acid (1.3 ml) in 100 mL DI water.

4. Preparation of the paper-based platform

The pattern was first designed using the Microsoft word software (Figure 61). The filter paper was placed under the blocking stencil, and then 20 mL of the solution of epoxy resin in curing agent at 2:1 v/v was poured onto the stencil and distributed using a squeegee. The epoxy resin solution needed to penetrate to the bottom of the filter paper. The patterned papers were then curing at room temperature for overnight. After curing, the patterned papers were ready to use.

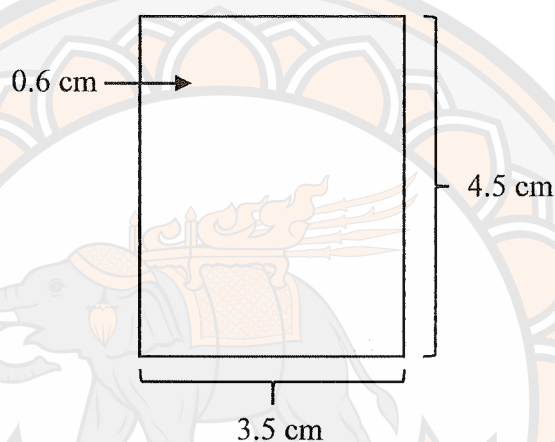


Figure 61 Pattern of paper-based platform

5. Optimization of ion-pair extraction conditions

The objective of this part of the work was to investigate the effect of the variables that impose on the ion-pair extraction process involved in the indirect determination of potassium. The four parameters are the selection of counter ion, pH of solution, concentration of dibenzo-18-crown-6, and the reaction time, were optimized to provide the lowest values of color intensity of remaining dyes in aqueous.

5.1 Selection of counter ion

300 μL of 20 and 120 mg L^{-1} potassium were added to 300 μL of each buffer with a pH of 3, 5, and 7. Then, 300 μL of 0.1% w/v dibenzo-18-crown-6, and 100 μL of 0.04% w/v congo red, malachite, methyl orange, bromophenol blue, bromothymol blue, and calmagite were added. The solutions were shaken, then the water phase was allowed to separate from the organic layer for 10 minutes.

5.2 pH of solution

For bromothymol blue; 300 μL of potassium solution at concentrations of 20, 40, 60, 80, 100, and 120 mg L^{-1} were added into 300 μL of the buffer with a pH of 3, 3.5, 4, 4.5, 5, 5.5, and 6. Then, 300 μL of 0.1% dibenzo-18-crown-6 and 100 μL of 0.04% w/v bromothymol blue were added. The solutions were shaken, then the water phase was allowed to separate from the organic layer for 10 minutes. After that, the water phase was measured at 430 nm by using a spectrophotometer.

For calmagite; 300 μL of potassium solution at concentrations of 20, 40, 60, 80, 100, and 120 mg L^{-1} were added into 300 μL of the buffer with a pH of 3, 3.5, 4, 4.5, 5, 5.5, and 6. Then, 300 μL of 0.1% dibenzo-18-crown-6 and 100 μL of 0.02% w/v calmagite were added. The solutions were shaken, then the water phase was allowed to separate from the organic layer for 10 minutes. After that, the water phase was measured at 530 nm by using a spectrophotometer (Figure 62).

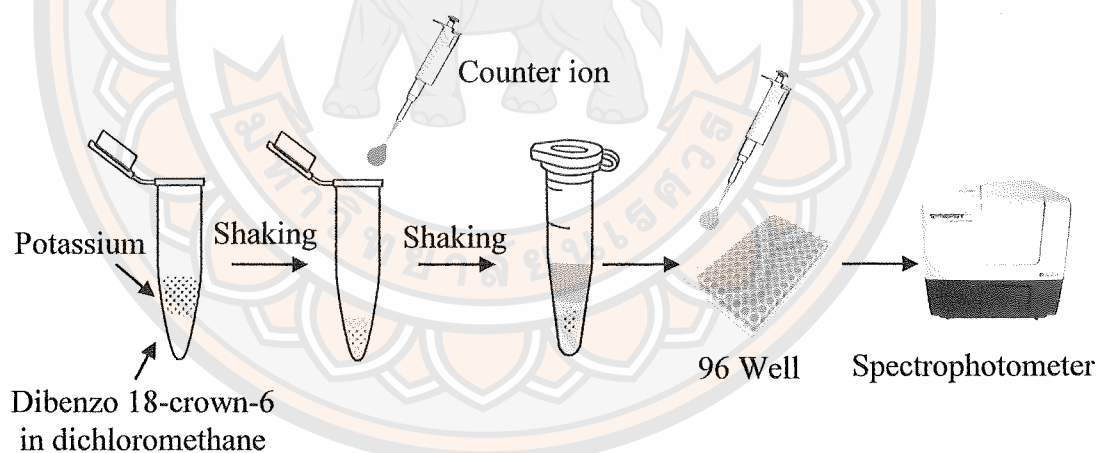


Figure 62 Process for the detection of potassium by using spectrophotometric method

5.3 Concentration of dibenzo-18-crown-6

For bromothymol blue; 300 μL of potassium solution at a concentration of 120 mg L^{-1} was added into 300 μL of the buffer with a pH of 5. Then, 300 μL dibenzo-18-crown-6 with concentrations in the range of 0.025–1.0% w/v and 100 μL of 0.04% w/v bromothymol blue were added. The solutions were shaken,

then the aqueous phase was allowed to separate from the organic layer for 10 minutes. After that, the aqueous phase was measured at 430 nm by using a spectrophotometer.

For calmagite; 300 μL of potassium solution at a concentration of 120 mg L^{-1} was added into 300 μL of the buffer with a pH of 3.5. Then, 300 μL dibenzo-18-crown-6 with concentrations in the range of 0.025–1.0% w/v and 100 μL of 0.02% w/v calmagite were added. The solutions were shaken, then the water phase was allowed to separate from the organic layer for 10 minutes. After that, the water phase was measured at 530 nm by using a spectrophotometer.

5.4 Reaction time

The experiments were carried out according to the procedures described in section 5.3, with the reaction times of 5, 10, 15, 20, 30, 40, 50, and 60 minutes. The dibenzo-18-crown-6, and bromothymol blue were set at 0.2% w/v, and 0.4% w/v, respectively, whereas the dibenzo-18-crown-6, and calmagite were set at 0.8% w/v, and 0.02% w/v, respectively.

6. Interference

The experiments were carried out using 300 μL of 100 mg L^{-1} NaCl, CuNO_3 , PbNO_3 , FeNO_3 , and MnNO_3 according to the procedures described in section 5.3, under optimum conditions.

7. Application to paper-based platform with smartphone readout

The proposed method for potassium detection was applied to paper-based platform couple with smartphone. The validation parameters included linearity, LOD, LOQ, precision, and accuracy, were evaluated under selected conditions.

7.1 Linearity

For bromothymol blue: 300 μL of potassium standard solution at concentrations of 20, 40, 60, 80, 100, and 120 mg L^{-1} were added into 300 μL of the buffer with a pH of 5. Then, 300 μL dibenzo-18-crown-6 with concentrations in the range of 0.2% w/v and 100 μL of 0.4% w/v bromothymol blue were added. The solutions were shaken, then the aqueous phase was allowed to separate from the organic layer for 10 minutes. After that, 5 μL of aqueous phase were dropped onto the circular areas on the paper-based platform, then photographed with a smartphone (iPhone 7s plus, Apple Inc.) in a photo light box. The images were then imported to RGB color value

software for measurement of their mean color intensities. A graph was produced to plot the linearity between the color intensity and the concentrations of potassium.

For calmagite: 300 μL of potassium standard solution at concentrations of 20, 40, 60, 80, 100, and 120 mg L^{-1} were added into 300 μL of the buffer with a pH of 3.5. Then, 300 μL dibenzo-18-crown-6 with concentrations in the range of 0.8% w/v and 100 μL of 0.02% w/v calmagite were added. The solutions were shaken, then the aqueous phase was allowed to separate from the organic layer for 10 minutes. After that, 5 μL of aqueous phase were dropped onto the circular areas on the paper-based platform, then photographed with a smartphone (iPhone 7s plus, Apple Inc.) in a photo light box. The images were then imported to RGB color value software for measurement of their mean color intensities. A graph was produced to plot the linearity between the color intensity and the concentrations of potassium (Figure 63).

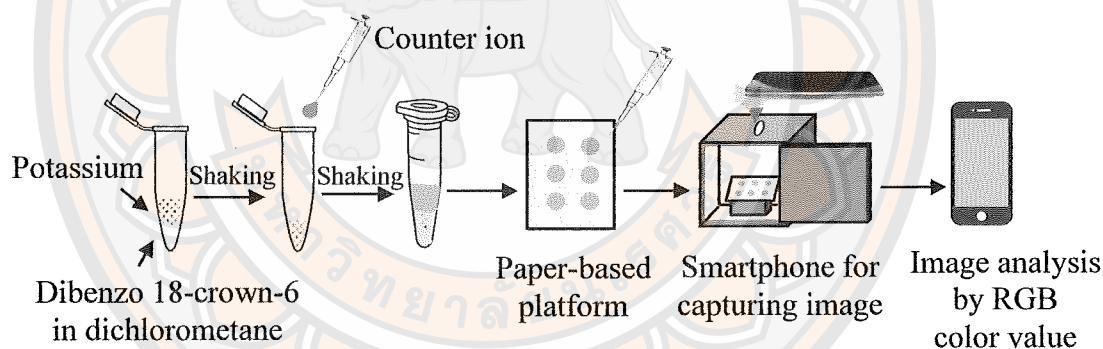


Figure 63 Process for the detection of potassium by using paper-based platform with smartphone readout

7.2 LOD and LOQ

The experiment was carried out according to the procedure as described in a section 7.1 under optimum conditions. The DI water was analyzed by using calmagite as counter ion in 10 replicates. The SD of the response and the slopes of the concentration curves of the calibration curves were used to estimate the LOD ($3\sigma/\text{slope}$) and LOQ ($10\sigma/\text{slope}$).

7.3 Precision

Evaluation of method repeatability (intraday precision) and reproducibility (interday precision) were performed. The potassium standard solution at the concentrations of 20, 60, and 100 mg L⁻¹ was analyzed. The experiment was carried out according to the procedure described in a section 7.1 under optimum conditions. Intraday precision was determined from six replications within 1 day, and the interday precision was analyzed in six replications on 5 days.

7.4 Accuracy and Recovery

Accuracy was evaluated across the specified range of the analytical procedure by a recovery study. The standard solution of the potassium was spiked into the soil samples extract in triplicate. The experiment was carried out according to the procedure described in a section 7.1 under optimum conditions. The recovery was determined as follows: (total potassium amount – original potassium amount in real sample)/potassium amount of added.

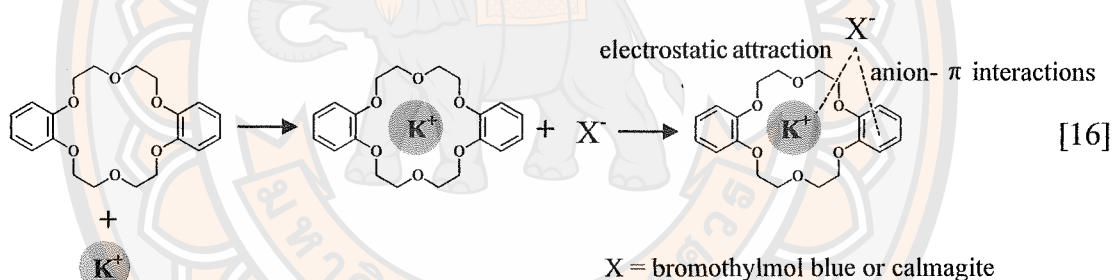
8. Application in real samples

The paper-based platform was applied to the determination potassium in soil. Seven soil samples were collected from rice fields in five provinces of Thailand: Phitsanulok, Sukhothai, Khamphaeng Phet, Sa Kaeo, and Ubon Ratchathani. All soil samples were dried in the open-air to remove the moisture, and then sieved to a particle size of 2 mm.

To validate the accuracy of the proposed method, 5.0 g of the soil sample was added in 7 centrifuge tubes. Then, 6 of the 7 samples were spiked with 0.5, 1.0, 1.5, 2.0, 2.5, and 3.0 mL of potassium standard solution to achieve concentrations of 20, 40, 60, 80, 100, and 120 mg L⁻¹, respectively. After that, adjusted to 25 mL of DI water and shaken for 15 min. The mixture was filtered through a filter paper (Whatman #5). The filtrate was then carried out according to the procedure as described in a section 7.1. The results from the paper-based platform were compared to spectrophotometry.

Results and discussion

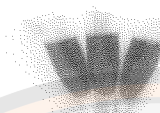

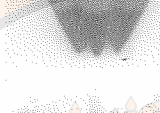
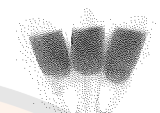
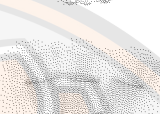

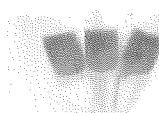

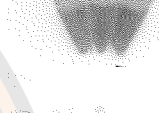

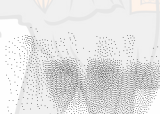




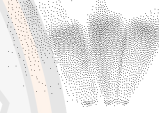

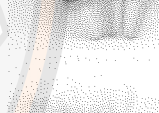
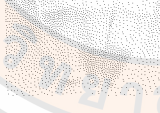
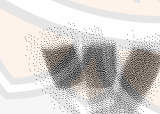

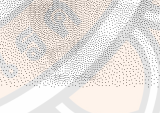


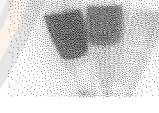
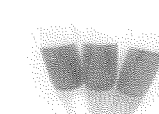

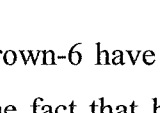
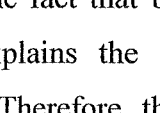
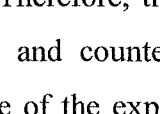
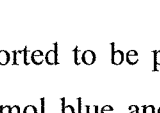
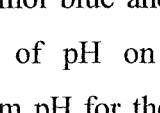
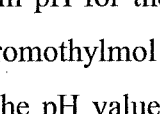
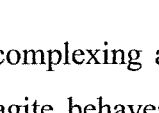
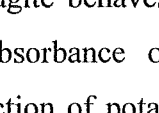
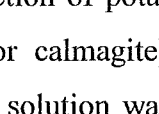
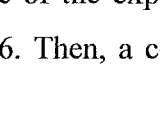


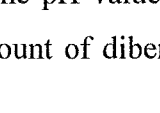


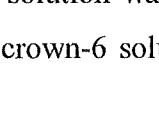


The indirect determination of potassium based on the ion-pair extraction of potassium ion into dichloromethane by using dibenzo-18-crown-6 and an excess amount of dyes (bromothymol blue or calmagite) as counter ion. It is well known that K^+ , which has a radius of 133 pm, fits very well into the cavity of 18-crown-6 (233). While in the presence of potassium and dibenzo-18-crown-6, K^+ can be well chelated with dibenzo-18-crown-6. Then when an excess dye was added, ion-pair formed between the positively charged of dibenzo-18 crown-6 - K^+ complex and dye anion through the electrostatic attraction and anion- π interactions (233), as shown in equation 16, and extracted into dichloromethane. When the extraction was complete, the remaining dye in aqueous phase was examined on a paper-based platform and digitized with a smartphone. A decrease in color intensity for dyes was proportional to the amount of potassium present, allowing the amount of potassium to be calculated.



1. Effect of selection of counter ions

Several colored dyes, including congo red, malachite, methyl orange, bromophenol blue, bromothymol blue, and calmagite, were used as counter ions. As shown in Table 15, the color intensity of congo red, malachite, methyl orange and bromophenol blue in both aqueous and organic phase with concentration of 20 and 120 mg L⁻¹ at all the pH levels, did not change when compared with the blank one. While the color intensity of bromothymol blue and calmagite changed at pH 3, 5, and 7. Therefore, bromothymol blue and calmagite, which are the anionic chromophoric reagents, were studied as counter ion for the ion pair extraction of potassium using dibenzo-18 crown-6.

Table 15 Comparison of potassium detection results by using varied counter ions at various pH levels

Counter ions	pH 3			pH 5			pH 7		
	Blank	20	120	Blank	20	120	Blank	20	120
Congo red									
Malachite									
Methyl orange									
Bromophenol blue									
Bromothymol blue									
Calmagite									

2. Effect of pH

Dibenzo-18-crown-6 have been reported to be proton complexing agents and this, together with the fact that bromothymol blue and calmagite behaves as a weak acid, probably explains the influence of pH on the absorbance of the dichloromethane extract. Therefore, the optimum pH for the extraction of potassium with dibenzo-18-crown-6 and counter ion (bromothymol blue or calmagite) was investigated. In the course of the experiment, the pH value of the solution was first adjusted to a range of 3–6. Then, a certain amount of dibenzo-18-crown-6 solutions

and counter ions (bromothymol blue or calmagite) were added into the potassium solutions with different pH values, and the reaction time lasted for 5 min. The absorbance of remaining dye in aqueous phase was measured by spectrophotometer for indirect determination of potassium. A graph plotted between absorbance and concentrations of potassium were constructed to find the linearity. The obtained linearity and correlation coefficient are shown in Table 16. When the pH is 5, and 3.5 for bromothymol blue and calmagite, respectively, the results showed the highest linearity. Therefore, a pH of 5 and 3.5 was chosen as the optimal for the detection of potassium by using bromothymol blue and calmagite, respectively.

Table 16 The effect of pH on linearity of potassium

pH	Bromothymol blue	Calmagite
3	$y = -6E-06x + 0.0625$ $R^2 = 0.0021$	$y = -0.001x + 0.5889$ $R^2 = 0.6926$
3.5	$y = -0.0001x + 0.0731$ $R^2 = 0.6791$	$y = -0.0013x + 0.6186$ $R^2 = 0.9935$
4	$y = -0.0002x + 0.0844$ $R^2 = 0.8437$	$y = -0.0009x + 0.5994$ $R^2 = 0.8161$
4.5	$y = -0.0009x + 0.1642$ $R^2 = 0.9511$	$y = -0.001x + 0.6278$ $R^2 = 0.5357$
5	$y = -0.001x + 0.1773$ $R^2 = 0.9858$	$y = -0.0011x + 0.6506$ $R^2 = 0.7567$
5.5	$y = -0.001x + 0.1818$ $R^2 = 0.9785$	$y = -0.001x + 0.6718$ $R^2 = 0.6863$
6	$y = -0.0011x + 0.2017$ $R^2 = 0.8841$	$y = -0.0017x + 0.7059$ $R^2 = 0.9772$

3. Effect of the dibenzo 18-crown-6 concentrations

The concentration of dibenzo-18-crown-6 for the extraction of potassium was varied from 0.025 to 1% w/v. Figure 64 shows how increasing dibenzo-18-crown-6 concentration caused decreasing absorbance of remaining dye in aqueous phase down to 0.2 and 0.8% w/v for bromothymol blue and calmagite, respectively. A high concentration of the crown ether required for efficient extraction of potassium due to the formation of a relatively weak complex between dibenzo-18-crown-6 and potassium. Consequently, a higher concentration of the crown ether is needed to push the complex formation equilibrium to completion (224). Therefore, 0.2 and 0.8% w/v dibenzo 18-crown-6 were selected to be the optimal conditions for bromothymol blue and calmagite, respectively.

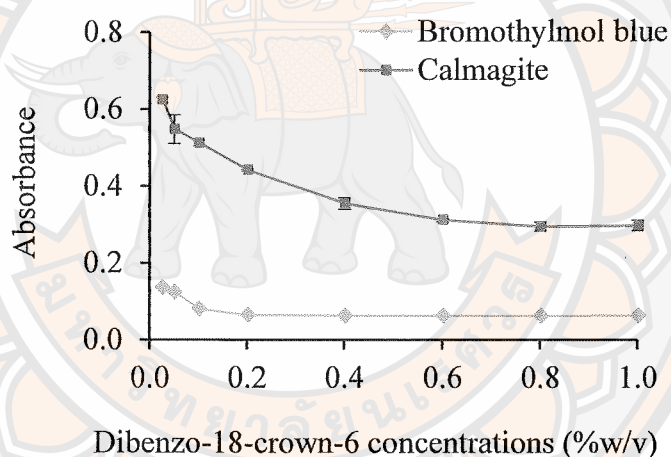


Figure 64 The effect of dibenzo-18-crown-6 concentrations

4. Effect of the reaction time

The effect of reaction time was also investigated, as shown in Figure 65. The absorbance of remaining dye in aqueous phase was observed to stabilize in about 5 min, and then became invariable. Therefore, the optimized reaction time selected was 5 min for potassium determination, using both bromothymol blue and calmagite.

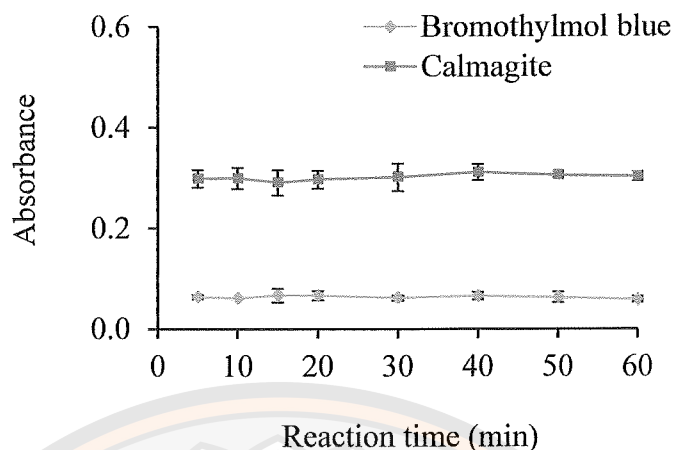


Figure 65 The effect of the reaction time

Under optimum ion pair extraction conditions, bromothymol blue and calmagite were used for the determination of potassium at pH 5 and 3.5, respectively. The optimum concentration of dibenzo-18-crown-6 was found to be 0.2 and 0.8% w/v for bromothymol blue and calmagite, respectively. The analysis of the reaction using this method was obtained in 5 min.

5. Effect of interference

In order to evaluate the selectivity of the detection system, the response of the detection to potassium was compared with five other ions, that were Na^+ , Cu^{2+} , Pb^{2+} , Fe^{2+} , and Mn^{2+} under the optimal experimental conditions. Furthermore, some transition metals could be eliminated by the addition of a masking agent such as EDTA as reported by other studies (223), therefore EDTA was added into the solution to mask transition metals. The absorbance of bromothymol blue and calmagite with and without EDTA are shown in Figure 6.6, compared with the blank one and other ions.

For bromothymol blue (Figure 66A): three ions, Pb^{2+} , Fe^{2+} , and Mn^{2+} changed the color of bromothymol from high color intensity to colorless, when without EDTA. However, with EDTA adding, the results showed that no significant change in the color intensity resulted for any of the ions. The one-way ANOVA showed that no significant change in the absorbance resulted for Na^+ , Cu^{2+} , Pb^{2+} , Fe^{2+} , and Mn^{2+} of the ions compared with the blank one, when added EDTA.

For calmagite (Figure 66B): four ions, Cu^{2+} , Pb^{2+} , Fe^{2+} , and Mn^{2+} changed the color of calmagite from high color intensity to weak color intensity, when without EDTA. However, with EDTA adding, the results showed that no significant change in the color intensity resulted for any of the ions. The one-way ANOVA showed that no significant change in the absorbance resulted for Na^+ , Cu^{2+} , Pb^{2+} , Fe^{2+} , and Mn^{2+} of the ions compared with the blank one, when added EDTA. Therefore, additional masking reagents, such as EDTA, are needed to eliminate the ions interference in the soil samples that contain high transition metals in its matrix.

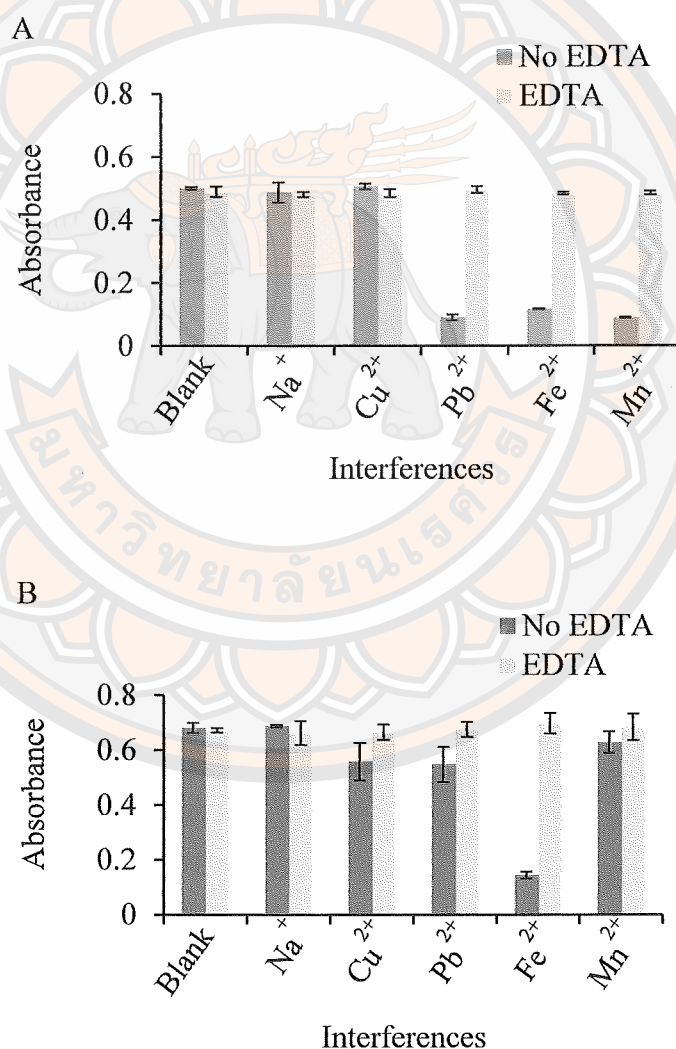


Figure 66 The effect of interfering ions with and without EDTA from the reaction of A) bromothymol blue, and B) calmagite

6. Paper-based platform in conjunction with smartphone for potassium determination

A paper-based platform coupled with smartphone was applied for determination of potassium, instead of spectrophotometric method. The solutions of aqueous phases were dropped on the paper-based platform, and then digitized and analyzed with a smartphone. This method is fast, low-cost, portable with high sensitivity, and does not require any complicated equipment.

For bromothymol blue: the linear range between 20–120 mg L⁻¹ was $y = 0.2176X + 213.2667$ with a correlation coefficient (R^2) of 0.7125 as shown in Figure 67A. It can be inferred from the calibration curves that the bromothymol blue has a less defined slope and a low correlation coefficient, which is not acceptable, because there is a weak color change on the paper-based platforms.

For calmagite: the linear range between 20–120 mg L⁻¹ was $y = 0.6919X + 172.9556$ with a correlation coefficient (R^2) of 0.9906 as shown in Figure 67B. The detection limit was determined to be 5.4 mg L⁻¹, and the limit of quantification was found to be 18.0 mg L⁻¹. To evaluate the precision of the paper-based platform, intra-repeatability ($n = 6$) and inter-reproducibility (5 days) were measured, both using a potassium concentration of 20, 60, and 100 mg L⁻¹, and expressed as %RSD. The percentage values of RSD for repeatability and reproducibility were 2.02–3.51% and 2.42–3.86%, respectively, indicating high precision.

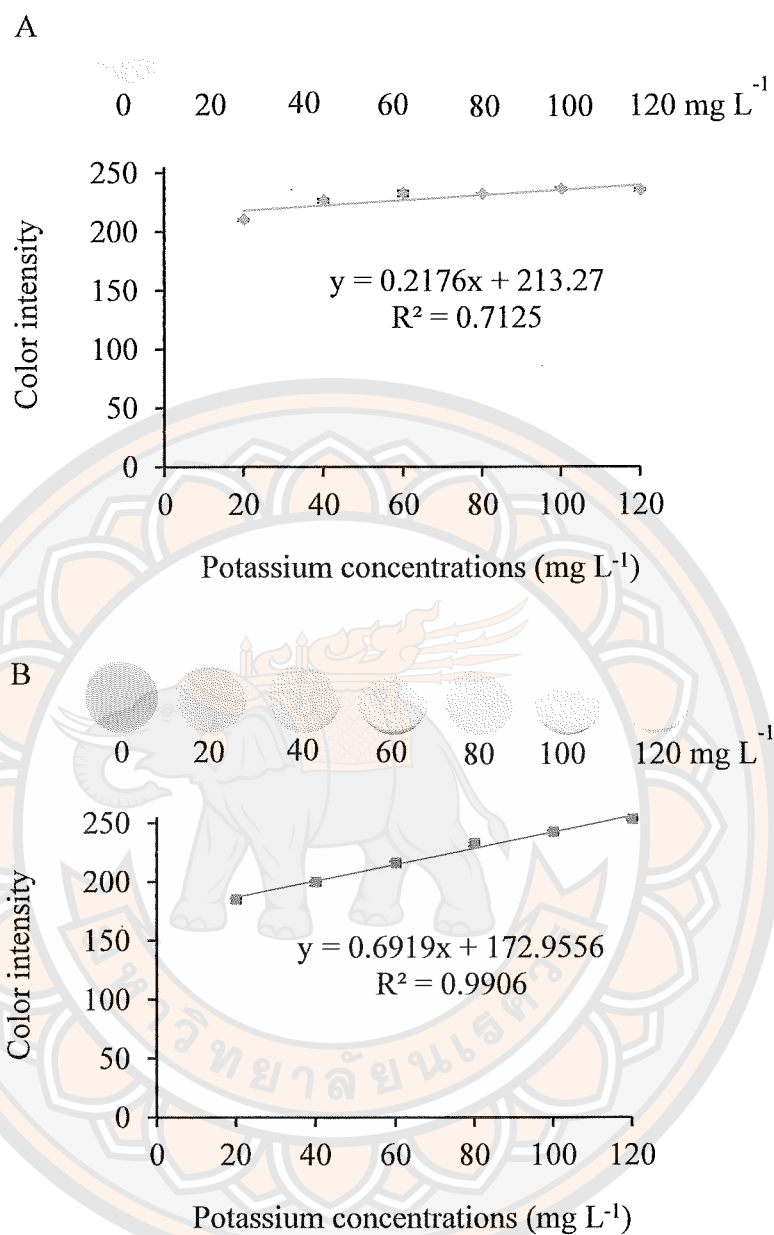


Figure 67 Calibration curve of potassium by using a paper-based platform:
A) bromothymol blue B) calmagite

7. Sample analysis

To assess the accuracy of the developed method, seven soil samples were analyzed by the paper-based platforms and the spectrophotometer method. In this study, 50 mg L⁻¹ of standard solution of potassium was added into the soil samples. The concentrations of potassium in the soil samples were obtained by calculation, which were then compared with the results of the spectrophotometer method.

The detailed results are shown in Table 17. It was found that the results detected by both methods were similar, and the recoveries were in the range of 83.8–117.4% which exhibited precisions of RSD in the range of 0.28–0.85%. Therefore, our developed method can be used for rapid colorimetric detection of potassium in soil samples. In order to validate the proposed method, a comparison between both the methods was carried out, by using the paired *t*-test, which proved that there was no significant difference between them ($t_{\text{stat}} = 0.37$, $t_{\text{critical}} = 2.31$), with a confidence level of 95%. Therefore, the paper-based platform associated with smartphone detection is reliable and considered as a promising method for potassium determination in soil samples.

Table 17 Comparison of potassium detection results from soil samples using the paper-based platform versus the spectrophotometric method

Sample	Added (mg kg ⁻¹)	Paper-based platform		Spectrophotometric method	
		Found (mg kg ⁻¹)	Recovery (%)	Found (mg kg ⁻¹)	Recovery (%)
Soil 1	0.0	ND	–	16.2 ± 9.4	–
	250.0	282.2 ± 7.2	112.9 ± 2.9	272.4 ± 6.7	102.5 ± 2.2
Soil 2	0.0	ND	–	21.7 ± 5.2	–
	250.0	282.2 ± 7.2	112.9 ± 2.9	294.0 ± 7.5	108.9 ± 1.9
Soil 3	0.0	ND	–	26.6 ± 7.3	–
	250.0	294.2 ± 11.0	117.7 ± 4.4	271.7 ± 4.8	98.1 ± 4.7
Soil 4	0.0	34 ± 4.2	–	32.8 ± 10.5	–
	250.0	296.6 ± 7.2	105.0 ± 1.7	282.2 ± 10.5	99.7 ± 4.2
Soil 5	0.0	55.7 ± 11.0	–	48.1 ± 8.3	–
	250.0	265.3 ± 4.2	83.8 ± 2.9	282.8 ± 8.7	93.9 ± 2.6
Soil 6	0.0	ND	–	26.6 ± 8.4	–
	250.0	284.6 ± 8.3	113.8 ± 3.3	286.7 ± 8.1	104.0 ± 4.5
Soil 7	0.0	ND	–	19.7 ± 5.2	–
	250.0	270.1 ± 11.0	108.0 ± 4.4	279.4 ± 6.3	103.9 ± 2.1

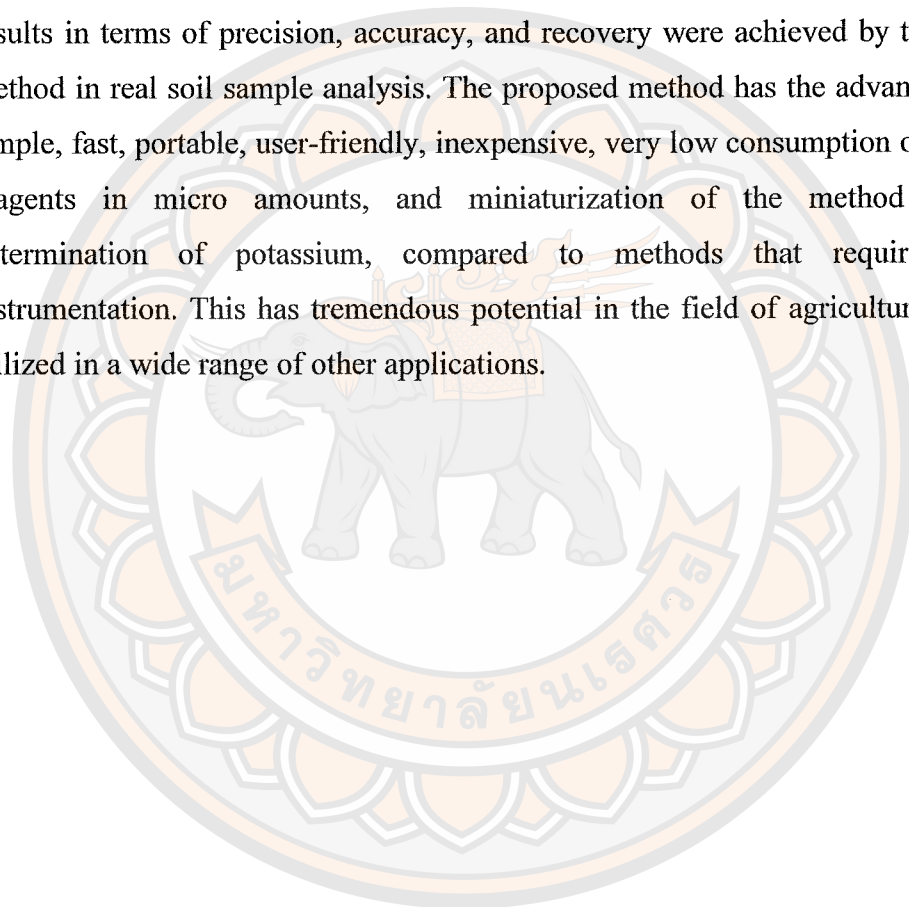
A comparative study of different methods from other studies is presented in Table 18, showing that the proposed method described here has advantages such as: low detection limits, fast, easy to use as well as the only materials needed are paper-based platforms, and a smartphone.

Table 18 Comparison of the features of the proposed method with those of other reported methods for potassium determination

Methods	Sample	Linear range	LOD	Reaction time (min)	Reference
Crown ether modified Au NPs sensor	Urine	0–200 μM	5.24 μM	20	(165)
Potassium ionophore I based on μPADs	Human serum	0.1–5.0 mM	0.1 mM	5	(166)
Aptamer-functionalized gold nanoparticles	Urine	5 nM – 1 μM	5 nM	—	(228)
Gold nanoparticle aggregation-based aptasensor	Urine	10 nM – 50 mM	4.4 nM	45	(229)
Ionophore-Based Titrimetric	Human serum	—	4.38 mM	30	(232)
Paper-Based Potentiometric Ion Sensing	Fluids and environmental or industrial	10^{-4} – 10^{-1} M	10^{-4} M	15	(234)
Dibenzo-18-crown-6 and counter ion based on paper-based plat form	Soil	20–120 mg L^{-1}	5.41 mg L^{-1}	5	This work

Conclusions

A simple indirect method base on the ion-pair extraction of potassium ion into dichloromethane by using dibenzo-18-crown-6 and an excess amount of calmagite as counter ion was combined with a paper-based colorimetric assay for determination of potassium. Colorimetric change of calmagite has been effectively integrated with smartphone assisted RGB color value application. Samples with transition metal matrix had no significant effect on the potassium determination, and satisfactory results in terms of precision, accuracy, and recovery were achieved by the developed method in real soil sample analysis. The proposed method has the advantage of being simple, fast, portable, user-friendly, inexpensive, very low consumption of sample and reagents in micro amounts, and miniaturization of the method for on-site determination of potassium, compared to methods that require expensive instrumentation. This has tremendous potential in the field of agriculture and can be utilized in a wide range of other applications.



CHAPTER VII

CONCLUSIONS

Conclusions

In this study, four (microfluidic) paper-based analytical devices were developed for the detection of primary macronutrients in soil including nitrate, ammonium, phosphate, and potassium. The fabrication method using a simple, inexpensive screen-printing method together with new hydrophobic materials was presented.

In the first part of this study, the fabrication of a microfluidic paper-based device for the detection of nitrate, was produced from beeswax which is a new environmentally friendly hydrophobic material with the screen-printing method. This method provided a well-defined hydrophobic barrier with an efficient resolution, good reproducibility and high stability without requiring organic solvents or complicated instruments. The μ PAD was successfully applied to determined nitrate in soil samples, using the Griess reaction and VCl_3 for the colorimetric assay. Consequently, the analytical results obtained by the μ PAD were in good agreement with those obtained by the spectrophotometric method. Therefore, this beeswax screen-printing method provides an alternative and inexpensive fabrication method for μ PADs. The proposed μ PAD, which is probably first used for the detection of nitrate in soil, is advantageous as a lower cost, simple, shorter detection time, and environmentally friendly device.

In the second part of this study, UV resin was used as a new hydrophobic material for the fabrication of 3D PADs. The advantages of using the UV resin are that it is commercially available, inexpensive, easy to use with a low toxicity, and delivers fast cure at room temperature. The PADs produced by this method were applied by carrying out the modified Berthelot reaction for colorimetric determination of ammonium, in which sodium salicylate and dichloroisocyanurate are used instead of toxic phenol and unstable hypochlorite, respectively. The developed 3D PAD, which is probably first used for the detection of ammonium in soil, was applied for the

determination of ammonium in soil samples, and no significant differences in the analytical results were observed compared to the spectrophotometric method. The developed 3D PAD exhibited rapid results, inexpensive, low consumption of reagents, and simplicity, in that it does not require instrumentation for the read-out.

In the third part of this study, a one-step fabrication method for μ PAD, using epoxy resin, as new hydrophobic material, in conjunction with the screen-printing method was described. This method was simple, fast, solvent and instrument free, and had a high production rate. The use of a μ PAD for the colorimetric detection of phosphate, was analyzed by using the molybdenum blue method with reducing agent stannous chloride which is more stable than ascorbic in previous work. The results obtained by the proposed method were in good agreement with those of the spectrophotometric method. These μ PADs have the advantage of being cost effective simple, and wide operating range, which makes it suitable for the determination of phosphate in soil samples.

The (μ)PADs were successfully developed by using new hydrophobic materials in conjunction with the screen-printing method. The beeswax is easy to make, inexpensive, and it is environmental friendly. UV resin are commercially available, inexpensive, easy to use with a low toxicity, and delivers fast cure at room temperature. Moreover, the epoxy resin was performed by using a single process at room temperature, which did not require complicated and expensive instruments. It has resistance to variety of chemicals and solvent free.

Finally, an indirect method for the determination of potassium, based on the ion-pair extraction using dibenzo-18-crown-6 and calmagite as the counter ion was described. When the extraction was complete, the remaining calmagite in aqueous phase was examined on a paper-based platform and digitized with a smartphone, allowing the amount of potassium to be determined. The proposed indirect method for potassium analysis is selectivity and simple, and specific compounds does not require. In addition, the developed analytical platform is rapid, cost-efficient, and potentially applicable at the point-of-need. The proposed approach was successfully applied to the detection of potassium in soil samples.

The summarize of the analytical performances of four developed methods for primary macronutrients, are described in Table 19.

Table 19 Summarize of the analytical performances of the four developed methods

Nutrients	Nitrate	Ammonium	Phosphate	Potassium
Fabrication methods	Beeswax screen-printing method	UV resin screen-printing method	Epoxy resin screen-printing method	Epoxy resin screen-printing method
Reaction time (min)	10	5	10	5
Linearity (mg L⁻¹)	0.5–40	10–100	0.5–40	20–120
Calibration curve	$y = 2.2341x + 26.998$	$y = 0.8343x + 32.691$	$y = 2.6426x + 14.6123$	$y = 0.6919x + 172.9556$
R²	0.9924	0.9963	0.9920	0.9906
LOD (mg L⁻¹)	0.41	0.50	0.25	5.41
LOQ (mg L⁻¹)	1.35	1.65	0.83	18.03
Intraday (%)	1.50–2.16	1.57–2.58	1.52–2.46	1.50–2.16
Interday (%)	1.15–2.24	1.86–3.81	1.89–2.74	1.15–2.24
Recovery (%)	88.4–99.8	95.5–107.5	88.8–101.0	83.8–117.7

Future works

An interesting topic for future work is the development of (μ)PADs for the simultaneous detection of nitrate, ammonium, phosphate, and potassium in soil samples. In addition, further development of these (μ)PADs as a simple, sensitive, and easy-to-use test kit are required to make them fully functional for Thai farmers.



REFERENCES

REFERENCES

1. Ramane DV, Patil SS, Shaligram A, editors. Detection of NPK nutrients of soil using fiber optic sensor. International Journal of Research in Advent Technology Special Issue National Conference ACGT 2015; 2015.
2. Rashid MM, Jahan M, Islam KS. Impact of nitrogen, phosphorus and potassium on brown planthopper and tolerance of its host rice plants. Rice Science. 2016;23(3):119-31.
3. Zhang J, Balkovič J, Azevedo LB, Skalský R, Bouwman AF, Xu G, et al. Analyzing and modelling the effect of long-term fertilizer management on crop yield and soil organic carbon in China. Science of The Total Environment. 2018;627:361-72.
4. Máximo W, Santos P, Mendonça E, Santos B, Paiva L. Nitrate (NO_3^-) and ammonium (NH_4^+) ratios for propagation of Eucalyptus hybrid in two different in vitro cultivation systems. Australian Journal of Crop Science. 2015;9:1242-8.
5. Kalayu G. Phosphate solubilizing microorganisms: promising approach as biofertilizers. International Journal of Agronomy. 2019;2019:4917256.
6. Pettygrove S, O'Geen T, Southard R. Potassium fixation and its significance for California crop production. Better Crops with Plant Food. 2011;95(4):16-8.
7. Akenga P, Ali S, Anam O, Amir Y, Waudo W. Determination of selected micro and macronutrients in sugarcane growing soils at Kakamega North District, Kenya. IOSR Journal of Applied Chemistry. 2014;7(7):34-41.
8. Yusof KM, Isaak S, Rashid NCA, Ngajikin NH. NPK detection spectroscopy on non-agriculture soil. Jurnal Teknologi. 2016;78(11):227–31.
9. Zhang Z, Lynch JP, Zhang B, Wang Q. Chapter 14-NPK deficiency modulates oxidative stress in plants. In Plant Macronutrient Use Efficiency. 2017;245-65.
10. Ma L, Duan T, Hu J. Application of a universal soil extractant for determining the available NPK: A case study of crop planting zones in central China. Science of The Total Environment. 2020;704:135253.
11. Ma L, Feng S, Reidsma P, Qu F, Heerink N. Identifying entry points to improve fertilizer use efficiency in Taihu Basin, China. Land Use Policy. 2014;37:52-9.

12. Khan M, Mobin M, Zahid A, Alamri S. Fertilizers and their contaminants in soils, surface and groundwater. Reference Module in Earth Systems and Environmental Sciences. 2017.
13. Shyla B, Mahadevaiah, Nagendrappa G. A simple spectrophotometric method for the determination of phosphate in soil, detergents, water, bone and food samples through the formation of phosphomolybdate complex followed by its reduction with thiourea. *Spectrochimica Acta Part A: Molecular and Biomolecular Spectroscopy*. 2011;78(1):497-502.
14. Caro CA, Bedioui F, Zagal JH. Electrocatalytic oxidation of nitrite on a vitreous carbon electrode modified with cobalt phthalocyanine. *Electrochimica Acta*. 2002;47(9):1489-94.
15. Mikuška P, Večeřa Z. Simultaneous determination of nitrite and nitrate in water by chemiluminescent flow-injection analysis. *Analytica Chimica Acta*. 2003;495(1):225-32.
16. Merusi C, Corradini C, Cavazza A, Borromei C, Salvadeo P. Determination of nitrates, nitrites and oxalates in food products by capillary electrophoresis with pH-dependent electroosmotic flow reversal. *Food Chemistry*. 2010;120(2):615-20.
17. Jedličková V, Paluch Z, Alušík Š. Determination of nitrate and nitrite by high-performance liquid chromatography in human plasma. *Journal of Chromatography B*. 2002;780(1):193-7.
18. Martinez AW, Phillips ST, Butte MJ, Whitesides GM. Patterned paper as a platform for inexpensive, low-volume, portable bioassays. *Angewandte Chemie International Edition*. 2007;46(8):1318-20.
19. Vidal E, Lorenzetti AS, Lista AG, Domini CE. Micropaper-based analytical device (μ PAD) for the simultaneous determination of nitrite and fluoride using a smartphone. *Microchemical Journal*. 2018;143:467-73.
20. Dungchai W, Chailapakul O, Henry CS. A low-cost, simple, and rapid fabrication method for paper-based microfluidics using wax screen-printing. *Analyst*. 2011;136(1):77-82.
21. Li X, Tian J, Garnier G, Shen W. Fabrication of paper-based microfluidic sensors by printing. *Colloids and Surfaces B: Biointerfaces*. 2010;76(2):564-70.

22. Liana DD, Raguse B, Gooding JJ, Chow E. Recent advances in paper-based sensors. *Sensors*. 2012;12(9):11505-26.
23. Jayawardane BM, McKelvie ID, Kolev SD. A paper-based device for measurement of reactive phosphate in water. *Talanta*. 2012;100:454-60.
24. Kim J-Y, Yeo M-K. A fabricated microfluidic paper-based analytical device (μ PAD) for in situ rapid colorimetric detection of microorganisms in environmental water samples. *Molecular & Cellular Toxicology*. 2016;12(1):101-9.
25. Kung C-T, Hou C-Y, Wang Y-N, Fu L-M. Microfluidic paper-based analytical devices for environmental analysis of soil, air, ecology and river water. *Sensors and Actuators B: Chemical*. 2019;301:126855.
26. Moniz T, Bassett CR, Almeida MIGS, Kolev SD, Rangel M, Mesquita RBR. Use of an ether-derived 3-hydroxy-4-pyridinone chelator as a new chromogenic reagent in the development of a microfluidic paper-based analytical device for Fe(III) determination in natural waters. *Talanta*. 2020;214:120887.
27. Trofimchuk E, Nilghaz A, Sun S, Lu X. Determination of norfloxacin residues in foods by exploiting the coffee-ring effect and paper-based microfluidics device coupling with smartphone-based detection. *Journal of Food Science*. 2020;85(3):736-43.
28. Weng X, Neethirajan S. Paper-based microfluidic aptasensor for food safety. *Journal of Food Safety*. 2018;38(1):e12412.
29. Chaikhan P, Udnan Y, Sananmuang R, Ampiah-Bonney RJ, Chuachuad Chaiyasith W. A low-cost microfluidic paper-based analytical device (μ PAD) with column chromatography preconcentration for the determination of paraquat in vegetable samples. *Microchemical Journal*. 2020;159:105355.
30. Jin L, Hao Z, Zheng Q, Chen H, Zhu L, Wang C, et al. A facile microfluidic paper-based analytical device for acetylcholinesterase inhibition assay utilizing organic solvent extraction in rapid detection of pesticide residues in food. *Analytica Chimica Acta*. 2020;1100:215-24.
31. Ng K, Gao B, Yong KW, Li Y, Shi M, Zhao X, et al. Paper-based cell culture platform and its emerging biomedical applications. *Materials Today*. 2017;20(1):32-44.
32. Tao FF, Xiao X, Lei KF, Lee I-C. Paper-based cell culture microfluidic system. *BioChip Journal*. 2015;9(2):97-104.

33. Musile G, Wang L, Bottoms J, Tagliaro F, McCord B. The development of paper microfluidic devices for presumptive drug detection. *Analytical Methods*. 2015;7(19):8025-33.
34. Hong B, Xue P, Wu Y, Bao J, Chuah YJ, Kang Y. A concentration gradient generator on a paper-based microfluidic chip coupled with cell culture microarray for high-throughput drug screening. *Biomedical microdevices*. 2016;18(1):21.
35. Ge L, Yan J, Song X, Yan M, Ge S, Yu J. Three-dimensional paper-based electrochemiluminescence immunodevice for multiplexed measurement of biomarkers and point-of-care testing. *Biomaterials*. 2012;33(4):1024-31.
36. Mao K, Min X, Zhang H, Zhang K, Cao H, Guo Y, et al. Paper-based microfluidics for rapid diagnostics and drug delivery. *Journal of Controlled Release*. 2020;322:187-99.
37. Yetisen AK, Akram MS, Lowe CR. Paper-based microfluidic point-of-care diagnostic devices. *Lab on a Chip*. 2013;13(12):2210-51.
38. de Souza FR, Alves GL, Coltro WKT. Capillary-driven toner-based microfluidic devices for clinical diagnostics with colorimetric detection. *Analytical Chemistry*. 2012;84(21):9002-7.
39. Arun K, Singh., Kamal K, Soan. *Soil Science*. Ranchi: State Agricultural Management and Extension Training Institute; 2012.
40. El-Ramady, Hassan R. Integrated nutrient management and postharvest of crops. *Sustainable Agriculture Reviews*. 2014;13:163-274.
41. Roy RN, Finck A, Blair GJ, Tandon HLS. *Plant nutrition for food security*. Rome, Italy FAO; 2006.
42. Jones JB. *Plant Nutrition and Soil Fertility Manual*. Florida. USA: CRC Press; 2012.
43. Handreck KA, Black ND. *Growing media for ornamental plants and turf*. Sydney, Australia: University of New South Wales Press; 2002.
44. Hofman G, Cleemput O. *Soil and Plant Nitrogen*. Paris: International Fertilizer Industry Association; 2004.
45. Hachiya T, Sakakibara H. Interactions between nitrate and ammonium in their uptake, allocation, assimilation, and signaling in plants. *Journal of Experimental Botany*. 2016;68(10):2501-12.

46. Pasquali CL, Gallego-Picó A, Hernando PF, Velasco M, Alegría JD. Two rapid and sensitive automated methods for the determination of nitrite and nitrate in soil samples. *Microchemical Journal*. 2010;94(1):79-82.
47. Chen J-F. Adsorption and diffusion of ammonium in soils. In: Zhu Z-l, Wen Q-x, Freney JR, editors. *Nitrogen in Soils of China*. Dordrecht: Springer Netherlands; 1997;87-111.
48. Courtney Johnson GA, Quirine Ketterings, Jen Beckman, Kristen Stockin. Nitrogen basics – The nitrogen cycle; [update 2005; cited 2019 Feb 3]. Available from: <http://cceonondaga.org/resources/nitrogen-basics-the-nitrogen-cycle>
49. Elhanafi L, Houhou M, Rais C, Mansouri I, Elghadraoui L, Greche H. Impact of excessive nitrogen fertilization on the biochemical quality, phenolic compounds, and antioxidant power of *sesamum indicum* L seeds. *Journal of Food Quality*. 2019;2019:9428092.
50. Douglas B. Beegle poa, and Philip T. Durst. Managing phosphorus for crop production. [update 2002; cited 2020 Feb 26]. Available from: <https://extension.psu.edu/programs/nutrient-management/educational/soil-fertility/managing-phosphorus-for-crop-production>
51. Menzies N. The science of phosphorus nutrition: from in thr soil, plant uptake, and plant response. [updated 2009; cited 2020 Mach 4]. Available from: <https://grdc.com.au/resources-and-publications/grdc-update-papers/tab-content/grdc-update-papers/2009/02/the-science-of-phosphorus-nutrition-forms-in-the-soil-plant-uptake-and-plant-response>
52. Malhotra H, Sharma S, Pandey R. Phosphorus nutrition: plant growth in response to deficiency and excess. *Plant Nutrients and Abiotic Stress Tolerance*. Singapore: Springer. 2018; 171-90.
53. Nowaki RHD, Parent S-É, Cecílio Filho AB, Rozane DE, Meneses NB, da Silva JADS, et al. Phosphorus over-fertilization and nutrient misbalance of irrigated tomato crops in Brazil. *Front Plant Sci*. 2017;8:825.
54. Montag Manufacturing. The agronomy corner. [update 2019; cited 2020 Mach 26]. Available from: https://www.montagmfg.com/wp-content/uploads/info_center/Agronomy_Corner_Potassium.pdf

55. Mahler RL. Nutrients plants require for growth. University of Idaho College of Agricultural and Life Science CIS. 2004;1124.
56. E.S. Marx JH, R.G. Stevens. Soil Test Interpretation Guide. [update 2018; cited 2019 Mach 5]. Available from:
<https://www.piercecountycd.org/DocumentCenter/View/670>
57. Land development department. State of soil and land resources of Thailand. Land development department and ministry of agriculture and cooperatives. Bangkok; 2015. Thailand.
58. Sackmann EK, Fulton AL, Beebe DJ. The present and future role of microfluidics in biomedical research. *Nature*. 2014;507(7491):181-9.
59. Yang Y, Noviana E, Nguyen MP, Geiss BJ, Dandy DS, Henry CS. Paper-based microfluidic devices: Emerging themes and applications. *Analytical chemistry*. 2017;89(1):71-91.
60. Li X, Ballerini DR, Shen W. A perspective on paper-based microfluidics: Current status and future trends. *Biomicrofluidics*. 2012;6(1):301-13.
61. Martinez AW, Phillips ST, Whitesides GM, Carrilho E. Diagnostics for the developing world: Microfluidic paper-based analytical devices. *Analytical Chemistry*. 2010;82(1):3-10.
62. Almeida MIGS, Jayawardane BM, Kolev SD, McKelvie ID. Developments of microfluidic paper-based analytical devices (μ PADs) for water analysis: A review. *Talanta*. 2018;177(Supplement C):176-90.
63. Satarpai T, Shiowatana J, Siripinyanond A. Paper-based analytical device for sampling, on-site preconcentration and detection of ppb lead in water. *Talanta*. 2016;154:504-10.
64. Liu C-C, Wang Y-N, Fu L-M, Chen K-L. Microfluidic paper-based chip platform for benzoic acid detection in food. *Food Chemistry*. 2018;249:162-7.
65. Xia Y, Si J, Li Z. Fabrication techniques for microfluidic paper-based analytical devices and their applications for biological testing: A review. *Biosensors and Bioelectronics*. 2016;77:774-89.
66. Sriram G, Bhat MP, Patil P, Uthappa UT, Jung H-Y, Altalhi T, et al. Paper-based microfluidic analytical devices for colorimetric detection of toxic ions: A review. *TrAC Trends in Analytical Chemistry*. 2017;93:212-27.

67. Asano H, Shiraishi Y. Development of paper-based microfluidic analytical device for iron assay using photomask printed with 3D printer for fabrication of hydrophilic and hydrophobic zones on paper by photolithography. *Analytica Chimica Acta*. 2015;883:55-60.
68. Yu L, Shi ZZ. Microfluidic paper-based analytical devices fabricated by low-cost photolithography and embossing of Parafilm®. *Lab on a Chip*. 2015;15(7):1642-5.
69. Morbioli GG, Speller NC, Cato ME, Cantrell TP, Stockton AM. Rapid and low-cost development of microfluidic devices using wax printing and microwave treatment. *Sensors and Actuators B: Chemical*. 2019;284:650-6.
70. Younas M, Maryam A, Khan M, Nawaz AA, Jaffery SHI, Anwar MN, et al. Parametric analysis of wax printing technique for fabricating microfluidic paper-based analytic devices (μ PAD) for milk adulteration analysis. *Microfluidics and Nanofluidics*. 2019;23(3):38.
71. Carrilho E, Martinez AW, Whitesides GM. Understanding wax printing: A simple micropatterning process for paper-based microfluidics. *Analytical Chemistry*. 2009;81(16):7091-5.
72. Ferreira FTSM, Mesquita RBR, Rangel AOSS. Novel microfluidic paper-based analytical devices (μ PADs) for the determination of nitrate and nitrite in human saliva. *Talanta*. 2020;219:121183.
73. Yamada K, Henares TG, Suzuki K, Citterio D. Paper-based inkjet-printed microfluidic analytical devices. *Angewandte Chemie International Edition*. 2015;54(18):5294-310.
74. Abe K, Suzuki K, Citterio D. Inkjet-printed microfluidic multianalyte chemical sensing paper. *Analytical Chemistry*. 2008;80(18):6928-34.
75. Henares TG, Yamada K, Takaki S, Suzuki K, Citterio D. "Drop-slip" bulk sample flow on fully inkjet-printed microfluidic paper-based analytical device. *Sensors and Actuators B: Chemical*. 2017;244:1129-37.
76. Sitanurak J, Fukana N, Wongpakdee T, Thepchuay Y, Ratanawimarnwong N, Amornsakchai T, et al. T-shirt ink for one-step screen-printing of hydrophobic barriers for 2D- and 3D-microfluidic paper-based analytical devices. *Talanta*. 2019;205:120113.

77. Sameenoi Y, Nongkai PN, Nouanthavong S, Henry CS, Nacapricha D. One-step polymer screen-printing for microfluidic paper-based analytical device (μ PAD) fabrication. *Analyst*. 2014;139(24):6580-8.
78. Teepoo S, Arsawiset S, Chanayota P. One-step polylactic acid screen-printing microfluidic paper-based analytical device: Application for simultaneous detection of nitrite and nitrate in food samples. *Chemosensors*. 2019;7(3):44.
79. de Oliveira R, Camargo F, Pesquero N, Faria R. A simple method to produce 2D and 3D microfluidic paper-based analytical devices for clinical analysis. *Analytica Chimica Acta*. 2017;957:40-6.
80. Spicar P, Toley B, Houghtaling J, Liang T, Yager P, Fu E. CO₂ laser cutting and ablative etching for the fabrication of paper-based devices. *Journal of Micromechanics and Microengineering*. 2013;23:067003.
81. Songjaroen T, Dungchai W, Chailapakul O, Laiwattanapaisa W. Novel, simple and low-cost alternative method for fabrication of paper-based microfluidics by wax dipping. *Talanta*. 2011;85(5):2587-93.
82. Cardoso TMG, Garcia PT, Coltro WKT. Colorimetric determination of nitrite in clinical, food and environmental samples using microfluidic devices stamped in paper platforms. *Analytical Methods*. 2015;7(17):7311-7.
83. Mathaweesansurn A, Thongrod S, Khongkaew P, Phechkrajang CM, Wilairat P, Choengchan N. Simple and fast fabrication of microfluidic paper-based analytical device by contact stamping for multiple-point standard addition assay: Application to direct analysis of urinary creatinine. *Talanta*. 2020;210:120675.
84. de Tarso Garcia P, Garcia Cardoso TM, Garcia CD, Carrilho E, Tomazelli Coltro WK. A handheld stamping process to fabricate microfluidic paper-based analytical devices with chemically modified surface for clinical assays. *RSC Advances*. 2014;4(71):37637-44.
85. Zhang Y, Zhou C, Nie J, Le S, Qin Q, Liu F, et al. Equipment-free quantitative measurement for microfluidic paper-based analytical devices fabricated using the principles of movable-type printing. *Analytical Chemistry*. 2014;86(4):2005-12.

86. Dornelas KL, Dossi N, Piccin E. A simple method for patterning poly(dimethylsiloxane) barriers in paper using contact-printing with low-cost rubber stamps. *Analytica Chimica Acta*. 2015;858(1):82-90.
87. Duangdeewong C, Sitanurak J, Wilairat P, Nacapricha D, Teerasong S. Microfluidic paper-based analytical device for convenient use in measurement of iodate in table salt and irrigation water. *Microchemical Journal*. 2020;152:104447.
88. Martinez AW, Phillips ST, Carrilho E, Thomas SW, Sindi H, Whitesides GM. Simple telemedicine for developing regions: Camera phones and paper-based microfluidic devices for real-time, off-site diagnosis. *Analytical Chemistry*. 2008;80(10):3699-707.
89. OuYang L, Wang C, Du F, Zheng T, Liang H. Electrochromatographic separations of multi-component metal complexes on a microfluidic paper-based device with a simplified photolithography. *RSC Advances*. 2014;4(3):1093-101.
90. Asano H, Shiraishi Y. Microfluidic paper-based analytical device for the determination of hexavalent chromium by photolithographic fabrication using a photomask printed with 3D printer. *Analytical Sciences*. 2018;34(1):71-4.
91. Martinez AW, Phillips ST, Wiley BJ, Gupta M, Whitesides GM. FLASH: A rapid method for prototyping paper-based microfluidic devices. *Lab on a chip*. 2008;8(12):2146-50.
92. Chaiyo S, Siangproh W, Apilux A, Chailapakul O. Highly selective and sensitive paper-based colorimetric sensor using thiosulfate catalytic etching of silver nanoplates for trace determination of copper ions. *Analytica Chimica Acta*. 2015;866:75-83.
93. Chaiyo S, Apiluk A, Siangproh W, Chailapakul O. High sensitivity and specificity simultaneous determination of lead, cadmium and copper using μ PAD with dual electrochemical and colorimetric detection. *Sensors and Actuators B: chemical*. 2016;233:540-9.
94. Fujisaki S, Shibata H, Yamada K, Suzuki K, Citterio D. Printed low-cost microfluidic analytical devices based on a transparent substrate. *Analyst*. 2019;144(8):2746-54.

95. Liu C-C, Wang Y-N, Fu L-M, Huang Y-H. Microfluidic paper-based chip platform for formaldehyde concentration detection. *Chemical Engineering Journal*. 2018;332:695-701.
96. Guzman JMCC, Tayo LL, Liu C-C, Wang Y-N, Fu L-M. Rapid microfluidic paper-based platform for low concentration formaldehyde detection. *Sensors and Actuators B: Chemical*. 2018;255:3623-9.
97. Schonhorn JE, Fernandes SC, Rajaratnam A, Deraney RN, Rolland JP, Mace CR. A device architecture for three-dimensional, patterned paper immunoassays. *Lab on a Chip*. 2014;14(24):4653-8.
98. Morbioli GG, Mazzu-Nascimento T, Milan LA, Stockton AM, Carrilho E. Improving sample distribution homogeneity in three-dimensional microfluidic paper-based analytical devices by rational device design. *Analytical chemistry*. 2017;89(9):4786-92.
99. Peters JJ, Almeida MIGS, O'Connor Šraj L, McKelvie ID, Kolev SD. Development of a micro-distillation microfluidic paper-based analytical device as a screening tool for total ammonia monitoring in freshwaters. *Analytica Chimica Acta*. 2019;1079:120-8.
100. Maejima K, Tomikawa S, Suzuki K, Citterio D. Inkjet printing: an integrated and green chemical approach to microfluidic paper-based analytical devices. *RSC Advances*. 2013;3(24):9258-63.
101. Xu C, Cai L, Zhong M, Zheng S. Low-cost and rapid prototyping of microfluidic paper-based analytical devices by inkjet printing of permanent marker ink. *RSC Advances*. 2015;5(7):4770-3.
102. Prabhu A, Giri Nandagopal MS, Peralam Yegneswaran P, Singhal HR, Mani NK. Inkjet printing of paraffin on paper allows low-cost point-of-care diagnostics for pathogenic fungi. *Cellulose*. 2020;27(13):7691-701.
103. Jutila E, Koivunen R, Bollström R, Gane P. Fully inkjet-printed glucose assay fabricated on highly porous pigment coating. *Microfluidics and Nanofluidics*. 2020;24(6):40.
104. Zhang H, Smith E, Zhang W, Zhou A. Inkjet printed microfluidic paper-based analytical device (μ PAD) for glucose colorimetric detection in artificial urine. *Biomed Microdevices*. 2019;21(3):48.

105. Jayawardane BM, Wongwilai W, Grudpan K, Kolev S, Heaven M, Nash D, et al. Evaluation and application of a paper-based device for the determination of reactive phosphate in soil Solution. *Journal of Environmental Quality*. 2014;43(3):1081-5.
106. Jayawardane BM, McKelvie ID, Kolev SD. Development of a gas-diffusion microfluidic paper-based analytical device (μ PAD) for the determination of ammonia in wastewater samples. *Analytical Chemistry*. 2015;87(9):4621-6.
107. Hamedpour V, Postma GJ, van den Heuvel E, Jansen JJ, Suzuki K, Citterio D. Chemometrics-assisted microfluidic paper-based analytical device for the determination of uric acid by silver nanoparticle plasmon resonance. *Analytical and Bioanalytical Chemistry*. 2018;410(9):2305-13.
108. Jiranusornkul N, Kraduangdej S, Niltawach N, Pimpin A, Srituravanich W. Development of a paper-based pressure sensor fabricated by an inkjet-printed water mask method. *Microsystem Technologies*. 2020;26(6):2117-21.
109. Li X, Tian J, Shen W. Progress in patterned paper sizing for fabrication of paper-based microfluidic sensors. *Cellulose*. 2010;17(3):649-59.
110. Namwong P, Jarujamrus P, Amatatongchai M, Chairam S. Fabricating simple wax screen-printing paper-based analytical devices to demonstrate the concept of limiting reagent in acid–base reactions. *Journal of Chemical Education*. 2018;95(2):305-9.
111. Mohammadi S, Maeki M, Mohamadi RM, Ishida A, Tani H, Tokeshi M. An instrument-free, screen-printed paper microfluidic device that enables bio and chemical sensing. *The Analyst*. 2015;140(19):6493-9.
112. Sun JY, Cheng CM, Liao YC. Screen printed paper-based diagnostic devices with polymeric inks. *Analytical sciences : the international journal of the Japan Society for Analytical Chemistry*. 2015;31(3):145-51.
113. Yao Y, Zhang C. A novel screen-printed microfluidic paper-based electrochemical device for detection of glucose and uric acid in urine. *Biomed Microdevices*. 2016;18(5):92.
114. Nuchtavorn N, Macka M. A novel highly flexible, simple, rapid and low-cost fabrication tool for paper-based microfluidic devices (μ PADs) using technical drawing pens and in-house formulated aqueous inks. *Analytica Chimica Acta*. 2016;919:70-7.

115. Bruzewicz DA, Reches M, Whitesides GM. Low-cost printing of poly(dimethylsiloxane) barriers to define microchannels in paper. *Analytical Chemistry*. 2008;80(9):3387-92.
116. Sousa LR, Duarte LC, Coltro WKT. Instrument-free fabrication of microfluidic paper-based analytical devices through 3D pen drawing. *Sensors and Actuators B: Chemical*. 2020;312:128018.
117. Nie J, Zhang Y, Lin L, Zhou C, Li S, Zhang L, et al. Low-cost fabrication of paper-based microfluidic devices by one-step plotting. *Analytical Chemistry*. 2012;84(15):6331-5.
118. Ghaderinezhad F, Amin R, Temirel M, Yenilmez B, Wentworth A, Tasoglu S. High-throughput rapid-prototyping of low-cost paper-based microfluidics. *Scientific Reports*. 2017;7(1):3553.
119. Amin R, Ghaderinezhad F, Li L, Lepowsky E, Yenilmez B, Knowlton S, et al. Continuous-ink, multiplexed pen-plotter approach for low-cost, high-throughput fabrication of paper-based microfluidics. *Analytical Chemistry*. 2017;89(12):6351-7.
120. Nie J, Liang Y, Zhang Y, Le S, Li D, Zhang S. One-step patterning of hollow microstructures in paper by laser cutting to create microfluidic analytical devices. *Analyst*. 2013;138(2):671-6.
121. Chen W, Fang X, Li H, Cao H, Kong J. A Simple Paper-Based Colorimetric Device for Rapid Mercury(II) Assay. *Scientific Reports*. 2016;6(1):31948.
122. Mu X, Zhang L, Chang S, Cui W, Zheng Z. Multiplex microfluidic paper-based immunoassay for the diagnosis of hepatitis C virus infection. *Analytical chemistry*. 2014;86(11):5338-44.
123. Feng Q-M, Cai M, Shi C-G, Bao N, Gu H-Y. Integrated paper-based electroanalytical devices for determination of dopamine extracted from striatum of rat. *Sensors and Actuators B: Chemical*. 2015;209:870-6.
124. Song M-B, Joung H-A, Oh YK, Jung K, Ahn YD, Kim M-G. Tear-off patterning: a simple method for patterning nitrocellulose membranes to improve the performance of point-of-care diagnostic biosensors. *Lab on a Chip*. 2015;15(14):3006-12.
125. Li X, Zwanenburg P, Liu X. Magnetic timing valves for fluid control in paper-based microfluidics. *Lab on a Chip*. 2013;13(13):2609-14.

126. Cai L, Wang Y, Wu Y, Xu C, Zhong M, Lai H, et al. Fabrication of a microfluidic paper-based analytical device by silanization of filter cellulose using a paper mask for glucose assay. *Analyst*. 2014;139(18):4593-8.
127. Evans E, Gabriel EFM, Coltro WKT, Garcia CD. Rational selection of substrates to improve color intensity and uniformity on microfluidic paper-based analytical devices. *Analyst*. 2014;139(9):2127-32.
128. Fang X, Wei S, Kong J. Paper-based microfluidics with high resolution, cut on a glass fiber membrane for bioassays. *Lab on a Chip*. 2014;14(5):911-5.
129. Chen X, Chen J, Wang F, Xiang X, Luo M, Ji X, et al. Determination of glucose and uric acid with bienzyme colorimetry on microfluidic paper-based analysis devices. *Biosensors and Bioelectronics*. 2012;35(1):363-8.
130. Rattanarat P, Dungchai W, Cate DM, Siangproh W, Volckens J, Chailapakul O, et al. A microfluidic paper-based analytical device for rapid quantification of particulate chromium. *Analytica chimica acta*. 2013;800:50-5.
131. Nie J, Zhang Y, Lin L, Zhou C, Li S, Zhang L, et al. Low-cost fabrication of paper-based microfluidic devices by one-step plotting. *Analytical Chemistry*. 2012;84(15):6331-5.
132. Rahbar M, Nesterenko PN, Paull B, Macka M. High-throughput deposition of chemical reagents via pen-plotting technique for microfluidic paper-based analytical devices. *Analytica Chimica Acta*. 2019;1047:115-23.
133. Fenton EM, Mascarenas MR, López GP, Sibbett SS. Multiplex lateral-flow test strips fabricated by two-dimensional shaping. *ACS Applied Materials & Interfaces*. 2009;1(1):124-9.
134. Curto VF, Lopez-Ruiz N, Capitan-Vallvey LF, Palma AJ, Benito-Lopez F, Diamond D. Fast prototyping of paper-based microfluidic devices by contact stamping using indelible ink. *RSC Advances*. 2013;3(41):18811-6.
135. Santhiago M, Nery EW, Santos GP, Kubota LT. Microfluidic paper-based devices for bioanalytical applications. *Bioanalysis*. 2014;6(1):89-106.
136. Akyazi T, Basabe-Desmonts L, Benito-Lopez F. Review on microfluidic paper-based analytical devices towards commercialisation. *Analytica Chimica Acta*. 2018;1001:1-17.

137. Dungchai W, Chailapakul O, Henry CS. Use of multiple colorimetric indicators for paper-based microfluidic devices. *Analytica Chimica Acta*. 2010;674(2):227-33.
138. Li Z, Zhu Y, Zhang W, Xu C, Pan Y, Zhao Y. A low-cost and high sensitive paper-based microfluidic device for rapid detection of glucose in fruit. *Food Analytical Methods*. 2017;10(3):666-74.
139. Silva TG, de Araujo WR, Muñoz RAA, Richter EM, Santana MHP, Coltro WKT, et al. Simple and sensitive paper-based device coupling electrochemical Sample pretreatment and colorimetric detection. *Analytical Chemistry*. 2016;88(10):5145-51.
140. Jarujamrus P, Meelapsom R, Naksen P, Ditcharoen N, Anutrasakda W, Siripinyanond A, et al. Screen-printed microfluidic paper-based analytical device (μ PAD) as a barcode sensor for magnesium detection using rubber latex waste as a novel hydrophobic reagent. *Analytica Chimica Acta*. 2019;1082:66-77.
141. Liu C, Gomez FA, Miao Y, Cui P, Lee W. A colorimetric assay system for dopamine using microfluidic paper-based analytical devices. *Talanta*. 2019;194:171-6.
142. Abdulsattar JO, Hadi H, Richardson S, Iles A, Pamme N. Detection of doxycycline hyclate and oxymetazoline hydrochloride in pharmaceutical preparations via spectrophotometry and microfluidic paper-based analytical device (μ PADs). *Analytica Chimica Acta*. 2020;1136:196-204.
143. Liu Y-C, Hsu C-H, Lu B-J, Lin P-Y, Ho M-L. Determination of nitrite ions in environment analysis with a paper-based microfluidic device. *Dalton Transactions*. 2018;47(41):14799-807.
144. Murray E, Nesterenko EP, McCaul M, Morrin A, Diamond D, Moore B. A colorimetric method for use within portable test kits for nitrate determination in various water matrices. *Analytical Methods*. 2017;9(4):680-7.
145. Jayawardane BM, Wei S, McKelvie ID, Kolev SD. Microfluidic paper-based analytical device for the determination of nitrite and nitrate. *Analytical chemistry*. 2014;86(15):7274-9.
146. Yuen SH, Pollard AG. Determination of nitrogen in agricultural materials by the nessler reagent. II.—Micro-determinations in Plant Tissue and in Soil Extracts. *Journal of the Science of Food and Agriculture*. 1954;5(8):364-9.

147. Krug FJ, Růžicka J, Hansen EH. Determination of ammonia in low concentrations with Nessler's reagent by flow injection analysis. *The Analyst*. 1979;104(1234):47-54.
148. Niedzielski P, Kurzyca I, Siepak J. A new tool for inorganic nitrogen speciation study: Simultaneous determination of ammonium ion, nitrite and nitrate by ion chromatography with post-column ammonium derivatization by Nessler reagent and diode-array detection in rain water samples. *Analytica Chimica Acta*. 2006;577(2):220-4.
149. Zhou L, Boyd CE. Comparison of nessler, phenate, salicylate and ion selective electrode procedures for determination of total ammonia nitrogen in aquaculture. *Aquaculture*. 2016;450:187-93.
150. Bower CE, Holm-Hansen T. A salicylate–hypochlorite method for determining ammonia in seawater. *Canadian Journal of Fisheries and Aquatic Sciences*. 1980;37(5):794-8.
151. Bolleter WT, Bushman CJ, Tidwell PW. Spectrophotometric determination of ammonia as indophenol. *Analytical chemistry*. 1961;33(4):592-4.
152. Weatherburn MW. Phenol-hypochlorite reaction for determination of ammonia. *Analytical chemistry*. 1967;39(8):971-4.
153. Afkhami A, Norooz-Asl R. Micelle-mediated extraction and spectrophotometric determination of ammonia in water samples utilizing indophenol dye formation. *Journal of the Brazilian Chemical Society*. 2008;19:1546-52.
154. Phansi P, Sumantakul S, Wongpakdee T, Fukana N, Ratanawimarnwong N, Sitanurak J, et al. Membraneless Gas-separation microfluidic paper-based analytical devices for direct quantitation of volatile and nonvolatile compounds. *Analytical Chemistry*. 2016;88(17):8749-56.
155. Cho YB, Jeong SH, Chun H, Kim YS. Selective colorimetric detection of dissolved ammonia in water via modified Berthelot's reaction on porous paper. *Sensors and Actuators B: Chemical*. 2018;256(Supplement C):167-75.
156. Nagul EA, McKelvie ID, Worsfold P, Kolev SD. The molybdenum blue reaction for the determination of orthophosphate revisited: Opening the black box. *Analytica Chimica Acta*. 2015;890:60-82.

157. Moonrungsee N, Pencharee S, Jakmunee J. Colorimetric analyzer based on mobile phone camera for determination of available phosphorus in soil. *Talanta*. 2015;136:204-9.
158. Deng S, Yang T, Zhang W, Ren C, Zhang J, Zhang Y, et al. Rapid detection of trichlorfon residues by a microfluidic paper-based phosphorus-detection chip (μ PPC). *New Journal of Chemistry*. 2019;43(19):7194-7.
159. Pinyorosphathum C, Rattanarat P, Chaiyo S, Siangproh W, Chailapakul O. Colorimetric sensor for determination of phosphate ions using anti-aggregation of 2-mercaptoethanesulfonate-modified silver nanoplates and europium ions. *Sensors and Actuators B: Chemical*. 2019;290:226-32.
160. Jacobs HRD, Hoffman WS. A new colorimetric method for the estimation of potassium. *Journal of Biological Chemistry*. 1931;93:685-91.
161. Looney JM, Dyer CG. A photoelectric method for the determination of potassium in blood serum. *The Journal of Laboratory and Clinical Medicine*. 1942;28(3):355-63.
162. Abdul-Fadl MA. Colorimetric determination of potassium by folin-ciocalteu phenol reagent. *Biochemical Journal*. 1949;44(3):282-5.
163. Whittles CL, Little RC. A colorimetric method for the determination of potassium and its application to the analysis of soil extracts. *Journal of the Science of Food and Agriculture*. 1950;1:323-9.
164. Song G, Sun R, Du J, Chen M, Tian Y. A highly selective, colorimetric, and environment-sensitive optical potassium ion sensor. *Chemical Communications*. 2017;53(41):5602-5.
165. Qiu J, Zhang Y, Dong C, Huang Y, Sun L, Ruan H, et al. Rapid colorimetric detection of potassium ions based on crown ether modified Au NPs sensor. *Sensors and Actuators B: Chemical*. 2019;281:783-8.
166. Gerold CT, Bakker E, Henry CS. Selective distance-based K^+ quantification on paper-based microfluidics. *Analytical Chemistry*. 2018;90(7):4894-900.
167. Norman RJ, Stucki JW. The determination of nitrate and nitrite in soil extracts by ultraviolet spectrophotometry. *Soil Science Society of America Journal*. 1981;45(2):347-53.

168. Berg, M, Meehan, M, Scherer, T. Nitrogen Behavior in the Environment. [updated 2017; cited 2019 April 3]. Available from: <https://www.ag.ndsu.edu/publications/environment-natural-resources/nitrogen-behavior-in-the-environment>.
169. USDA Natural Resources Conservation Service. Soil Quality Indicators. [updated 2014; cited 2019 April 3]. Available from: https://www.nrcs.usda.gov/wps/PA_NRCSCconsumption/download?cid=stelprdb1243373&ext=pdf.
170. Flynn R. Interpreting soil tests: Unlock the secrets of your soil: Extension Service, Circular 676. USA: College of Agriculture, Consumer and Environmental Sciences, New Mexico State University; 2015.
171. Jones JB. Laboratory guide for conducting soil tests and plant analysis. Florida, USA: CRC Press; 1930.
172. López Pasquali CE, Fernández Hernando P, Durand Alegría JS. Spectrophotometric simultaneous determination of nitrite, nitrate and ammonium in soils by flow injection analysis. *Analytica Chimica Acta*. 2007;600(1):177-82.
173. Li X, Tian J, Nguyen T, Shen W. Paper-based microfluidic devices by plasma treatment. *Analytical Chemistry*. 2008;80(23):9131-4.
174. Zhang Y, Ren T, He J. Inkjet printing enabled controllable paper superhydrophobization and its applications. *ACS Applied Materials & Interfaces*. 2018;10(13):11343-9.
175. Li Z, Li F, Xing Y, Liu Z, You M, Li Y, et al. Pen-on-paper strategy for point-of-care testing: Rapid prototyping of fully written microfluidic biosensor. *Biosensors & bioelectronics*. 2017;98:478-85.
176. Wang S, Ge L, Song X, Yu J, Ge S, Huang J, et al. Paper-based chemiluminescence ELISA: Lab-on-paper based on chitosan modified paper device and wax-screen-printing. *Biosensors and Bioelectronics*. 2012;31(1):212-8.
177. Zhang W, Lu P, Qian L, Xiao H. Fabrication of superhydrophobic paper surface via wax mixture coating. *Chemical Engineering Journal*. 2014;250:431-6.
178. Jusoh N, Othman N. Stability of water-in-oil emulsion in liquid membrane prospect. *Malaysian Journal of Fundamental and Applied Sciences*. 2017;12.

179. Liu Z, Yu J, Lin W, Yang W, Li R, Chen H, et al. Facile method for the hydrophobic modification of filter paper for applications in water-oil separation. *Surface and Coatings Technology*. 2018;352:313-9.
180. Miranda KM, Espey MG, Wink DA. A rapid, simple spectrophotometric method for simultaneous detection of nitrate and nitrite. *Nitric Oxide*. 2001;5(1):62-71.
181. García-Robledo E, Corzo A, Papaspyrou S. A fast and direct spectrophotometric method for the sequential determination of nitrate and nitrite at low concentrations in small volumes. *Marine Chemistry*. 2014;162:30-6.
182. Jayawardane BM, Wei S, McKelvie ID, Kolev SD. Microfluidic paper-based analytical device for the determination of nitrite and nitrate. *Analytical Chemistry*. 2014;86(15):7274-9.
183. Carmona FdC, Anghinoni I, Cao EG. Dynamics of ammonium and pH in the solution of soils with different salinity levels, growing irrigated rice. *Revista Brasileira de Ciência do Solo*. 2012;36:401-9.
184. Zhao-liang Z, Qi-xiao W, Freney JR. *Nitrogen in soils of China*: Springer Science & Business Media; 2012.
185. Brandes JA, Devol AH, Deutsch C. New developments in the marine nitrogen cycle. *Chemical Reviews*. 2007;107(2):577-89.
186. Hodges SC. *Soil fertility basics*. Soil Science Extension. USA: North Carolina State University; 2010.
187. Thompson J, Morrison G. Determination of organic nitrogen. Control of variables in the use of nessler's reagent. *Analytical Chemistry*. 1951;23(8):1153-7.
188. Tzollas NM, Zachariadis GA, Anthemidis AN, Stratis JA. A new approach to indophenol blue method for determination of ammonium in geothermal waters with high mineral content. *International Journal of Environmental Analytical Chemistry*. 2010;90(2):115-26.
189. Patton CJ, Crouch SR. Spectrophotometric and kinetics investigation of the Berthelot reaction for the determination of ammonia. *Analytical Chemistry*. 1977;49(3):464-9.
190. Searle PL. The berthelot or indophenol reaction and its use in the analytical chemistry of nitrogen. A review. *Analyst*. 1984;109(5):549-68.

191. Ma J, Li P, Lin K, Chen Z, Chen N, Liao K, et al. Optimization of a salinity-interference-free indophenol method for the determination of ammonium in natural waters using o-phenylphenol. *Talanta*. 2018;179:608-14.
192. Sasongko A. Ammonia determination in bottled water using spectrophotometer: Comparison between nessler and berthelot methods. 2018;7(1):9.
193. Law K-Y. Definitions for hydrophilicity, hydrophobicity, and superhydrophobicity: Getting the basics right. *The Journal of Physical Chemistry Letters*. 2014;5(4):686-8.
194. Dai C, Yang L, Xie J, Wang T-J. Nutrient diffusion control of fertilizer granules coated with a gradient hydrophobic film. *Colloids and Surfaces A: Physicochemical and Engineering Aspects*. 2020;588:124361.
195. Cogan D, Cleary J, Fay C, Rickard A, Jankowski K, Phelan T, et al. The development of an autonomous sensing platform for the monitoring of ammonia in water using a simplified Berthelot method. *Analytical Methods*. 2014;6(19):7606-14.
196. Krom MD. Spectrophotometric determination of ammonia: a study of a modified Berthelot reaction using salicylate and dichloroisocyanurate. *The Analyst*. 1980;105(1249):305-16.
197. Nguyen TH, Mugerli L, Rivron C, Tran-Thi TH. Innovative colorimetric sensors for the selective detection of monochloramine in air and in water. *Sensors and Actuators B: Chemical*. 2015;208:622-7.
198. Shoji T, Nakamura E. Flow injection analysis with spectrophotometry for ammonium ion with 1-naphthol and dichloroisocyanurate. *Journal of Flow Injection Analysis*. 2009;26(1):37.
199. Rhine E, Mulvaney R, Pratt E, Sims G. Improving the Berthelot reaction for determining ammonium in soil extracts and water. *Soil Science Society of America Journal*. 1998;62(2):473-80.
200. Apilux A, Siangproh W, Praphairaksit N, Chailapakul O. Simple and rapid colorimetric detection of Hg(II) by a paper-based device using silver nanoplates. *Talanta*. 2012;97:388-94.
201. Nieder R, Benbi DK, Scherer HW. Fixation and defixation of ammonium in soils: a review. *Biology and Fertility of Soils*. 2011;47(1):1-14.

202. Jaikang P, Paengnakorn P, Grudpan K. Simple colorimetric ammonium assay employing well microplate with gas pervaporation and diffusion for natural indicator immobilized paper sensor via smartphone detection. *Microchemical Journal*. 2020;152:104283.
203. Meena VS. *Role of Rhizospheric Microbes in Soil*. Singapore: Springer Nature Singapore; 2018.
204. Vance CP, Uhde-Stone C, Allan DL. Phosphorus acquisition and use: Critical adaptations by plants for securing a nonrenewable resource. *New Phytologist*. 2003;157(3):423-47.
205. De Borba BM, Jack RF, Rohrer JS, Wirt J, Wang D. Simultaneous determination of total nitrogen and total phosphorus in environmental waters using alkaline persulfate digestion and ion chromatography. *Journal of Chromatography A*. 2014;1369:131-7.
206. Pradhan S, Pokhrel MR. Spectrophotometric determination of phosphate in sugarcane juice, fertilizer, detergent and water samples by molybdenum blue method. *Scientific World*. 2013;11:58-62.
207. Ivanov K, Zapryanova P, Petkova M, Stefanova V, Kmetov V, Georgieva D, et al. Comparison of inductively coupled plasma mass spectrometry and colorimetric determination of total and extractable phosphorus in soils. *Spectrochimica Acta Part B: Atomic Spectroscopy*. 2012;71-72(Supplement C):117-22.
208. Legiret F-E, Sieben VJ, Woodward EMS, Abi Kaed Bey SK, Mowlem MC, Connelly DP, et al. A high performance microfluidic analyser for phosphate measurements in marine waters using the vanadomolybdate method. *Talanta*. 2013;116:382-7.
209. Yang C, Sun X, Liu B, Lian H. Determination of total phosphorus in water sample by digital imaging colorimetry. *Chinese Journal of Analytical Chemistry*. 2007;35(6):850-3.
210. Carrilho E, Martinez A, Whitesides G. Understanding wax printing: A simple micropatterning process for paper-based microfluidics. *Analytical chemistry*. 2009;81:7091-5.

211. Waghwani B, Balpande S, Kalambe J. Development of microfluidic paper based analytical device for detection of phosphate in water. *International Journal of Innovative Technology and Exploring Engineering (IJITEE)*. 2019;8(6S):592-5.
212. Racicot JM, Mako TL, Olivelli A, Levine M. A Paper-based device for ultrasensitive, colorimetric phosphate detection in seawater. *Sensors*. 2020;20(10):2766.
213. Sparks D, Huang P. Physical chemistry of soil potassium. Potassium in agriculture. 1985:201-76.
214. Hafsi C, Debez A, Abdelly C. Potassium deficiency in plants: effects and signaling cascades. *Acta Physiologiae Plantarum*. 2014;36(5):1055-70.
215. Wang Y, Wu W-H. Plant sensing and signaling in response to K⁺ deficiency. *Molecular Plant*. 2010;3(2):280-7.
216. Sattar A, Naveed M, Ali M, Zahir ZA, Nadeem SM, Yaseen M, et al. Perspectives of potassium solubilizing microbes in sustainable food production system: A review. *Applied Soil Ecology*. 2019;133:146-59.
217. Wang NCY, Rice GE, Teuschler LK, Colman J, Yang RSH. An in silico approach for evaluating a fraction-based, risk assessment method for total petroleum hydrocarbon mixtures. *Journal of Toxicology*. 2012;2012:410143.
218. Lalitha M, Dhakshinamoorthy M. Forms of soil potassium-a review. *Agricultural Reviews*. 2014;35(1):64-8.
219. Prajapati K, Modi H. The importance of potassium in plant growth-a review. *Indian Journal of Plant Sciences*. 2012;1(02):177-86.
220. Mouhamad R, Atiyah A, Iqbal M. Behavior of potassium in soil: a mini review. *Chemistry International*. 2016;2:47-58.
221. Rao CS, Srinivas K. Potassium dynamics and role of non-exchangeable potassium in crop nutrition. *Indian Journal of Fertilisers*. 2017;13:80-94.
222. Xiao-lei W, Hai-qiu Y, Ning L, Bing Y, Jing W, Xing-tao L, et al. Some physiological characteristics in maize (*Zea mays* L.) inbred lines tolerant to low potassium from grain filling to maturity. *African Journal of Agricultural Research*. 2012;7(11):10.5897.

223. Escobar R, Lamonedá C, de Pablos F, Guiraúm A. Ion-pair extraction and spectrophotometric determination of potassium using dibenzo-18-crown-6 and bromothymol blue. *Analyst*. 1989;114(4):533-5.
224. Dadfarnia S, Shamsipur M. Extraction-spectrophotometric determination of potassium by dibenzo-18-crown-6 and calmagite and its application to biological fluids. *Analytical Letters*. 1992;25(1):11-20.
225. Chen Z, Guo J, Ma H, Zhou T, Li X. A simple colorimetric sensor for potassium ion based on DNA G-quadruplex conformation and salt-induced gold nanoparticles aggregation. *Analytical Methods*. 2014;6(19):8018-21.
226. Li L, Li W. Colorimetric kinetic determination of potassium ions based on the use of a specific aptamer and catalytically active gold nanoparticles. *Microchimica Acta*. 2015;182(13):2307-12.
227. Lin S-Y, Liu S-W, Lin C-M, Chen C-h. Recognition of potassium ion in water by 15-crown-5 functionalized gold nanoparticles. *Analytical Chemistry*. 2002;74(2):330-5.
228. Chen Z, Huang Y, Li X, Zhou T, Ma H, Qiang H, et al. Colorimetric detection of potassium ions using aptamer-functionalized gold nanoparticles. *Anal Chim Acta*. 2013;787:189-92.
229. Naderi M, Hosseini M, Ganjali MR. Naked-eye detection of potassium ions in a novel gold nanoparticle aggregation-based aptasensor. *Spectrochimica acta Part A, Molecular and biomolecular spectroscopy*. 2018;195:75-83.
230. Lapresta-Fernández A, Capitán-Vallvey LF. Scanometric potassium determination with ionophore-based disposable sensors. *Sensors and Actuators B: Chemical*. 2008;134(2):694-701.
231. Wang X, Qin Y, Meyerhoff ME. Paper-based plasticizer-free sodium ion-selective sensor with camera phone as a detector. *Chemical Communications*. 2015;51(82):15176-9.
232. Zhai J, Xie X, Cherubini T, Bakker E. Ionophore-based titrimetric detection of alkali metal ions in serum. *ACS Sensors*. 2017;2(4):606-12.
233. Frański R, Gierczyk B, Schroeder G. Anion- π interactions—interactions between benzo-crown ether metal cation complexes and counter ions. *Journal of the American Society for Mass Spectrometry*. 2009;20(2):257-62.

234. Lan W-J, Zou XU, Hamed MM, Hu J, Parolo C, Maxwell EJ, et al. Paper-based potentiometric ion sensing. *Analytical Chemistry*. 2014;86(19):9548-53.

